The development of a thermal storage system for a solar driven aqua ammonia heat pump

A.P.J de Beer

orcid.org/0000-0001-7405-5205

Dissertation submitted in fulfilment of the requirements for the degree *Master of Engineering in Mechanical Engineering* at the North-West University

Supervisor: Prof. C.P Storm

Graduation May 2018

Student number: 22788913

Abstract

The development of a thermal heat storage system for a solar driven aqua ammonia heat pump is of significant importance to make a truly effective alternative power refrigeration system. This dissertation includes a preliminary design for the specific application as well as verification of the suitability of the design choices made. Literature gives a vast array of methods and materials that can be used for thermal heat storage. Packed beds normally store thermal energy that is provided by solar air heaters. However, this design included a packed bed storage system that uses a water glycol mixture as the heat transfer fluid. After constructing a test bed, multiple runs were completed, using water as the heat transfer fluid, to test the effectiveness of this unconventional method. Amongst others, the project involved determining the pressure drop across the system, the density of the storage material and the void fraction of the packing method. The results showed that the effectiveness of this design was 76.5 % under ideal circumstances. This compares well to other thermal energy storages systems. In conclusion, the study showed that a packed bed storage system using a water glycol mixture as heat transfer fluid is a viable thermal heat storage solution. The project recommendations suggested that the further research can be conducted regarding the shape of the storage material to reduce cost and the void fraction in the system.

Key words: Thermal heat storage, aqua ammonia, packed beds, specific heat capacity

Declaration

I, Abri de Beer 22788913 have read the information above and understand it. I know what plagiarism is and am aware of the consequences of committing plagiarism. I further declare:

1. that the text and bibliography of this paper reflect the sources I have consulted, and
2. that sections with no source references are my own ideas, arguments and/or conclusions.

SIGNATURE: _____ DATE: 2018/05/02

Acknowledgments

I would like to thank my supervisor Prof. C. Storm as well as Prof. J. Markgraaff for the academic support and guidance. I would also like to thank my wife Anika for the moral support. And last but not least my Mother Annelie and Father Attie which through their hard work made it possible to pursue my dreams.

"Even the smallest person can change the course of the future."

Queen Galadriel (Lord of the Rings)

Table of contents

Table of figures

List of tables

Nomenclature

List of symbols

Symbol	Description	Unit
c_d	Drag coefficient for a packed bed, as used in the RUC Model	-
f_{er}	Ergun Friction Factor	-
Ψ	Sphericity	-
E	Quality factor from ASME B 31.3	-
F	Drag Factor of Plessis and Woudberg (2008)	-
Re_{er}	Ergun definition of the Reynolds number	-
Re_p	Particle Reynolds number	-
Y	Coefficient of material from ASME B 31.3	-
n	Number of storage material elements	-
ε	Void fraction	-
$NumberOfCubes$	Number of storage material elements needed for adequate energy storage	-
Eff	Effectivity of storage system	%
T_{max}	Maximum temperature	C
T_{min}	Minimum temperature	C
G	Air mass flux.	g/s m^2
Q_{latent}/q_{latent}	Latent Heat	J

Symbol	Description	Unit
$Q_{sensible,solid}$	Sensible Heat of Solidification	J
$Q_{sensible,liquid}$	Sensible Heat of Melting	J
$Q_{sensible}$	Sensible heat	J
Q_{total}/q_{total}	Total heat	J
h_m	Enthalpy of melting	J
c_p	Specific Heat	J/kg.K
c_{pf}	Specific heat capacity of HTF at constant pressure	J/kg.K
c_s	Specific heat capacity of solid	J/kg.K
cp_{STM}	Specific heat capacity of storage material	J/kg.K
T_f	HTF temperature	K
T_s	Solid temperature	K
T_1	Initial temperature	K
T_2	Final temperature	K
T_m	Temperature of melting	K
ΔT	Temperature difference	K
T	Temperature	K
m_{cube}	Mass of storage material elements	kg
$m_{s_{seg}}$	Mass of solid in segment	kg
m_{STM}	Mass storage material	kg
m_s	Mass of solid	kg

Symbol	Description	Unit
m	Mass	kg
m_{pipe_E}	Mass of empty pipe	kg
m_{pipe_F}	Mass of filled pipe	kg
m_{HTF}	Mass of heat transfer fluid in pipe	kg
μ_f	HTF (dynamic) viscosity	kg/m.s
ρ_a	HTF density	kg/m^3
ρ_f	Density of HTF	kg/m^3
ρ	Density	kg/m^3
ρ_{STM}	Density of heat storage material	kg/m^3
$\dot{m}_f$	Mass flow rate of HTF through bed	kg/s
G_{CW}	Air mass flux as used by Chandra and Whillit.	kg/s m^2
μ_a	Dynamic viscosity of HTF	kg/s.m
G	Mass velocity of HTF or mass flow rate of HTF per unit bed cross-sectional area	kg/s.m
Sb	Maximum bending stress in pipe	kPa
A_{cs}	Cross-sectional area of test section perpendicular to flow direction	m
D_c	Equivalent diameter	m
d_s	Lengths dimension of a solid cube within the RUC	m
Δx	Discrete segment length of bed	m

Symbol	Description	Unit
C	Circumference	m
H	Height	m
h	Plenum side length	m
L	Length	m
L_p	Pipe length	m
W	Width	m
D	Particle hydraulic/equivalent diameter or size	m
L	Flow-wise length of bed	m
L	Span length	m
d	Side length of a cubic RUC	m
D_{pipe_O}	Outside diameter of pipe/housing.	m
D_{pipe_I}	Inside diameter of pipe/housing.	m
L	Maximum allowable length between supports	m
r_{pipe_O}	Outside radius of pipe	m
r_{pipe_I}	Inside radius of pipe	m
t	Wall thickness	m

Symbol	Description	Unit
y_a	Allowable deflection	m
D_s	Length dimension of solid cube within RUC.	m
v_s	Superficial speed through porous medium	m/s
v_s	Superficial speed through porous medium.	m/s
v_b	Average interstitial speed (air speed between rocks).	m/s
A	Area	m^2
A_p	Pipe cross sectional area	m^2
A_{cs}	Cross-sectional area of test section perpendicular to flow direction.	m^2
A_s	Total surface area of solid particle in bed/RUC volume.	m^2
V_s	Solid volume	m^3
V_{STM}	Volume heat storage material	m^3
V_{cube}	Volume of storage material elements	m^3
V_f	Void volume/Fluid volume	m^3
V_o	Total volume	m^3
V	Volume	m^3
I	Moment of Inertia	m^4
w_c	Concentrated weight on pipeline	N

Symbol	Description	Unit
w_{pipe_F}	Weight of filled pipe	N
w_{con}	Weight of concentrated masses on pipeline ex flanges	N
w	Uniformly distributed weight of pipeline	N/m
wf	Weight of fluid per unit length	N/m
wp	Weight of pipe per unit length	N/m
P_b	Bed pressure	N/m^2
E	Modulus of elasticity	N/m^2
P	Pressure of the fluid in pipe	N/m^2
S	Allowable stress	N/m^2
$\frac{\Delta p}{L}$	Pressure gradient	$N/m^2/m$
$PriceOfCubes$	Total price of elements needed for adequate energy storage	R
$HousingPrice$	Total price of thermal heat store housing	R
$MouldPrice$	Price of storage element mould	R
$TotalPrice$	Total price of energy storage system	R
$\dot{Q}$	Heat flow rate	W
$Q_{ToBeStored}$	Amount of energy stored	W

Symbol	Description	Unit
$Q_{in_{6hours}}$	Amount of energy that is received from the CSP in 6 hours	W
$Q_{pump_{1hour}}$	Energy to be stored to let pump run one hour	W
$Q_{pump_{24hours}}$	Energy to be stored to let pump run 24 hours	W
$Q_{PumpDesigned}$	Energy consumed by bubble pump	W.h
Q_{in}	Amount of energy that is received from the CSP per hour.	W.h
λ	Thermal conductivity	W/m.K
M	Index	$Ws^{-0.5}/m^2K$

Abbreviations

Abbreviation	Description
NWU	North-West University
PV	Photovoltaic
CST	Concentrated Solar Thermal
HTF	Heat Transfer Fluid
PCM	Phase Change Materials
CSP	Concentrated Solar Power
pH	Power of Hydrogen
TES	Thermal Energy Storage
RUC	Representative Unit Cell
EES	Engineering Equation Solver
NTU	Number of Transfer Units
STM	Storage Material

Units

Symbol	**Description**
m	Meter
N	Newton
J	Joule
W	Watt
s	Second
K	Kelvin

1 Introduction

1.1 Background

The technology on which pump-less aqua ammonia absorption refrigeration is based, is more than a hundred years old. The same restriction that led to the development of the system is now relevant once more – the availability of cheap reliable electricity. A hundred years ago, there was a lack of electrical infrastructure in South Africa and other developing countries, not only the lack of renewable energy that drives this innovation, but also the lack of a reliable electricity supply. (van der Walt, 2012:1)

Heating and cooling using solar power is simple, while generating shaft power (electricity) from the sun has many more losses associated with it. *Van de Walt* argued that, a solar thermal power aqua-ammonia absorption heat pump used for refrigeration is a much more efficient way of using solar power for refrigeration than relying on a compressor-driven system (van der Walt, 2012:1).

Using solar power for refrigeration is not a new concept. Over the years several manufacturers of refrigerators have designed solar-powered pump-less aqua ammonia absorption refrigeration. These refrigerators were mostly aimed at the camping market. The technology, however, never really took off as it was very inefficient and struggled to supply reliable cooling (van der Walt, 2012:1).

The main problem is that the energy source (namely the sun) is inconsistent. Even in South Africa which has a very high level of solar radiation one can only bargain on about six hours of intense sunshine a day. Because of this, the design of such refrigerators used a large refrigeration setup to quickly cool to desired temperature during the available time in the day. They then relied on good insulation to keep the system cool during the night. This design has some merit in theory but in practice it is woefully inadequate. As the design has such a large refrigeration system it needs a large heat input making solar thermal collectors very large and cumbersome. Secondly, if it is an overcast day there is no cooling, and if this happens one or two days in a row the spoiling of food becomes a reality. The user must also manage his/her usage of the system very carefully to avoid the unnecessary opening of the refrigerator at times when it is not cooling to avoid heating of the system.

When optimizing the system, it is important to address some of the issues discussed above. Thus, if it is possible to keep the system running 24/7 it would give the user a backup for overcast days as well as making the management of the system easier.

The North-West University (NWU) under the leadership of Prof C Storm is doing exactly that. They have designed a solar-powered pump-less aqua ammonia absorption refrigerator that addresses the problems that have kept this technology out of mainstream usage. This was done by making the system smaller and optimizing it to its full potential enabling them to keep the system running 24 hours a day with the solar energy captured during the day.

The solar collectors of the above-mentioned mobile test rig deliver 30 *kW.h* in a six-hour day nominal, at a best and worst scenario of 140 °*C* and 100 °*C* respectively. Prof Storm and his team intend to optimize the technology by making the refrigeration cycle run for a 24 *h* day at a 0.9 *kW.h* supply at 90 °*C* and 60 °*C* at best and worst case respectively. The difference in input and output of the heat store regarding quantity of heat as well temperature differences should cater for pre-empted loss of efficiency of the heat store conservatively. The remainder is intended to cater for cloudy days.

A critical parameter of this absorption heat pump cycle is the required system pressure that of the latter is dictated by the condenser outlet temperature. The system pressure thus has to be at least the equivalent saturation pressure of ammonia for that temperature. Due to seasonal heat sink temperature variances the ideal system pressure will thus have to vary. An innovation of this project is that the system pressure will vary and an overpressure for worst case scenario will not be implemented. The resulting innovation is that an optimum generator temperature has been determined for each varying system pressure (done in another project, see Section 1.5). It is also important to note that the system will be using a water glycol mixture as the heat transfer fluid.

The design described above will bring about a revolution in the use of such system, as it will now make it much more attractive to use not only in the industry but also making it a serious contender for industrial use.

The research done in this dissertation forms part of this larger project. A number of sub-projects focus on the design of the solar collectors, heat sink, bubble pump and mounting trailer whereas this study focuses on the thermal heat storage system.

1.2 Problem statement

- Since the heat pump will be operating 24 *h* a day and the usable sun radiation is only 6 *h* a day, a heat store is necessary.
- Due to the optimum generator temperatures and load, varying with the seasons. The required heat store needs to be designed for the worst-case scenario as per Section 1.1

1.3 Objectives

Objectives to be completed are the following:

- To identify by research and testing, a suitable thermal heat storage material.
- To design the thermal heat storage system regarding size, thermodynamic design approach and other specifications, based on the properties of the selected thermal heat storage material.
- Designing a heat store according to the selected thermal heat storage material and within the restrictions of the available space in the mobile test rig.
- Manufacturing and assemble the said thermal heat storage system or a portion thereof depending on available facilities and funds.
- Perform tests on the above-mentioned thermal heat storage system and perform interpretation and evaluation of the results.

1.4 Research methodology and experimental procedure

The research methodology and experimental procedure to be followed is listed below:

- Preform a literature survey regarding thermal heat storage systems, storage materials and thermal heat storage system setups. Other information will serve as secondary background.
- Develop a concept design in which some aspects of the literature are investigated further in order to proceed with the detailed design. These aspects include, storage material and storage material shape the pressure drop over the thermal heat storage system and the thermal heat storage system housing.
- Produce a detailed design using the technical information gathered in the concept design phase.
- Manufacture the test rig in accordance with the detailed design.
- Construct the test rig while also identifying, calibrating and installing the measuring equipment to be used during the experiments.
- Execute the following tests:

    - Specific heat of storage material
    - Thermal heat storage system void fraction.
    - Thermal heat storage material density.
    - Pressure difference over the thermal heat storage system.
    - Thermal store efficiency.
- Calculate and interpret all the tests results.
- Make a conclusion and recommendation using the test results.

1.5 Scope and limitations

- The following is not included in the study: the calculation of the optimum generator temperature, derived from the different system pressures, which is dictated by heat sink seasonal temperatures. These parameters are given.
- The size and capacity of this thermal heat store is only matched to the test model and quantities mentioned in background Section 1.1.
- This study focuses only on the macroscopic first law approach of heat in vs heat out and overall efficiency. It does not endeavour to perform detailed calculations and evaluation of heat transfer within the elements in the packed bed itself.
- This study does not include the way in which the system pressure is varied according to different heat sink temperatures.

1.6 Structure of dissertation

1. **Introduction**

   The introduction gives a brief background that explains the need for the project. The problem is then stated as well as the objectives of the project. Furthermore, the experimental procedure and scope are defined.

2. **Literature study**

   The literature study gives a broad overview of all the components in the thermal heat storage system. This section, however, places more emphasis on the thermal energy storage system that is found in a concentrated solar thermal system, and reviews available storage technologies.

3. **Concept design**

   Preliminary component selection is done by using the literature study. However, more in-depth studies are done to give an explanation of component choice as well as bringing chosen individual components together for the first iteration design.

4. **Detailed design and manufacturing**

   Design is finalised and manufacturing starts.

5. **Test execution**

   The test is executed and the test data is gathered.

6. **Calculations and interpretation of results**

   The raw test data is processed to a usable form after which calculations are performed and results interpreted.

7. **Conclusions and recommendations**

   Using the interpretation of the results a conclusion is drawn and recommendations made to better any aspect of the dissertation.

8. **References and Bibliography**

   References contain specific citing in the text of all proceeding chapters. Bibliography contains documents and citing which were necessary for background knowledge, applicable technical information ext., but which were not specifically cited or referred to in the text of the proceeding chapters.

9. **Appendices**

2 Literature study

The main focus of the literature study is on thermal heat stores and suitable materials described in Sections 2.4-2.7. In addition, it was found necessary to include literature on prereferral upstream and downstream systems. This knowledge serves as background knowledge in the design of the thermal heat store. These systems are described in Sections 0-2.3.

2.1 Pump-less absorption refrigeration

The development of the absorption cycle can be dated back to the 1700s. It was known that ice could be produced by evaporating pure water from a vessel contained in an evacuated chamber in the presence of sulphuric acid. In 1820, ice was being made from water in a vessel which was connected to a second vessel containing the sulphuric acid. The major problem was air leakage into the evacuated chamber and the corrosive nature of sulphuric acid. In 1859 Ferdinand Carre invented a system that used water/ammonia as the working fluid. This system was what would become the basic design of early refrigeration (Srikhirin *et al.*, 2001:343).

Thus, the ammonia water-based system is one of the oldest refrigeration systems. These systems are not only used in refrigeration but also in air conditioning. This system can have very small or large refrigeration capacities.

Refrigeration systems can have several configurations with some incorporating compressors while others are pump-less systems. The refrigeration cycles also differ in the chemicals used for the refrigeration process. This project will be incorporated into a pump-less triple vapour refrigeration system using an aqua ammonia solution, thus, only this system will be briefly discussed.

The most common place one would be able to find one of the above-mentioned refrigeration systems would be in a caravan because electricity is not always available when camping and one does not want to use the battery power for refrigeration as a gas absorption refrigerator is normally used, and this only needs a heat input to function. This heat input is normally achieved using a propane flame.

The refrigeration process is explained using Figure 1.

The process begins in the generator by boiling the dissolved ammonia water mixture. The generator is heated to the boiling point of ammonia. Since the ammonia has a lower boiling point than water the ammonia boils and the vapour leave the generator and enters the condenser. The evaporated water is trickled back to the generator via pipes from the separator. In the condenser, the ammonia cools and returns to its liquid state cooling its surroundings.

The ammonia now flows down to the hydrogen-filled chamber called the evaporator or freezing unit. In this low-pressure chamber, the ammonia expands and cools down. This is the cooling action of the refrigerator. Due to the evaporation in the evaporator the ammonia is now again in its gaseous form. The ammonia then travels through a second heat provider that provides additional cooling, and returning the ammonia to a liquid form again

A device called an absorber then lets water flow through the evaporator. Ammonia easily dissolves in the water but the hydrogen not. The water ammonia mixture then returns to the generator and the process starts again (David, 2015).

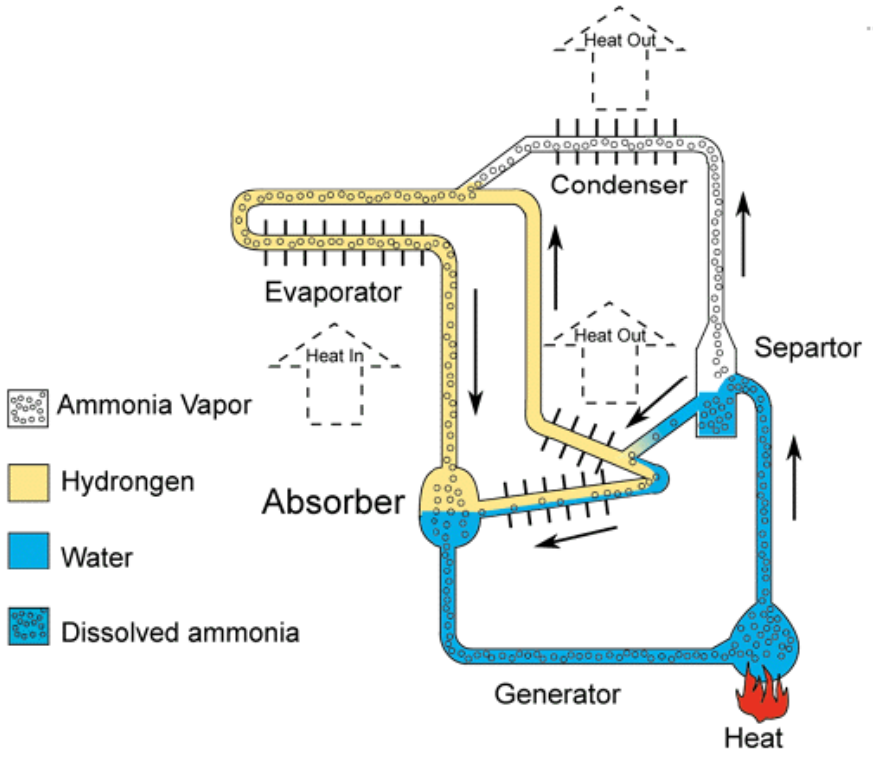

Figure 1: Schematic representation of a triple fluid vapour absorption refrigeration system (Department of Electrical Engineering Indian Institute of Technology, 2008:809)

2.2 Solar thermal refrigeration and cooling

As fossil fuels become scarcer and a large-scale energy crisis becomes a real possibility, scientists have increasingly focused more on solar energy. Solar energy is the result of electromagnetic radiation released from the sun by the thermonuclear reactions occurring inside its core. Solar refrigeration is a system where solar energy is used for refrigeration purposes (Ullah *et al.*, 2013:500).

Cooling can be achieved by means of two basic methods. Firstly, by the use of PV (photovoltaic) based systems, where the solar energy is converted into electricity to power compressor driven refrigeration. Electricity can be used to power an element for adsorption refrigeration, and secondly by the use of solar thermal energy. This system is used as a heat source for systems such as the one illustrated in Figure 1 (Ullah *et al.*, 2013:501).

The refrigeration system as designed by Prof Storm will use a solar thermal energy system, and thus, only this system will be looked at.

2.3 Concentrated solar thermal

Concentrated solar thermal (CST), is a system that concentrates a large area of sunlight onto a small receiver area (Camacho *et al.*, 2012:11). This energy is used to heat using a heat transfer fluid. CSTs can be used as a heat source for conventional power plants and a range of industrial processes. The sunlight is concentrated using a variety of mirror configurations. These configurations include:

a. parabolic troughs;
b. solar dishes;
c. linear Fresnels; and
d. solar power towers.

The main purpose of this technology is to produce as high as possible temperatures and, therefore, high thermodynamic efficiencies (Camacho *et al.*, 2012:12).

2.3.1 Concentrated solar thermal system setup

In a conventional CST system, there are three major components namely the solar collector (mirrors), solar receiver and thermal heat storage system as seen in Figure 2.

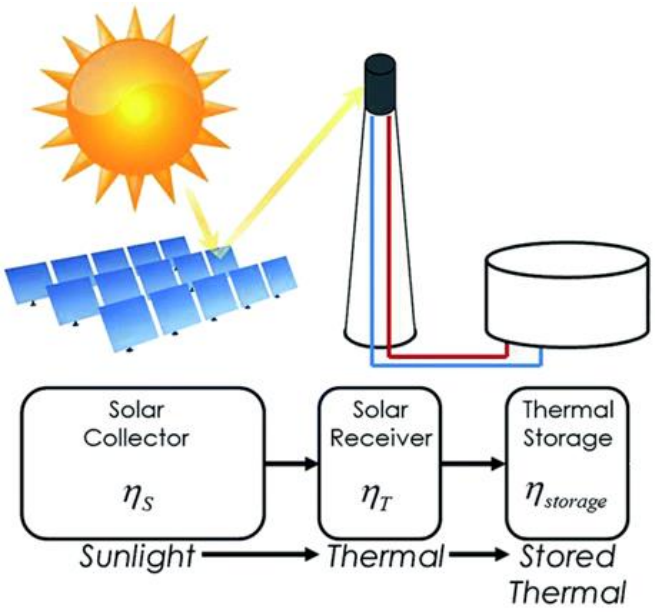

Figure 2: Simple diagram of a CST system (Henry & Prasher, 2015:1819)

This project focuses on the development of a thermal heat storage system; thus, all other components will not be elaborated upon.

2.4 Thermal heat storage system

Because of the intermitted nature of solar energy systems uptake of this technology has been slow. To increase utilization in the heating and cooling, process heat and power generating sectors two main solutions to this irregularity have been used, one being used to operate a hybrid system (solar+fossil) or to use thermal heat storage systems (Tamme *et al.*, 2012:10552).

Thermal heat storage is a physical or chemical process that takes place in the storage tank during the charging and discharging periods. The storage system consists of a tank, storage medium and a charge discharge device. The thermal energy is transferred from the solar receiver to storage (charging) and from storage to a conversion system (discharging) using a heat transfer fluid (HTF).

Thermal heat storage systems are based on:

- Sensible thermal heat storage in saturated liquids;
- Sensible thermal heat storage in solids;
- Latent thermal heat storage; and
- Thermochemical storage.

Solar heat pump thermal heat storage.

Both liquids and solids are used for the storage of sensible heat where phase change materials are normally used in latent thermal heat storage. Chemical storage requires a chemical requires that is completely reversible and that that equilibrium temperature be the same as the charge/ discharge temperature (Camacho *et al.*, 2012:21). An overview of thermal heat storage materials can be seen in Figure 3.

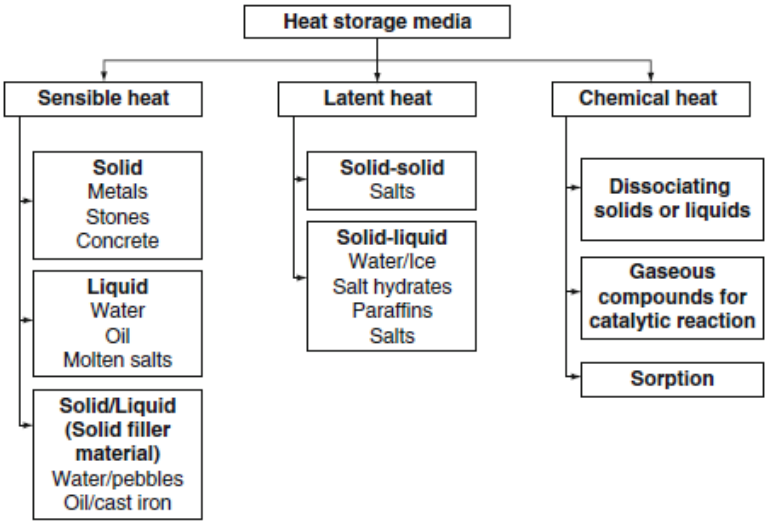

Figure 3: Overview of thermal heat storage media with examples (Tamme *et al.*, 2012:10553)

2.4.1 Principles of sensible heat

Sensible heat will always result in an increase or decrease of the materials' temperature. All materials are able to absorb and store energy (Tamme *et al.*, 2012:10552) because they have mass m and c_p at constant pressure. For a temperature difference $\Delta T=T_2-T_1$ this heat equates to

$$Q_{sensible} = m.c_p.(T_2 - T_1) \quad (1)$$

T_2 is the temperature of the material the end of the heat absorbing process and T_1 is the temperature at the beginning of the process (Tamme *et al.*, 2012:10553).

2.4.2 Principles of latent heat

Materials used for latent thermal heat storage are most commonly known as phase-change materials (PCM), this is due to the fact that they change their phase from solid to liquid and vice versa. The change in phase of the material is coupled with the absorption of heat, when the material melts and does a heat release during solidification. The phase change of the material occurs at the melting temperature or T_m. At this temperature when heat is added the

material melts but shows no sign of an increase in temperature. Thus, the heat that is added cannot be sensed and appears to be latent.

The heat stored with phase change amounts to

$$q_{latent} = \Delta h_m \quad (2)$$

where Δh_m is the latent heat (enthalpy) of melting. When the material is heated from initial temperature T_1 to the melting point T_m and it is then heated further to T_2, the total heat stored is

$$Q_{total} = Q_{sensible,solid} + Q_{latent} + Q_{sensible,liquid} \quad (3)$$

$$Q_{total} = q_{total}.m \quad (4)$$

(Tamme *et al.*, 2012:10557).

2.4.3 Principles of thermochemical storage

Reversible thermochemical reactions can be used for storing thermal heat energy. This energy is in a chemical compound created by an endothermic reaction. This energy is then recovered again by recombining the compound during an exothermic reaction. The heat stored and released is equivalent to the total heat of the chemical reaction (Tamme *et al.*, 2012:10561).

2.5 Heat transfer fluid

For purposes of explaining heat transfer fluids a parabolic concentrated solar power plant will be used as backdrop. This can be done as the purpose of the heat transfer fluid does not change even if system application charges.

During power generation, the heat transfer fluid used in the direct concentrated solar power (CSP) system is normally water, whereas the indirect system, uses a HTF where heat is later liberated to water in the steam generator. In the indirect method, there is a separate cycle for the heat transfer fluid as shown in Figure 4. The other cycle is a normal Rankine cycle used for power production (Kumar V & Sharma, 2014:239).

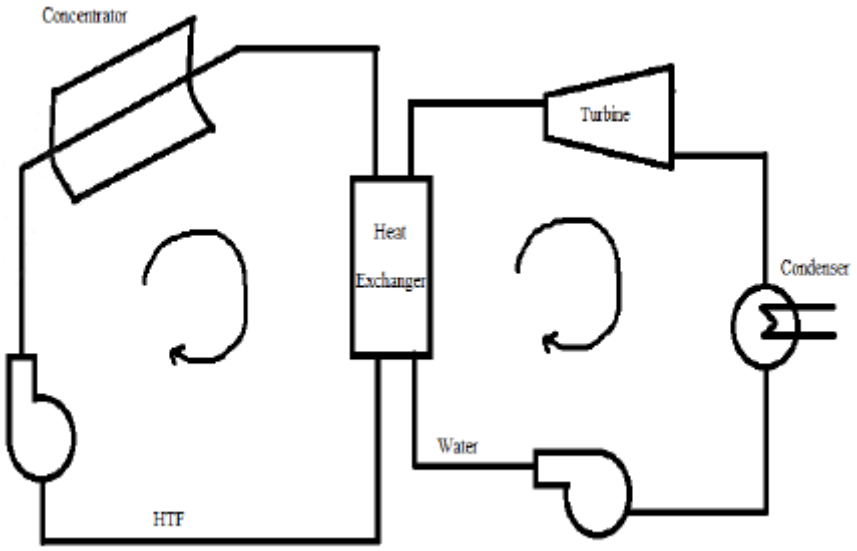

Figure 4: Basic layout of CSP plant used in power generation (Kumar V & Sharma, 2014:239)

2.5.1 Selection of heat transfer fluids

The most commonly used HTF materials in CSP plants are air, water, molten salts, glycol based, glycerol based and synthetic oils. Nowadays water and air are not used as regularly due to the fact that heating increases their volume. This leads to an increase in heat exchanger size for acceptable heat transfer effectiveness. This increases the investment cost of such a system (Kumar V & Sharma, 2014:239).

At high temperatures water, will get oxidized quickly. This tends to lead to a significantly higher corrosion rate in the pipes. Molten salts on the other hand tend to solidify at lower temperatures.

All HTF have a specific temperature range at which they are used to avoid problems such as discussed above. Glycol-based fluids are used in applications of under 175°*C* whereas synthetic fluids are used at temperatures in the range of 400°*C (Kumar V & Sharma, 2014:239)*.

In colder regions where temperatures drop below 0°*C,* water cannot be used as it will freeze. In a situation like that a HTF with anti-freeze properties would be selected with a minimum of a 20-year lifespan. Adding anti-freeze to water has a negative impact on system performance as it increases the boiling point. This in turn increases power consumption as the anti-freeze will increase the water's viscosity. The heat transfer efficiency also decreases because of the introduction of anti-freeze (Kumar V & Sharma, 2014:239).

Solar heat pump thermal heat storage.

When looking at corrosion it is important to note that salts are corrosive and that the corrosion cannot be stopped by the addition of corrosion inhibiters. Glycols and alcohols without corrosion inhibiters will also lead to corrosion. Glycols produce acids during oxidation, and this in turn results in a lower pH at higher temperature. Acid will then form which is corrosive in nature. pH buffers should thus be used to keep HTF neutral, along with proper corrosion inhibiters. Corrosion can also be minimized by proper material selection (Kumar V & Sharma, 2014:239). Materials must be kept in a passive state as a material in an active state has a higher corrosion rate (Kumar V & Sharma, 2014:240).

The toxicity of the HTF must also be considered. Glycols and alcohols are classified as moderately toxic. Systems using alcohols must be handled with care as it is flammable. Amongst the glycols, propylene glycol is seen as a safe alternative. The propylene glycol is an attractive option as HTF because of its anti-freeze, non-corrosive, heat transfer properties and relatively low cost (Kumar V & Sharma, 2014:240).

The concentration must be kept between *20%-65%*. Where concentration is too high it must be diluted with de-ionized water. Concentrations higher than *65%* will increase the load on the system. The HTF must also not be over-diluted for example; propylene glycol is over-diluted leads to corrosion and bio-fouling (Kumar V & Sharma, 2014:240).

2.5.2 Criteria for selection of HTF

Below are selection criteria as set out by (Kumar V & Sharma, 2014:240) for the use in CSP design. The criteria are as follows:

- High operating temperature;
- Stability at high temperature:
- Low material and transport cost:
- Non-corrosive:
- Safe to use:
- Low vapour pressure:
- Product life cycle:
- Low freezing point: and
- Low viscosity.

2.5.3 Heat transfer fluids used

Table 1 below contains HTFs mainly used in CSP.

Table 1: Heat transfer fluids mainly used in CSP (Kumar V & Sharma, 2014:240)

HTF	T_{max} (K)	C_p (KJ/kg.K)	ρ (kg/m^3)	K (W/m.K)	μ (mPa.s)
Xceltherm	580	3	672.36	0.113	0.252
Biphenyl	500	2.03	869	0.118	0.32
Phenyl-naphthalene	600	2.6	849	0.077	0.11
Dowtherm A	678	2.73	672.5	0.0771	0.12
Therminol 66	648	-	1011	0.09	0.29
Nitrate Salts	873	1.495	1899	-	3.26
Hitec	720	2.319	1992	-	6.37

*Source: NREL, ORNL for Heat Transfer Fluids

2.6 Storage materials

The heat in a thermal energy storage system is stored in a storage material. There are three main groups of storage materials, viz. solids, liquids and phase-change materials.

2.6.1 Solid storage materials

Solid thermal heat storage materials can be utilized in a wide temperature range, with some solids being able to handle temperatures up to 1000°*C*. Solids are often chemically inert and have a low vapour pressure. The vessel housing the material is often simpler and cheaper than that used for liquid storage mediums.

Solid storage materials can be classified as metals and non-metals. For lower temperatures rock and soil can be used in a ground storage system as it is cheap and abundant. For higher temperatures, rocks, such as granite, quartzite and basalt, as well as pebbles can be used (Tamme *et al.*, 2012:10553).

Typically, metals have a higher thermal conductivity but due to their higher cost metals are less attractive than non-metals. Metals' high thermal conductivity makes them ideal for fast charge and discharge systems.

Heat transfer in systems, using solid materials for TES, usually uses an additional fluid as a heat carrier (e.g., water, steam, oil, molten salt) for the charge and discharge process. The heat carrier fluid can be in direct contact with the solid or the heat transfer can be indirect. A direct contact design makes use of a packed bed of solid material in a container. This system

can also use a more defined arrangement such as a regular array of checker bricks. These beds provide a large heat transfer area with only small internal heat losses. Particle beds, however, have a few drawbacks including large pressure drops across the system as well as the large storage area normally associated with the use of solid materials. To compensate for the loss in pressure, compressors or pumps are used. As the solid storage material is in direct contact with the fluid heat carriers, the solids must be chosen carefully. This is done by taking into account the properties of the solids with regards to fluid flow, heat transfer, particle size and thermal cycling.

Indirect contact systems are used in situations where direct contact is not economical or feasible. This can be done if the heat carrier fluid is pressurized, or incompatible with the storage medium (Tamme *et al.*, 2012:10555).

2.6.2 Liquid storage materials

The most widely used liquid for thermal heat storage is water. Water has several advantages:

1. It is inexpensive;
2. It has a relatively high heat diffusivity and relatively low thermal diffusivity which is an advantage for thermal stratification in hot-water storage tanks;
3. Can easily be stored in a range of containers;
4. Control of water flow can be done very accurately;
5. Water can be used directly used without heat exchangers; and
6. Is easily mixable with additives.

The major disadvantage of using water is:

1. It has a limited operation range (0°*C*-100°*C*);
2. It is corrosive; and
3. It has a high vapour pressure.

The water vapour pressure can be reduced when a mixture of chemicals is applied (Tamme *et al.*, 2012:10555).

Molten salts instead of water are usually used in applications with a temperature higher than 100°*C* (Tamme *et al.*, 2012:10556). The advantages of using molten salt are the low cost, low vapour pressure and thermal stability. Because of the low vapour pressure low pressure vessels can be used. Many salts can also be used in air without significant degradation.

Further liquid storage materials are available. These include a range of natural as well as synthetic oils (Tamme *et al.*, 2012:10557).

2.6.3 Phase change storage material

As mentioned, Phase Change Material (PCMs) are used for latent thermal heat storage. The thermal energy is transferred when the material changes from solid to liquid, or liquid to solid. Initially, PCMs perform the same as conventional storage materials; their temperature rises as they absorb heat. But then unlike sensible thermal heat storage materials PCMs will absorb and release heat at a nearly constant temperature. Some studies have shown that PCMs can store 5-14 times more heat per unit volume than sensible thermal heat storage materials like water, masonry, or rock (Sharma *et al.*, 2009:321).

PCM can be classified as shown Figure 5.

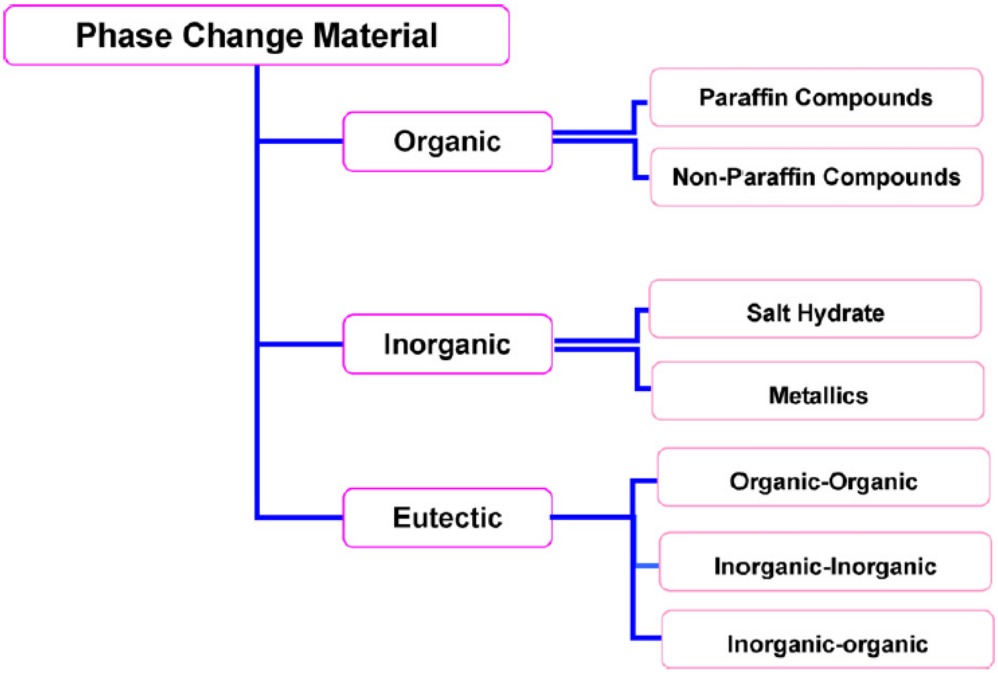

Figure 5: Classification of PCMs (Sharma *et al.*, 2009:323)

2.6.3.1 Organic phase change materials

Organic phase change materials can be further divided into paraffin and non-paraffin. This group of PCMs include congruent melting which means they melt and freeze repeatedly without phase segregation and consequent degradation.

Paraffins

Paraffins consist of a mixture of strait chain *n*-alkanes $CH_3–(CH_2)–CH_3$. The crystallization of the (CH3)-chain releases a large amount of latent heat. Both the melting point and heat of fusion increase with chain length.

There are some favourable characteristics such as congruent melting and good nucleation properties. Where some undesirable characteristics are:

- low thermal conductivity;
- no compatibility with the plastic container; and
- moderately flammable (Sharma *et al.*, 2009:323).

Non-paraffin

This category has the most phase change materials with a wide range of properties. Each of the materials has its own properties unlike the paraffins which have very similar properties. Some of the features of these materials are:

- high heat of fusion;
- in flammability;
- low thermal conductivity;
- low flash points;
- varying level of toxicity; and
- instability at high temperatures (Sharma *et al.*, 2009:324).

2.6.3.2 Inorganic phase change materials

Inorganic phase change materials can be further classified as salt hydrates or metallic substances. These materials do not super-cool appreciably and their heat of fusion does not degrade with thermal cycling.

Salt hydrates

These materials may be regarded as inorganic salts or alloys. They typically form water-form crystalline solids of general formula AB $n$$H_2O$. The solid-liquid transformation is actually the dehydration of hydration of the salts although thermodynamically it is seen as melting and freezing. Salt hydrates normally melt to either a salt hydrate with fewer moles or to its anhydrous form.

According to Shame *et al.* the most attractive properties of salt hydrates are:

- high latent heat of fusion per unit volume;
- relatively high thermal conductivity (almost double of the paraffins); and
- small volume changes on melting (Sharma *et al.*, 2009:325).

Metallic

This category consists of low melting metals and metal eutectics. Metals have not been serious contenders for use as PCMs because of the weight penalties, but because of their high heat of fusion per volume they become more attractive in constricted areas.
Some of the features of these materials are:

- low heat of fusion per unit weight;
- high heat of fusion per unit volume;
- high thermal conductivity;
- low specific heat; and
- relatively low vapour pressure (Sharma *et al.*, 2009:326).

2.6.3.3 Eutectic

A eutectic is a minimum melting point composition of two or more components, each melting and freezing congruently to form a mixture of the components during crystallization. These materials nearly always melt and freeze without segregation (Sharma *et al.*, 2009:326).

2.7 Energy storage

Energy storage is employed in solar thermal energy systems to store the excess energy produced during times of high solar availability for use in times of lower solar availability. There is a wide variety of storage systems that can be used. However, practical design considerations (e.g., operating experience) tend to limit the number of sub-systems that can be used (Stine & Geyer, 2001). In this section, different storage systems will be examined.

2.7.1 Sensible thermal heat storage

Sensible thermal heat storage is seen as the simplest form of storing thermal energy. In the simplest configuration, the cold fluid to be heated is contained in an insulated tank, it is then heated by a hot fluid from the field of solar collectors as illustrated in Figure 6 (Stine & Geyer, 2001).

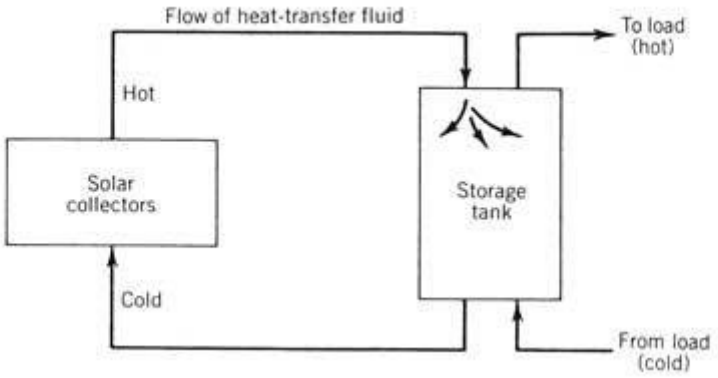

Figure 6: Single-tank sensible-thermal heat storage (Stine & Geyer, 2001)

In most industrial applications, the fluid in the storage tank and collectors is the same. Thus, no heat exchanger is shown in sensible thermal heat storage (Stine & Geyer, 2001).

The problem with the single tank storage system is that the storage fluid reaches an average temperature between the starting storage temperature and collector temperature. In storage systems, and the designer is interested in the quality of the energy. When the amount of energy delivered by the collector is insufficient to heat the all the storage fluid to that of the collector fluid, a significant loss in energy quality is to be expected (Stine & Geyer, 2001).

Energy quality is imperative in the design of high-temperature thermal heat storage systems, otherwise there would be no need to use high-temperature solar collectors that will decrease the collectors' efficiency. A multi-stage storage as illustrated in Figure 7 is used to avoid this. (Stine & Geyer, 2001).

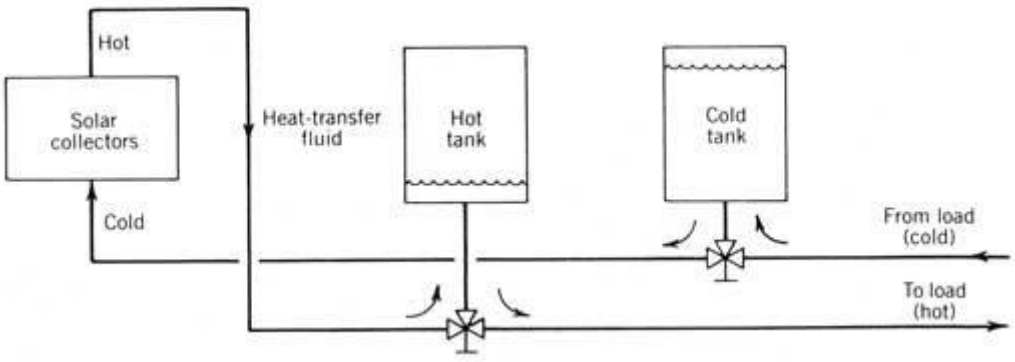

Figure 7: Multi-tank sensible thermal heat storage (Stine & Geyer, 2001)

Solar heat pump thermal heat storage.

2.7.1.1 Multi-tank storage

The logic that drives one to use more tanks is the fact that, as the number of tanks increases, the tank volume decreases. In a two-tank system, as in Figure 7: Multi-tank sensible thermal heat storage, each tank must be able to hold all the fluid in the system. Thus, the tankage volume must be twice that of the fluid volume. If three tanks of equal volume are used, any two of the three tanks must be able to hold all the fluid in order to separate the cold and hot fluid. A basic three-tank system is outlined in Figure 8 (Stine & Geyer, 2001:no pagination).

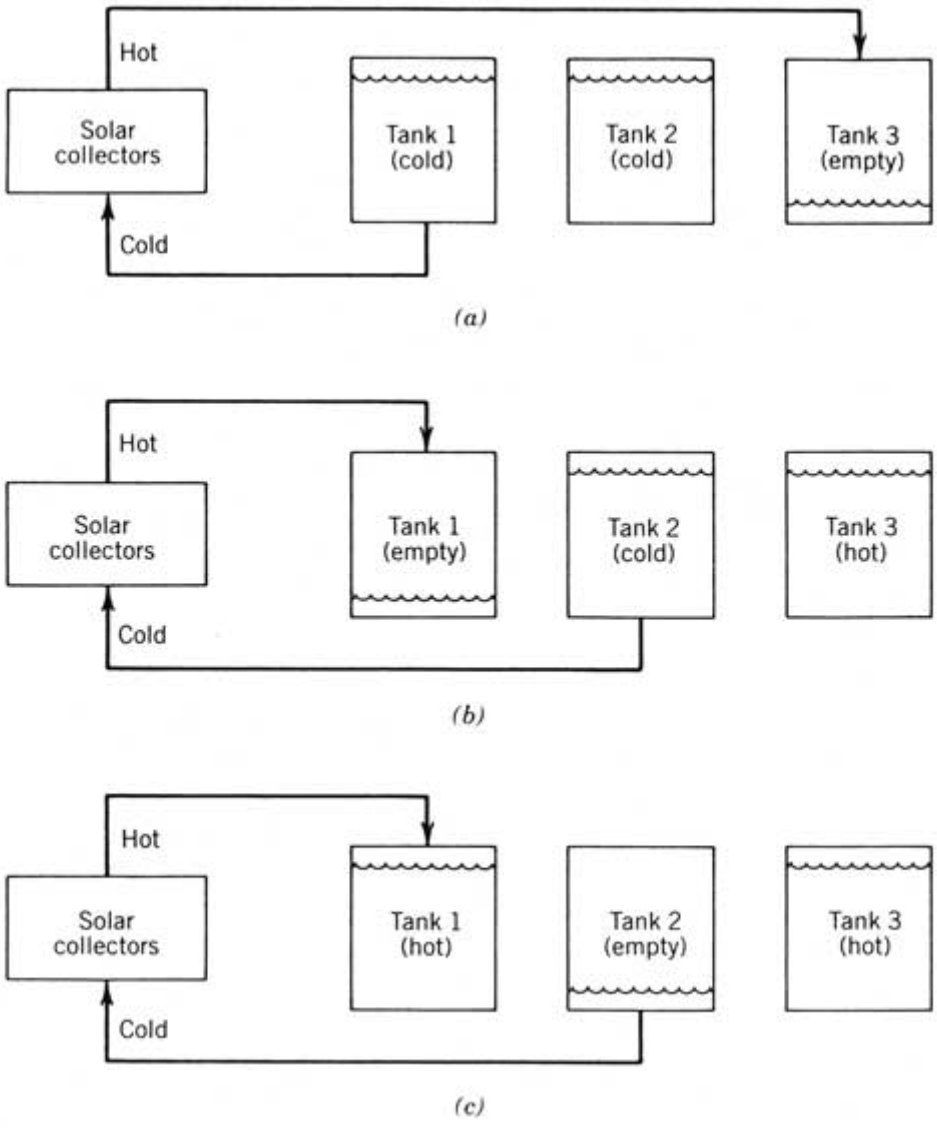

Figure 8: Three-tank sensible-thermal heat storage: (a) start up; (b) midday; (c) end of day (Stine & Geyer, 2001: no pagination)

If the volume of the tanks were the only cost parameter when designing one could reason that the more tanks in the system, the better. But as the number of tanks increases the complexity

of the controls increases as well as the complexity of the pluming that connects the tanks. Larger tanks also lose less heat per volume of hot fluid than small tanks (Stine & Geyer, 2001:no pagination).

2.7.1.2 Thermocline energy storage

The ultimate reduction in storage volume is achieved when the volume of the storage is precisely that of the fluid in the system. This is achieved in the thermocline storage system as the hot and cold fluid occupies the same tank (Stine & Geyer, 2001:no pagination).

At the start of the process the storage tank contains only cold water. As energy becomes available cold water is extracted from the bottom of the tank and heated. The hot storage fluid is then put back into the top of the storage tank. The hot fluid will float on top of the cold fluid as it is less dense creating what is known as a thermocline (Stine & Geyer, 2001:no pagination). A visual illustration of this phenomenon can be seen in Figure 9.

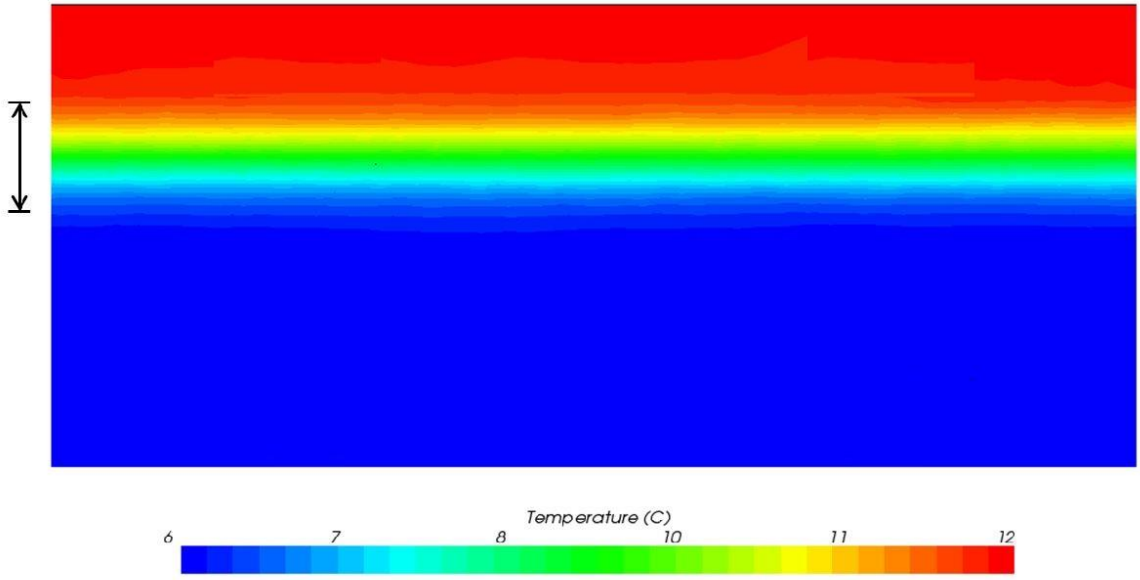

Temperature distribution in tank at arbitrary point in time. The thermocline is visualised by the transition between hot (red) and cold (blue) fluids.

Figure 9: Thermal stratification in a thermal tank (Anon, 2014a)

2.7.1.3 Mixed-media thermocline storage

If the volume of the tank is reduced sufficiently, the next step is to reduce the cost by investigating the storage fluid. Organic oils are normally used in high-temperature solar energy storage to avoid phase change. Although less expensive than high pressure plumbing, organic oils are not cheap. Mixed-media thermocline storage aims to reduce the volume of these oils

by replacing some of it with a cheaper alternative such as rock. One example of this storage method is shown in Figure 9 (Stine & Geyer, 2001: no pagination).

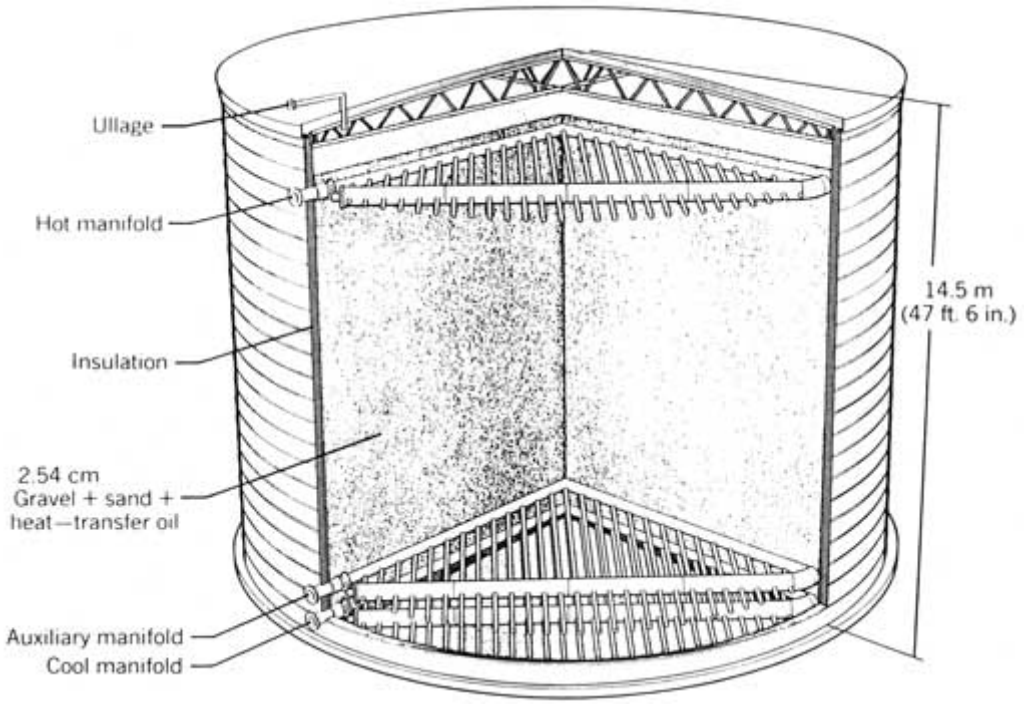

Figure 10: Mixed-media thermal heat storage unit, central receiver installation at Barstow, CA (Stine & Geyer, 2001: no pagination)

In a mixed-media unit the stability of the hot storage fluid in the presence of rock is very important. Of particular concern is the potential for the catalytic degradation of the fluid (Stine & Geyer, 2001: no pagination).

The strength of the tank with respect to thermal ratcheting must also be considered. As the tank and its contents heat up the internal volume increases. This in turn lets the solid media settle. When the tank then cools during the discharging phase, stress builds up at the bottom of the tank as the solid media is compressed. Thus, when designing the tank special consideration must be taken to avoid ruptures due to this phenomenon (Stine & Geyer, 2001:no pagination).

2.7.1.4 High-temperature sensible thermal heat storage

The ability to store high temperature thermal energy is mostly limited by the availability of heat transfer fluids. Above 400°C most organic oils tend to thermally decompose. For high temperature applications fluids, such as molten salts, liquid metals or air are typically used (Stine & Geyer, 2001: no pagination).

Solar heat pump thermal heat storage.

Basic problems for systems using molten salts and liquid metals are solidification at low temperature. Thus, auxiliary heat is needed in these systems. This can result in increased system complexity and thus cost (Stine & Geyer, 2001: no pagination).

High-temperature air systems normally use some sort of inert rock as storage material. Figure 11 illustrates a designed storage system that uses helium instead of air. The hot gas flows over the magnesium oxide bricks that store the heat. Helium is mostly used instead of air because of the poor heat-transfer characteristics of air (Stine & Geyer, 2001: no pagination).

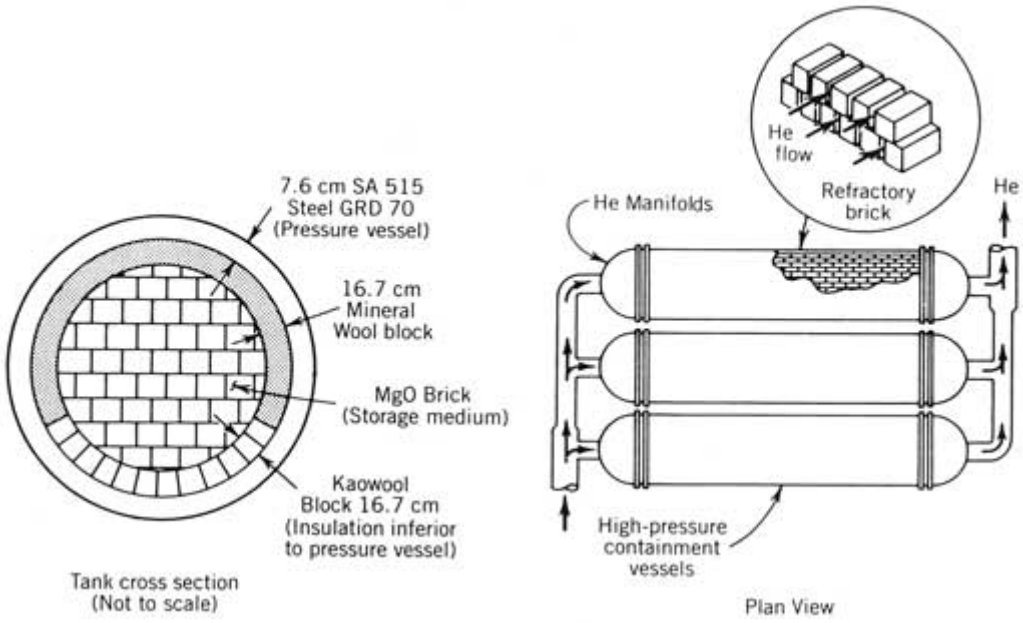

Figure 11: High-temperature sensible-thermal heat storage unit using helium as the HTF (Stine & Geyer, 2001: no pagination)

2.7.1.5 Pressurized fluids (steam or water)

The cost of most storage systems is strongly influenced by the cost of the storage fluid. The cost of organic oils can be quite high. The mixed-media storage system is one example of attempts to reduce the cost (Stine & Geyer, 2001:no pagination).

The use of water or steam is another way of cost saving. Although the fluid cost saving is significant, this is usually surpassed by the expense of the pressurized storage tanks (Stine & Geyer, 2001: no pagination).

2.7.2 Latent thermal heat storage systems

One limiting factor of sensible thermal heat storage is that the capacity of most materials to store sensible heat is relatively low. Latent heat energy storage can provide much higher

energy density storage. Because of the higher energy density of storage in latent heat systems the storage tank size as well as cost can be reduced (Stine & Geyer, 2001:no pagination).

A typical high temperature latent thermal heat storage system can be seen in

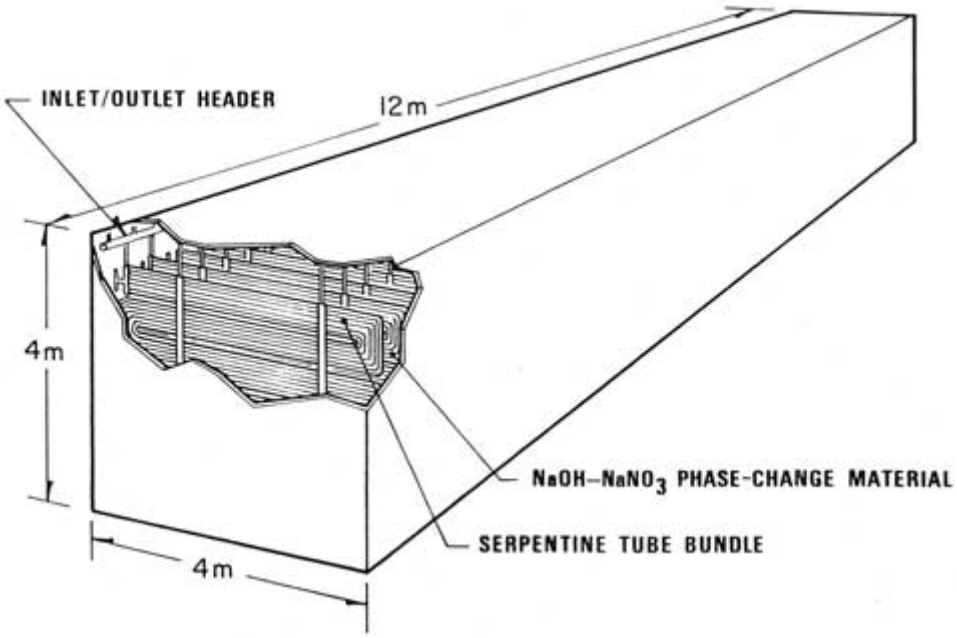

Figure 12: Latent-heat thermal energy storage module (Stine & Geyer, 2001: no pagination)

As the storage material transitions from a solid to a liquid and vice versa, the storage material cannot be pumped through the collector fields. This results in the need to incorporate a heat exchanger into the system. The heat exchanger must be carefully designed to accommodate the typical low thermal diffusivity of the solid material. These types of heat exchangers typically result in increased system costs compared to systems that use sensible heat (Stine & Geyer, 2001:no pagination).

Other characteristics that adversely affect design of latent thermal heat storage systems as listed by Grodzka in Stine and Geyer (2001) and include:

1. Cost of the more effective latent thermal heat storage materials are high;
2. Some of the materials are not pure materials but rather mixtures that tend to separate into their components on repeated freeze thaw cycling;
3. Some of the latent thermal heat storage materials such as NaOH can react violently if in contact with organic heat transfer oils that are normally used in solar collectors;
4. Supercooling of material can occur on solidification (Stine & Geyer, 2001: no pagination).

Solar heat pump thermal heat storage.

2.7.3 Thermochemical energy storage

Thermochemical energy storage is an energy storage system where thermal energy is used to rapture chemical bond in a reversible fashion. The rapture purpose requires a large amount of energy, thus resulting in energy storage. The products of a thermochemical reaction are normally non-reactive at ambient temperatures. However, at elevated temperatures the energy storage reaction reverses, forming the original chemical system with the release of heat (Stine & Geyer, 2001:no pagination).

An example of such a storage system is the dissociation of water. At temperatures in excess of 2000°C, water is desiccated into hydrogen and oxygen:

$$2H_2O + thermal\ energy = 2H_2 + O_2 \quad (5)$$

The reverse reaction,

$$2H_2 + O_2 = 2H_2O + thermal\ energy \quad (6)$$

will not proceed at low temperatures without a catalyst.

The reasons for the interest in thermochemical energy storage systems are:

1. Because the chemical reactions are so energetic, large quantities of energy can be stored in a small amount of material;
2. As the energy-releasing reaction seldom proceeds at room temperature, the energy can be stored indefinitely at room temperature without energy loss;
3. Because of the high-energy storage density and stability at low temperature the stored thermal energy can be transported (Stine & Geyer, 2001: no pagination).

2.8 Cost of storage

Sensible heat is the type of storage most often used for thermal heat storage (Stine & Geyer, 2001: no pagination). Thus, having a quick way of doing cost estimations before designing can be imperative. The following section will contain a brief discussion on the cost of sensible thermal heat storage.

As per Anonymous in Stine and Geyer (2001), Atomics International concluded that the cost (in 1976 dollars) of sensible thermal heat storage can be approximated by:

Solar heat pump thermal heat storage.

$$Storage\ cost = tank\ cost\ (\$) + oil\ cost\ (\$) \tag{7}$$

$$= 352 \times (vol, ft^3)^{0.515} + (oil\ cost, \$/ft^3) \times (vol, ft^3) \tag{8}$$

This relationship is felt to be valid for tanks in the range of $4.2\,m^3$ $(150\,ft^3)$ to $42\,000\,m^3$ $(150\,000\,ft^3)$. The capital cost must be corrected for inflation in order to use the equation with current oil prices (Stine & Geyer, 2001: no pagination).

The equation can also be used to estimate cost of mixed media storage. This is done by multiplying the tank volume by void fraction to obtain the oil volume in the tank. The equation is only suitable for preliminary mixed media storage as the cost of a reinforced tank to hold the rock may be large (Stine & Geyer, 2001:no pagination).

For oil costs of about $\$790\,m^3$ the cost of the oil begins to exceed the costs in the equation above at storage sizes near $14\,m^3$ $(250\,ft^3)$. Thus, in these cases the next equation can be used:

$$Storage\ cost = Oil\ cost \tag{9}$$

With some manipulation and the introduction of storage capacity the following equation can be derived:

$$Storage\ cost = (storage\ energy\ capacity) \times \left(\frac{oil\ cost\ per\ unit\ volume}{(oil\ density) \times (oil\ heat\ capacity) \times (storage\ \Delta T)}\right) \tag{10}$$

Using some nominal physical properties can help for early calculations. Many of the high temperature oil heat transfer fluids used in solar collectors have heat capacity in the range of $2.1 - 2.5\ kJ/kg°C$ and densities in the range of $780 - 900\ kg/m^3$ in the temperature range of $150 - 370\ °C$. Using nominal values of $2.3\ kJ/kg°C$ and $840\ kg/m^3$ for oil heat and capacity respectively, we can express the equation as:

$$\frac{Storage\ cost}{Energy\ stored} = 1.86.\ C_{oil}.\frac{V_{oil}}{\Delta T \eta_{stor}} \tag{11}$$

Where

$C_{oil} = cost\ of\ oil\ (\$/m^3)$

$V_{oil} = void\ fraction\ of\ oil\ (1\ for\ non-mixed\ media\ oil\ system)$

$\Delta T = collector\ field\ (storage)\ tempreture\ change\ (°C)$

$\eta_{stor} = efficiency\ of\ thermal\ storage\ system\ (Q_{out}/Q_{in})$

(Stine & Geyer, 2001: no pagination)

2.9 Summary

The most important points emenating from the literature study to be considered in the design of the thermal heat storage system are the following:

- From the literature it is clear that a good choice of energy stoare type is sensible thermal heat storage in solids. This is due to the fact that the other option namely latent thermal heat storage and thermocline thermal heat storage both can not accommodate different inlet and outlet tempretures. This will be investigated in the following chapters.
- Regarding phase change materials economy weight and size would be best, but they are ruled out due to the fact that different inlet and outlet tempretures will be used. Multiple tanks at close tempreture intervals will defeat the purpose of size and cost anywhy.
- The storage material to be used was norrowed down to being a solid. As this will give the simplets setup as well as being robust which is very important as the rig will be mobile.
- A single or multiple in line tank, sensible thermal heat storage system setup will be further scrutenized during the design stage.

3 Concept design

This chapter will concentrate on, the choice of the thermal heat storage material, storage material shape, calculation of the pressure drop over the system and the calculation the maximum distance between the supports on the system. This section will however not include the design calculations or the thermal heat storage capacity as of yet, this will be done more extensively in Chapter 4 and will be based on the thermal heat storage system capacity as mentioned in Section 1.1.

3.1 Qualitative design considerations

There are several design considerations to keep in mind during the design process. Mostly the requirements were given through by Prof C. Storm in order for the simplification of the integration process into the bigger refrigeration setup. Consideration must be given to the following aspects:

- Cost considerations;
- Ease of manufacturing;
- Robustness;
- To evaluate the sizing to comply with the mobile facility.; and
- Low maintenance.

3.2 Storage material

When considering the storage material to be used it is critical to keep the design considerations as set out in Section 3.1 in mind. When considering a liquid (as opposed to a solid) as a possible storage material there are some drawbacks in the specific application. The fact that systems will be mobile will give rise to several different obstacles that are not in play in a stationary system. When considering a fluid as storage medium it must be kept in mind that the fluid will tend to slosh about when the system is moved around, and this will inevitably lead to damage in the system especially if it is a large volume of fluid. However, a liquid will be used as a heat transfer fluid as mentioned in Section 1.1 and 1.2 on the upstream and downstream sides of the thermal heat storage system.

Next is the consideration of a system that uses a phase change material (PCM) as storage medium. Although PCM's are seen as one of the best types of storage materials available for thermal heat storage it is unsuited for this application. The fact that the generator in the aqua ammonia refrigeration cycle has to be run in a wide range of temperatures makes PCM's unsuited. With PCMs you are restricted to storing heat at very narrow ΔT. There are ways of increasing the range of temperature heat can be stored at in a system using a PCM. This

includes mixing of a few different PCM's with different phase change temperatures. This, however, increases the cost as well as the fact that the system must be increased in size dramatically (Kantole, 2012:85)

This leaves thermochemical storage systems as well as systems using solid materials. Due to the lack of literature and expertise available when it comes to the use of a thermochemical system a solid material shall be used and thus examined further.

3.2.1 Storage material selection

Emphasis will be placed on the use of a castable solid in the form of a ceramic. The material must be castable in order to have control over the material shape and in so doing maximize the efficiency of the thermal energy store (TES). Evidence exists that a structured bed of uniform pebbles will give rise to a reduction in the pressure drop through a TES system (Markgraaff, 2010:9).

Apart from the cost of materials key performance indicators for thermal heat storage design include the volumetric storage capacity $(kWh/m^3.K\ or\ J/m^3.K)$, the thermal conductivity $(W/m.K)$ and the maximum operation temperature capability. The effusivity off the thermal inertia $\left(\lambda\rho C_p\right)^{0.5}$ as a performance indicator is critical as it includes thermal conductivity *(λ),* which needs to be as high as possible in order to ensure effective heat transfer. Although these performance indicators are required for evaluation it is shown by Ashby (as per Markgraaff, 2010:10) that using the index $M = \lambda/a^{0.5}$, where a is the thermal diffusivity, more effectively maximizes the thermal heat storage capacity of a solid thermal heat storage material (Markgraaff, 2010:10). Using concrete as a lower limit for thermal conductivity and cost extended to the cost of graphite and silicone as the upper limit. Data in Table 2 are basic data by Ashby (as per Markgraaff, 2010:10) on candidate TES materials.

Table 2: Material properties of candidate TES materials (Markgraaff, 2010:10)

Material Generic	Density ρ $kg/m^3 \times 10^3$	Thermal Conductivity λ $W/m.K$	Specific Heat C_p J/kgK	Max Operating Temp T $°C$
Granite	2.59-2.66	2-4	800-900	400
Alumina	3.3-3.98	12-39	830-955	1800
Spinel	9.20-9.60	13-17	800-820	2000
SiC	2.20-2.70	31-39	660-670	1600
Concrete	2.20-2.60	0.8-1.0	1000-1182	560
Graphite	1.88-2.24	1.0-2.0	681-752	2690
Graphite	1.60-1.70	44-48	850-940	2690

The concrete with pozzolan binder presented in Table 3 is about 23 times less expensive than granite, with the concrete and granite having volumetric capacities of about 3000 and 2390 kJ/m^3K respectively (Markgraaff, 2010:10). A limiting factor in the use of these materials is their service temperature, their limited thermal conductivity as exemplified by the calculated effusivities and their expected susceptibility to thermal cycling (Markgraaff, 2010:11).

Table 3: Volume storage capacity and effusivities of candidate TES materials selected on the basis of the maximized material index (Markgraaff, 2010:10)

Material Generic	Storage Capacity (ρC_p) $Jm^{-3}K^{-1} \times 10^6$	Effusivity $(\rho\lambda C_p)^{0.5}$ $Jm^{-2}K^{-1}s^{-0.5} \times 10^3$	Index $M = \lambda/a^{0.5}$ $\frac{Ws^{-0.5}}{m^2}.K \times 10^3$	Relative Cost
Granite	2.39	3.09	1.55	1.0
Alumina	3.80	12.18	1.95	1.6
Spinel	7.87	11.57	2.80	1.6
SiC	1.80	8.40	1.35	10
Concrete	3.07	1.33	1.48	-23
Graphite	1.68	1.84	1.30	9.0
Graphite	1.59	8.76	1.26	9.0

Granite, alumina and spinel are shown to have high service temperatures, and with alumina sintered to a density of 95%, the service temperature can be increased to 1600°C. Furthermore, spinel exhibits a volume storage capacity of about three times that of granite or

concrete. The data presented in Table 3: Volume storage capacity and effusivities of candidate TES materials selected on the basis of the maximized material index, is that of a generic spinel. This refers to a magnesium spinel which contributes to the cost factor. Cr-and Fe-spinels are cheaper and refractories with these spinels can be produced to compete with the cost of granite. Spinels that include refractories have the added benefit of being castable (Markgraaff, 2010:11). Of the materials considered graphite and pyrolytic graphite cannot be used if the heat transfer fluid (HTF) is air (Markgraaff, 2010:12).

From Table 2 and 3 above granite emanated as the most common storage material in Republic of South Africa (RSA) (Markgraaff, 2010:12), but from the evaluation above it is clear that a spinel would be a better choice of thermal heat storage material for this system.

3.2.2 Storage material shape

A packed bed (any shape) storage system uses the heat capacity of a bed of loosely packed elements to store energy. A fluid is then circulated through the bed to add or remove energy. A variety of solids may be used, rock being the most widely used material (Duffie & Beckman, 2013:384).

The use of a packed beds has significant advantages. The fact that storage material is in the form of loose packed elements greatly increases available heat transfer areas in the system. Packed beds can also make use of non-uniform elements of similar size thus making cost of material preparation minimal. Moulded elements can be used in cases where more precise control of pressure drop and heat transfer across the bed is needed.

Singh *et al* (2013) concluded that the use of spherical elements with a lowest void fraction will result in the best thermo-hydraulic properties, while cubic elements with highest void fraction have the lowest friction factor and thus the least amount of pressure lost.

3.2.2.1 Void fraction (bed porosity)

The void fraction refers to the space in the packed bed left open after it has been filled by storage elements. The void fraction is dependent on the shape of the elements as well as the pattern of packing.

The void fraction can be defined as the ratio ε of the void volume V_f to the total volume V_o of a sample including both void and solid (Kenneth, 2010:16).

$$\varepsilon = \frac{V_f}{V_o} \tag{12}$$

If the value is 1 it implies an empty space; if it is 0 it refers to a solid. The simplest way of measuring porosity is by simply filling the packed bed with water. The porosity of the bed will vary in a randomly packed bed. The porosity of crushed rock is 0.44 and 0.45 (Kenneth, 2010:17).

Singh *et al* (2006 & 2013) did research on the Nusselt number and friction factor of beds with different shape elements. During the research, they also made observations on the void fractions of the different setups. During tests the smallest void fraction for spherical elements was found to be 0.275 with a rhombohedral packing (Singh *et al.*, 2013:23). The next closest packing was produced with taped packing (***ε=0.360)*** in which elements were filled by vigorously shaking the bed. When the bed is filled randomly a void faction of 0.410 was obtained. A cubical packed bed will result in a void fraction of 0.48 (Singh *et al.*, 2013:25).

3.3 Pressure drops

The classical equation used for the prediction of the pressure drop through a packed bed is the Ergun equation, which is based on the hydraulic radius method. This study will also use the representative unit cell (RUC) model, which is based on a numerical method instead of a semi-empirical basis used by Ergun (Kenneth, 2010:20).

Singh *et al* (2006) present a correlation for calculating the friction factor and pressure drop, determined experimentally, that is based on the sphericity *Ψ* of the storage elements.

3.3.1 The Ergun equation

Du Plessis and Woudberg (2008) as per Kenneth (Kenneth, 2010:21) give a simplified derivation of the Ergun equation. For a Newtonian fluid with laminar flow in the Darcy regime (where $Re_p \rightarrow 0$), the Blake-Kozeny equation gives an estimated pressure drop of:

$$-\frac{\Delta p}{L} = \frac{150(\varepsilon - 1)^2}{\varepsilon^3}\frac{\mu_f v_s}{D^2} \tag{13}$$

The Bruke-Plummer equation models the Forchheimer regime of flow to account for flow at higher Reynolds numbers:

$$-\frac{\Delta p}{L} = \frac{175(\varepsilon - 1)}{\varepsilon^3}\frac{\rho_f v_s^2}{D} \tag{14}$$

Ergun (1952) as per (Kenneth, 2010:21) combines the Darcy and Forchheimer flow equations by simple addition:

$$-\frac{\Delta p}{L} = \frac{150(\varepsilon - 1)^2}{\varepsilon^3}\frac{\mu_f v_s}{D^2} + \frac{175(\varepsilon - 1)}{\varepsilon^3}\frac{\rho_f v_s^2}{D} \tag{15}$$

The equation may also be written in terms of the friction factor (Bennet & Myers, 1962) as per Kenneth (Kenneth, 2010:21):

$$f_{er} = \frac{\Delta p}{L}\frac{D\varepsilon^3}{v_s^2 \rho_f (1 - \varepsilon)} \tag{16}$$

where f_{er} is the friction factor with the proposed relation of $f_{er}=1.75+1.50/Re_{er}$. Where Ergun defines the Reynolds number as per Kenneth (Kenneth, 2010:1):

$$Re_{er} = \frac{\rho_f v_s D}{\mu_f (1 - \varepsilon)} \tag{17}$$

3.3.2 The Representative Unit Cell model (RUC)

The RUC method takes into account the physics of the fluid flow in the porous space more carefully. It produces results that are similar to those of the Ergun equation in the region where the Ergun equation is normally accepted and used (Kenneth, 2010:22).

The RUC is defined by as per Kenneth (2010) as “the smallest rectangular control volume into which the average geometric property of the granular packed bed is embedded.” Figure 13 shows the control volume on which the method is based, where V_s is the solid volume, V_f is the fluid volume and V_o is the total volume. d represents the side length of a cubic RUC, and d_s represents the lengths dimension of a solid cube within the RUC (Kenneth, 2010:22).

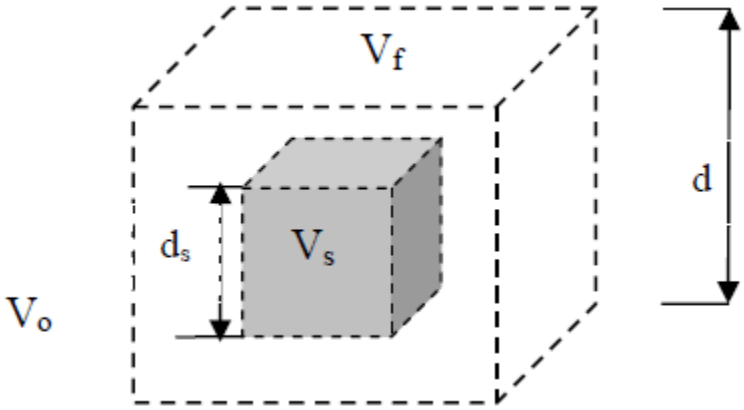

Figure 13: Diagram of RUC (Kenneth, 2010:22)

The relationship between the cell length and the solid cube length, for an isotropic medium, is given by:

$$d_s = (1-\varepsilon)^{\frac{1}{3}} d \tag{18}$$

The value of d_s is equal to the hydraulic diameter of the solid particle.
As per Kenneth (2010) use is made of the RUC to predict the pressure drop in the flow regime of $Re_p \approx 10000$.

Where Re_p is given as:

$$Re_p = \frac{\rho_f v_s D_s}{\mu_f} \tag{19}$$

with the superficial speed being defined as:

$$v_s = \frac{\dot{m}_f}{\rho_f A_{cs}}$$

Drag F can be defined as:

$$-\frac{\Delta p}{L} = \mu_f v_s F \tag{20}$$

where, in a randomly packed isotropic granular bed, F is given by:

$$Fd_s = \frac{25.4(1-\varepsilon)^{\frac{3}{4}}}{\left(1-(1-\varepsilon)^{\frac{1}{3}}\right)\left(1-(1-\varepsilon)^{\frac{2}{3}}\right)^2} + \frac{c_d(1-\varepsilon)}{2\varepsilon\left(1-\left(1-\varepsilon^{\frac{2}{3}}\right)\right)^2}\left(\frac{\rho_f v_s d_s}{\mu_f}\right) \quad (21)$$

(Kenneth, 2010:1)

Kenneth (2010) states that for two-dimensional flow over a cube drag coefficient c_d may be taken as 1.1. However, it has also been suggested that values of 2 or 1.9 can be more applicable to packed beds.

The RUC pressure drop equation in terms of particle Reynolds number is:

$$Fd_s = \frac{\mu_f v_s}{d_s^2}\left(\frac{25.4(1-\varepsilon)^{\frac{3}{4}}}{\left(1-(1-\varepsilon)^{\frac{1}{3}}\right)\left(1-(1-\varepsilon)^{\frac{2}{3}}\right)^2} + \frac{c_d(1-\varepsilon)}{2\varepsilon\left(1-\left(1-\varepsilon^{\frac{2}{3}}\right)\right)^2}\, Re_p\right) \quad (22)$$

The equation is applicable to calculate an isothermal pressure drop over a bed. If the HTF temperature shows a significant change over a packed bed, the average temperature is used (Kenneth, 2010:23).

3.3.3 Correlation of Singh *et al*.

Singh *et al.* (2006) and Singh *et al.* (2013) developed a correlation for the Nusselt number and friction factor by taking into account the system parameters on them to maximize system stratification. The Nusselt number was maximised for $\Psi=1$ and at a minimum at void fraction $\varepsilon=0.275$ whereas the friction factor is found to be a minimum for cubical elements $\Psi=0.8$ and a maximum at $\varepsilon=0.48$. The stratification coefficient has been found to be a maximum for the minimum void fraction and element $\Psi=1$. The thermal efficiency of the collector is increased by stratification.

Chandra and Willits proposed a Reynolds number (*Re)* while Kulakowski and Schmidt's friction factor *(f)* as per (Singh *et al.*, 2013:27) is expressed as:

$$Re = \frac{GD_c}{\mu_a} \quad (23)$$

$$f = \frac{\Delta P_b \rho_a D_c}{LG^2} \quad (24)$$

where *G* is mass velocity (mass flow rate of air/bed cross-sectional area).

A correlation for the friction factor that can be seen as reasonably accurate is given by:

$$f = 374.765(Re)^{-0.6482}(\varepsilon)^{-0.7878}(\Psi)^{2.5246} \times \exp[(9.7487(ln\Psi)^2] \quad (25)$$

Where Singh *et al*. (2006) used another range of parameters as given in Table 4 set the friction factor correlation as:

$$f = 4.466(Re)^{-0.2}(\Psi)^{0.696}(\varepsilon)^{-2.945} \times \exp[(11.85(ln\Psi)^2] \quad (26)$$

Table 4: Range of parameters of the investigations of Singh *et al* (2006) and Singh *et al* (2013) (Singh *et al.*, 2013:27)

Sr. no.	Parameter	Singh *et al*. (2013)	Singh *et al* (2006)
1.	Aspect ratio (bed size to element size ratio)	10	3.2-4.8
2.	Sphericity *(Ψ)* and voidage *(ε)*	0.65 (0.275, 0.36, 0.42, 0.48) 0.71 (0.275, 0.36, 0.42, 0.48) 0.75 (0.275, 0.36, 0.42, 0.48) 0.80 (0.275, 0.36, 0.42, 0.48) 1.00 (0.275, 0.36, 0.42, 0.48)	0.56 (0.40) 0.63 (0.40) 0.72 (0.306, 0.40, 0.45, 0.54, 0.63) 0.80 (0.40) 1.00 (0.40)
3.	Mass velocity	0.155-0.266 kg/s.m^2	0.155-0.266 kg/s.m^2
4.	Corresponding Reynolds number	503-866	1257-2157 for *Ψ=0.55* 1047-1797 for *Ψ=0.63* 1257-2157 for *Ψ=0.72* 1558-2674 for *Ψ=0.80* 1139-1955 for *Ψ=1.00*

3.3.4 Engineering Equation Solver (EES) method

Engineering Equation Solver (EES) is a programme widely used by NWU as well as in the wider engineering industry. EES has a built-in function for calculating a range of variables that are instrumental in the design of a packed bed system.

The function is the Call Packed Sphere function, the function as used in EES can be seen below:

PackedSpheres (Fluid$, m_dot, d, A_fr, L, T, P: f, h, NTU)

The function returns the friction factor (f), heat transfer coefficient (h) and the number of transfer units for a well-packed matrix of spheres.

The function calculates the fluid properties at the stated pressure and temperature, and the Reynolds number for the sphere diameter. The EES function is built on a hydraulic Reynolds number.

The pressure can be determined using the following equation:

$$\frac{\Delta P}{P_1} = \frac{G^2}{2g_c}\frac{v_1}{P_1}\left[(1+p^2)\left(\frac{v_2}{v_1}-1\right)+f\frac{A}{A_c}\frac{v_m}{v_1}\right] \quad (27)$$

3.3.5 Pressure loss across a single-tank mixed thermocline storage unit

The pressure drops over a thermocline unit was calculated as follows by Chandra and Willet.

$$\Delta P = \frac{LG}{\rho_f D_c}\varepsilon^{-2.6}[1.7+\frac{185}{Re}] \quad (28)$$

Where *Re* can be expressed by

$$Re = \frac{GD_s}{\mu_f} \quad (29)$$

And *G* as

$$G = \frac{4\dot{m}}{\pi D_c^2} \quad (30)$$

(Tesfay & Venkatesan, 2013:360)

3.4 Heat transfer

3.4.1 The effectiveness Number of Transfer Units (NTU) method of Hughes

The NTU method of Hughes is a numerical approximation related to the Schumann model. The bed is divided into segments *Δx* along the flow direction. The temperature is assumed to be uniform across each bed segment. If the HTF temperature is assumed to have an exponential profile, then the HTF temperature may be found from the effectiveness-NTU equation.

The fluid equation is given by (Kenneth, 2010:38):

$$T_{f,i+1} = T_{f,i} - \left(T_{f,i} - T_{s,i}\right)\left(1 - e^{-NTU\left(\frac{\Delta x}{L}\right)}\right) \tag{31}$$

where *i* represents the segment, number being considered. Since the NTU applies to the whole bed, it is scaled by *Δx/L*, to give a NTU number that applies to a single segment.

An energy balance for the solid elements can be written in equation form as (Kenneth, 2010:38):

$$m_{s_{seg}} c_s \left(\frac{dT_s}{dt}\right) = \dot{Q} = \dot{m}_f c_{pf}\left(T_{f,i} - T_{s,i}\right)\left(1 - e^{-NTU\left(\frac{\Delta x}{L}\right)}\right) \tag{32}$$

where $m_{s\ seg}$ is the mass of the elements in bed segment *Δx.* Rearrangement of the above equations gives (Kenneth, 2010:38):

$$\left(\frac{dT_s}{dt}\right) = \frac{L}{\Delta x}\frac{\dot{m}_f c_{pf}}{m_s c_s}\left(T_{f,i} - T_{s,i}\right)\left(1 - e^{-NTU\left(\frac{\Delta x}{L}\right)}\right) \tag{33}$$

since $m_{s\ seg}$ is mass of a single segment it can be expressed in terms of total bed mass as (Kenneth, 2010:38):

$$m_{s_{seg}} = m_s \Delta x / L \tag{34}$$

3.5 Housing

Since the internal pressure that the housing will experience in the test setup and the actually rig (see Section 6.4) is relatively low and due to cost restrictions, a suitable length of scrap pipe was obtained. This mild steel pipe has a 2 *mm* wall thickness and a diameter of 330 *mm*. This also complied to the available space in the mobile rig (for the test rig see Section 4.2). The pipe will be fitted with flanges on both ends onto which the endplates can be bolted. It is planned that this pipe will be mounted to the trailer using steel struts spaced evenly along the length of the system. These struts will be designed by the team installing the system onto the trailer.

The housing will be covered in insulation to keep the heat loss in the system to a minimum, where after it will be covered with a cladding material to protect the insulation. As mentioned, no in-depth heat transfer calculations are intended for this heat loss. Any heat loss will thus be incorporated in the storage of the elements during testing. The flow and the temperature difference will thus be a nett thermal heat storage (storage minus losses).

3.5.1 Span between pipe supports

Cross-country pipelines are supported throughout their lengths by supports commonly placed at regular intervals (Vakharia & Farooq A, 2009:46). Although the storage system is not a pipeline the same method for calculating maximum span between two supports can be used. This is due to the fact that high pressure pipeline design is done with great attention to safety thus making it ideal in the development of a safe support structure for the thermal store. The method of calculation to be used was developed by Vakharia and Farooq (2009) and is an alternative to the standard ASME code.

The maximising of the distance between supports will minimize the number of supports needed on a pipe, and thus reduce the total cost of the pipeline. Supports for pipelines must be spaced with respect to the following three considerations:

a. Ability to place the support at some design required location;
b. Keeping sag in pipe section in limits to permit good drainage; and
c. Avoiding excessive bending stresses due to concentrated and uniform stresses between supports (Vakharia & Farooq A, 2009:46).

The formulae for the calculation of the bending stress and deflections are derived from the well-known beam formula:

Maximum bending stress (Vakharia & Farooq A, 2009:47):

$$S_b = \frac{(0.0624wL^2 + 0.1248w_cL)D}{I} \quad (35)$$

In *N/m²*

Maximum deflection (Vakharia & Farooq A, 2009:47):

$$y = \frac{5wL^4 + 8w_cL^3}{384EI} \quad (36)$$

In *m*

Where, *w* = uniformly distributed weight of pipeline in *N/m*

w_c = concentrated weight on pipeline in *N*

L = Span length in *m*

D = Outside diameter of pipe in *m*

d = Inside diameter of pipe in *m*

E = Modulus of elasticity of pipe in *N/m²*

I = Moment of Inertia of pipe in *m⁴*

The maximum bending stress in a pipe is taken as 30% of the maximum allowable stress.

Calculation of total weight (Vakharia & Farooq A, 2009:47):

$$Total\ weight = weight\ of\ pipe\ (wp) + weight\ of\ fluid\ (wf) \quad (37)$$

Weight of pipe:

Thickness of pipe can be calculated as (Vakharia & Farooq A, 2009:47):

$$t = \frac{PxD}{2(S_aE + PY)} \quad (38)$$

Where, *P* = Pressure of the fluid in pipe in N/m²

S_a = Allowable stress in pipe in N/m²

E = Quality Factor from ASME B 31.3

Y = Coefficient of material from ASME B 31.3

This is used to calculate the required thickness of the pipe to comply with the ASME code for a certain pressure. Otherwise where pipe thickness is known it can be used instead. From

the calculated thickness a suitable schedule of pipe can be selected thus giving the pipes inside diameter.

Annular cross section of pipe (Vakharia & Farooq A, 2009:47):

$$Annular\ cross\ section = \frac{\pi}{4}(D^2 - d^2) \tag{39}$$

Hence the unit weight of the pipe (Vakharia & Farooq A, 2009:47):

$$wp = Annular\ cross\ section \times density\ of\ pipe\ material \tag{40}$$

Unit weight of fluid (Vakharia & Farooq A, 2009:47):

$$wf = \frac{\pi}{4} d^2 \times density\ of\ fluid\ (N/m) \tag{41}$$

The pipe thickness is calculated (or given) first. Then the moment of inertia and total weight of pipe are calculated. All the variables are inserted into the maximum bending stress formula to calculate maximum span between supports. To verify results, it is stated that the maximum deflection of pipe may not exceed *L*/600 (Vakharia & Farooq A, 2009:47).

4 Detailed design and manufacturing

The design of the experimental setup will focus on fluid process aspects for thermal heat storage and not the mechanical strength and durability of the components.

The test rig will be an open system and use water as the HTF as mentioned in Section 1.2 where the final product will be using a water glycol mixture as the HTF.

4.1 Detailed design calculations

The detailed design calculations are based on the full-scale system with the variables taken to be that as found in the literature study. Thus, it might not be a real reflection of the reality.

4.1.1 Storage material cost calculation

Energy

These energy calculations where performed by the using Engineering Equation Solver (EES) software program. The equations below are exactly the “formatted” equations as per the abovementioned EES program. All parameters, input values and results are explained in the three tables below respectively.

Amount of energy captured by the CSP in one day.

$$Q_{in_{6hours}} = Q_{in} \times 6 \tag{42}$$

Number of hours the pump can run with energy captured by the CSP in one day. This includes the loss in the storage system.

$$Q_{pump_{1hour}} = Q_{PumpDesigned} \times \left(1 + \frac{100 - Eff}{100}\right) \tag{43}$$

$$HoursPumpCanRun = \frac{Q_{in_{6hours}}}{Q_{pump_{1hour}}} \tag{44}$$

Amount of energy that can be stored in one day.

$$Q_{ToBeStored} = Q_{in_{6hours}} - Q_{pump_{1hour}} \times 6 \tag{45}$$

Size

Solar heat pump thermal heat storage.

Size of storage system needed to run the pump for a 24-hour period.

$$Q_{pump_{24hours}} = Q_{pump_{1hour}} \times 24 \tag{46}$$

$$m_{STM} = \frac{Q_{pump_{24hours}} \times 3600}{cp_{STM} \times (T_{max} - T_{min})} \tag{47}$$

$$V_{STM} = \frac{m_{STM}}{\rho_{STM}} \tag{48}$$

$$V_{cube} = d^3 \tag{49}$$

$$m_{cube} = V_{cube} \times \rho_{STM} \tag{50}$$

$$NumberOfCubes = \frac{m_{STM}}{m_{cube}} \tag{51}$$

Price

Price of storage material.

$$PriceOfCubes = NumberOfCubes \times CubePrice \tag{52}$$

$$TotalPrice = PriceOfCubes + MouldPrice + HousingPrice \tag{53}$$

Table 5: Parameters for storage material cost calculation equations for detailed design

Symbol	Unit	Description
$Q_{in6Hours}$	[W]	Amount of energy that is received from the CSP in 6 hours.
$Q_{pump1hour}$	[W]	The size of the bubble pump in the cycle.
HoursPumpCanRun	[h]	The number of hours the bubble pump can run using a single day's sun energy.
$Q_{ToBeStored}$	[J]	Energy to be stored in system from using one day's charge.
$Q_{pump24hours}$	[J]	Amount of energy bubble pump uses in a 24-hour period.
m_{STM}	[kg]	Mass of storage material needed storage system.
V_{STM}	[m^3]	Volume of storage material.
V_{cube}	[m^3]	Volume of storage material elements.
m_{cube}	[kg]	Mass of storage material elements.
NumberOfCubes	[-]	Number of storage material elements needed for adequate energy storage.
PriceOfCubes	[R]	Total price of elements needed for adequate energy storage.
TotalPrice	[R]	Total price of energy storage system.

Table 6: Inputs for storage material cost calculation equations for detailed design

Symbol	Magnitude and unit	Description
Q_{in}	4804 [W.h]	Energy delivered by CSP on a clear day in March (CSP designers).
$Q_{PumpDesigned}$	900 [W.h]	Energy consumed by bubble pump (cycle designers).
T_{max}	140 [°C]	Maximum temperature in system (CSP designers).
T_{min}	100 [°C]	Minimum temperature in system (CSP designers).
cp_{STM}	820 [J/kg.K]	Specific heat of the storage material (Burg Refractories).
ρ_{STM}	9600 [kg/m^3]	Density of storage material(Section 3.2.1).
d_c	0.05 [m]	Side length of storage material cube (Burg Refractories).
CubePrice	14.26 [R]	Price of an individual cube (Burg Refractories).
MouldPrice	1800 [R]	Price of cube mould (Burg Refractories).
Housing	10000 [R]	Estimated price for manufacturing of storage system housing (estimated value).
Eff	82.5 [%]	Estimated effectivity of storage system (Kantole, 2012:75).

Table 7: Results for storage material cost calculation equations for detailed design

Symbol	Unit	Magnitude
$Q_{in6hours}$	[W]	28824
$Q_{pump1hourwatt}$	[W]	1058
$Q_{ToBeStored}$	[W]	27767
V_{STM}	[m^3]	0.2902
m_{STM}	[kg]	2786
V_{cube}	[m^3]	0.000125
m_{cube}	[kg]	1.2
PriceOfCubes	[R]	33102
HoursPumpCanRun	[h]	27.26
NumberOfCubes	[-]	2321

The most important design elements calculated in this section is the mass of storage material that will be needed (2786 *kg*). the number individual elements this equates to (2610) and the total volume of all these elements (0.2902 m^3). It can also be seen how long the pump can run solely for the thermal heat store (27.26 h). The mass of storage material needed is quite high. It is thus necessary to find a balance between price, mass and heat storage capacity.

4.1.2 Storage material housing size

After the number of storage material elements is calculated in Section 4.1.1 the size of the storage system housing can be calculated.

Firstly, cross sectional area of the pipe used for the storage system housing is calculated as follows:

$$A_p = \pi \times (d - (t_{wall} \times 2)) \tag{54}$$

Thereafter calculating the volume, the storage material is going to take up.

$$V_{STM} = d_c^3 \times n \times (1 + \epsilon) \tag{55}$$

Finally, the length of pipe needed for the body of the storage system can be calculated. It is important to note that this pipe can be made in more than one section if the pipe is deemed too long to handle.

$$L_p = \frac{V_{STM}}{A_p + h \times 2} \tag{56}$$

Table 8: Parameters for storage material housing size for detailed design

Symbol	Unit	Description
V_{STM}	[m^3]	Storage material volume (section 4.1.1).
A_p	[m^2]	Cross sectional area of pipe.
L_p	[m]	Length of storage system body.

Table 9: Inputs for storage material housing size for detailed design

Symbol	Magnitude and unit	Description
d	0.327 [m]	Outside diameter of pipe.
n	2321 [-]	Number of cubes needed in storage system (section 4.1.1).
d_c	0.05 [m]	STM cube side length (Burg Refractories).
epsilon	0.275 [-]	Void fraction (section 3.2.2).
t_{wall}	0.002 [m]	Pipe wall thickness (measured value).
h	0.1 [m]	Plenum size (measured value).

Table 10: Results for storage material housing size for detailed design

Symbol	Unit	Magnitude
A_p	[m^2]	0.08197
L_p	[m]	4.533

The system will be housed in a standard size steel pipe. The inside diameter of this pipe is 323 *mm* and it has a wall thickness of 2 *mm*. This section calculates the total length needed of this pipe for the storage system (4.533 *m*). The suitability of the pipe is calculated in Section 4.1.3.

4.1.3 Calculation of the maximum span between supports

The maximum bending stress is taken at 30 % of the allowable stress.

$$S_b = S_a \times 30\% \tag{57}$$

Calculation of the various pipe dimensions

$$D_{pipe_I} = D_{pipe_O} - 2 \times (t_c + C_a) \tag{58}$$

$$r_{pipe_O} = \frac{D_{pipe_O}}{2} \tag{59}$$

$$r_{pipe_I} = \frac{D_{pipe_I}}{2} \tag{60}$$

Mass of empty pipe per unit length

When calculating the mass of the empty pipe the fittings and water boxes are not included.

$$m_{pipe_E} = \frac{\rho_{pipe} \times \pi \times \left(D_{pipe_O}^2 - D_{pipe_I}^2\right)}{4} \tag{61}$$

Mass of heat transfer fluid in pipe per unit length

When calculating the mass of the HTF the fact that the HTF can only occupy the void space left by the STM is taken into account.

$$m_{HTF} = \frac{\rho_{HTF} \times \pi \times D_{pipe_I}^2}{4} \times \epsilon \tag{62}$$

Mass of storage material in pipe per unit length

The mass of the STM is estimated by simplifying its form to be that of the inside of the pipe but taking into account the void fraction of the packing configuration to be used.

$$m_{STM} = \frac{\rho_{STM} \times \pi \times D_{pipe_I}^2}{4} \times (1 - \epsilon) \tag{63}$$

Total mass of pipe per unit length

By adding the pipe, HTF fluid and STM mass the total pipe mass when it is full (in use).

$$m_{pipe_F} = m_{pipe_E} + m_{HTF} + m_{STM} \tag{64}$$

Weight of full pipe per unit length

The unit weight of the full pipe is calculated to be used in further calculations.

$$w_{pipe_F} = m_{pipe_F} \times 9.81 \tag{65}$$

Moment of inertia

The moment of inertia for the pipe is calculated for two pipe choices. The subscript c indicates that it is the pipe that will be used in the building, where the other is the pipe with wall thickness as calculated using inside pressure as the only force acting on pipe as per ASME code.

$$I = \frac{\pi(D_{pipe_O}^4 - D_{pipe_I}^4)}{64} \tag{66}$$

Maximum bending stress

When calculating, the maximum bending stress the same subscript convention is used.

$$S_b = \frac{\left(0.0624 \times w_{pipe_F} \times L^2 + 0.1248 \times w_{con} \times L\right) \times D_{pipe_O}}{I} \tag{67}$$

Maximum deflection

$$y = \frac{5 \times w_{pipe_F} \times L^4 + 8 \times w_{con} \times L^3}{384 \times E \times I} \tag{68}$$

Thickness of pipe due to inside pressure

The thickness of the pipe is calculated using only the internal pressure as the only force acting upon the pipe. The calculation method is as set out by ASME B31.3.

$$t = \frac{P_{pipe_I} \times D_{pipe_O}}{2 \times \left(S_a \times E_{Constant} \times P_{pipe_I} \times Y_{Constant}\right)} \tag{69}$$

Maximum deflection cannot exceed

To test whether the maximum deflection is within code the following allowable maximum deflections are calculated. Thus, the maximum deflection in the setup must be less than that given by the formulae below to be acceptable.

$$y_a = L/600 \tag{70}$$

Table 11: Parameters for calculation of the maximum span between supports equations for detailed design

Symbol	Unit	Description
L	[m]	Maximum allowable length between supports.
I	[m^4]	Moment of Inertia.
S_b	[kPa]	Maximum bending stress in pipe.
D_{pipeI}	[m]	Inside diameter of pipe.
m_{pipeE}	[kg]	Mass of empty pipe.
m_{pipeF}	[kg]	Mass of filled pipe.
m_{STM}	[kg]	Mass of storage material in pipe.
m_{HTF}	[kg]	Mass of heat transfer fluid in pipe.
w_{pipeF}	[N]	Weight of filled pipe
r_{pipeI}	[m]	Inside radius of pipe.
r_{pipeO}	[m]	Outside radius of pipe.
w_{con}	[N]	Weight of concentrated masses on pipeline ex flanges.
t	[m]	Wall thickness
y_a	[m]	Deflection
Maximum bending stress can be taken as 30% of allowable stress		

Table 12: Inputs for calculation of the maximum span between supports equations for detailed design

Symbol	Magnitude and unit	Description
ρ_{STM}	9600 [kg/m^3]	Density of storage material.
ρ_{HTF}	1000 [kg/m^3]	Density of heat transfer fluid.
ρ_{pipe}	7850 [kg/m^3]	Density of pipe material.
ε	0.275 [-]	Void fraction of packing configuration (section 3.2.2).
S_a	115.1e3 [kPa]	Allowable stress in pipe.
$E_{Constant}$	0.7 [-]	Quality factor from ASME B31.3 Table A-1A or A-1B.
$Y_{constant}$	0.4 [-]	Coefficient of material from ASME B31.3.
w_{con}	0 [N]	Concentrated weight on pipeline.
C_a	0 [m]	Corrosion allowance.
E	195122e3 [kPa]	Modulus of elasticity of pipe.
t_c	0.002 [m]	Pipe wall thickness (measured value).
D_{pipeO}	0.327 [m]	Outside diameter of pipe (measured value).
P_{pipeI}	101 [kPa]	Pressure inside storage system.

Table 13: Results for calculation of the maximum span between supports equations for detailed design

Symbol	Unit	Magnitude
t	[m]	0.0000002050
L	[m]	2.765
y_a	[m]	0.004609
y	[m]	0.0008635

This section calculates the maximum space between the support struts (2.765 *m*).

4.1.4 Pressure drop calculations

When calculating, the pressure drop over the system all the different methods of calculations were combined into one programme. It was also taken into account that different equations only apply in different Re number bands. The different pressure drop results will be compared to the pressure drop in the experiment as explained in Chapter 5.

Cross-sectional area of test section perpendicular to flow direction

$$A_{cs} = \pi \left(\frac{D_{pipe_I}}{2}\right)^2 \tag{71}$$

Total surface area of solid particles in bed/RUC volume

$$A_s = 4\pi \left(\frac{D_{h_c}}{2}\right)^2 \tag{72}$$

Mass flow rate of fluid flowing through bed cross section

$$\dot{m_{HTF}} = v_s \rho_{HTF} A_{cs} \tag{73}$$

Fluid mass flux

$$G = \frac{\dot{m_{HTF}}}{A_{cs}} \tag{74}$$

The Ergun Equation

Ergun defines the Reynolds number as follows:

$$Re_{er} = \frac{\rho_{HTF} v_s D_c}{\mu_{HTF}(1-\epsilon)} \tag{75}$$

The Ergun Equation is only defined in the range of $Re_{er} = 0\ to\ 3000$. If the answer falls outside of this range the answer will be 0.

Thus:

$$If\ Re_{er} \geq 0\ and\ Re_{er} \leq 3000 \tag{76}$$

Then

$$-\frac{\Delta p_{er}}{L}=\frac{150(\varepsilon-1)^2}{\varepsilon^3}\frac{\mu_{HTF}v_s}{D_c^2}+\frac{175(\varepsilon-1)}{\varepsilon^3}\frac{\rho_{HTF}v_s^2}{D_c} \tag{77}$$

The Representative Unit Cell method

The pressure drop using the RUC method is calculated as follows:

The relationship between shell length and solid cube length is:

$$D_s=(1-\epsilon)^{\frac{1}{3}}D_c \tag{78}$$

The RUC method defines the Reynolds number as:

$$Re_p=\frac{\rho_{HTF}v_sD_c}{\mu_{HTF}} \tag{79}$$

The pressure drop across the system in terms of the Reynolds number:

$$\frac{\Delta p_{RUC}}{L}=\frac{\mu_{HTF}v_s}{D_s^2}\left(\frac{25.4(1-\varepsilon)^{\frac{3}{4}}}{\left(1-(1-\varepsilon)^{\frac{1}{3}}\right)\left(1-(1-\varepsilon)^{\frac{2}{3}}\right)^2}+\frac{c_d(1-\varepsilon)}{2\varepsilon\left(1-\left(1-\varepsilon^{\frac{2}{3}}\right)\right)^2}Re_p\right) \tag{80}$$

Singh *et al* (2006)

Using Singh *et al* (2006) pressure drop in terms of friction factor equations causes the pressure drop to be calculated as follows:

The friction factor calculation was deconstructed to ease solving of the calculation equations 87 and 88 are solved separately as portions of equations 89:

$$x_{06}=\ln(\Psi) \tag{81}$$

$$y_{06}=\exp(11.85(x_{06}^2)) \tag{82}$$

$$f_{06}=4.466Re_p^{-0.2}\Psi^{0.696}\epsilon^{-2.945}y_{06} \tag{83}$$

Singh *et al*. (2006) only define this in the range of $Re_p = 1558\ to\ 2674$ and $G = 0.155\ to\ 0.266$. If the answer falls outside of this range the answer will be 0.

$$\Delta p_{Singh_{06}} = \frac{f_{06} L G^2}{\rho_{HTF} D_s} \tag{84}$$

Singh *et al* (2013)

Using Singh *et al* (2013), the pressure drop in terms of friction factor equations the pressure drop is calculated as follows:

The friction factor calculation was deconstructed to ease solving of the calculation equations 91 and 92 are solved separately as portions of equations 93:

$$x_{13} = \ln(\Psi) \tag{85}$$

$$y_{13} = \exp(9.7478(x_{13}^2)) \tag{86}$$

$$f_{13} = 374.765 Re_p^{-0.6842} \Psi^{2.5246} \epsilon^{-0.7878} y_{13} \tag{87}$$

Singh *et al.* (2013) is only defined in the range of $Re_p = 503\ to\ 866$ and $G = 0.155\ to\ 0.266$. If the answer falls outside this range the answer will be 0.

$$\Delta p_{Singh_{13}} = \frac{f_{13} L G^2}{\rho_{HTF} D_s} \tag{88}$$

Chandra and Willits

The pressure drop calculation according to Chandra and Willits was calculated as follows:

$$G_{CW} = \frac{4\dot{m}_{HTF}}{\pi D_{h_c}^2} \tag{89}$$

$$Re_{CW} = \frac{G_{CW}}{\mu_{HTF}} \tag{90}$$

$$\Delta p_{CW} = \left(\frac{L G_{CW}^2}{\rho_{HTF} D_s}\right) \times \epsilon^{-2.6} \times \left(\frac{1.7 + 185}{Re_{CW}}\right) \tag{91}$$

Table 14: Parameters for system pressure drop equations for detailed design

Symbol	Unit	Description
v_s	[m/s]	Superficial speed through porous medium.
u_b	[m/s]	Average interstitial speed (air speed between rocks).
A_{cs}	[m^2]	Cross-sectional area of test section perpendicular to flow direction.
A_s	[m^2]	Total surface area of solid particle in bed/RUC volume.
G	[kg/s m^2]	Air mass flux.
G_{CW}	[kg/s m^2]	Air mass flux as used by Chandra and Whillit.
D_s	[m]	Length dimension of solid cube within RUC.

Table 15: Inputs for system pressure drop equations for detailed design

Symbol	Magnitude and unit	Description
L	5.25 [m]	Length of pipe (Section 4.1.2).
D_{pipeI}	0.323 [m]	Inside diameter of pipe (measured value).
epsilon	0.275 [-]	Void fraction (section 3.2.2).
μ_{HTF}	0.3544E-03 [kg/ms]	Dynamic viscosity of water.
ρ_{HTF}	1000 [kg/m^3]	Specific weight of HTF.
D_{hc}	0.05 [m]	Particle hydraulic/equivalent diameter or size.
D_c	0.05 [m]	Particle diameter (Burg Refractories).
ψ	0.8 [-]	Sphericity factor.
$\dot{m}_{HTF}$	0.017 [kg/s]	Mass flow rate of fluid flowing through bed cross section (CSP designers).
D_{RUCsl}	0.05 [m]	RUC model solid cube side length.
c_d	[-]	Drag coefficient for a packed bed, as used in the RUC model

Table 16: Results for system pressure drop equations for detailed design

Symbol	Unit	Magnitude
Δp_{RUC}	[N/m^2]	1.365
Δp_{er}	[N/m^2]	55.88
$\Delta p_{Singh06}$	[N/m^2]	0
$\Delta p_{Singh13}$	[N/m^2]	0
Δp_{CW}	[N/m^2]	475.1

An equation is not chosen as of yet as this will only be done after the testing phase. The disparity between the answers can be contributed to the fact that these equations are derived from equations that use air as a heat transfer media. Section 6.4 will make a verdict on which, if any, of these equations are the most realistic in this specific application.

4.1.5 System charging time

It was decided by the team the heat store will first be charged (heated up to capacity) without the heat pump cycle operating. This will prevent the heat pump initially to run as designed (optimal parameters).

The calculations used in the EES programme are based on the information as set out in Section 3.4.1. Furthermore Kenneth (2010) was used as a template for the calculation.

The E-NTU model is written in the form of multiple nested loops with the outer nested loop increasing in time steps and the inner loop incrementing the segment position.

Firstly a few standard variables are calculated as below:

Volume of single storage element

$$Volume = D_{particle}^3 \tag{92}$$

Particle hydraulic/equivalent diameter or size

$$D = Volume^{\frac{1}{3}} \tag{93}$$

Radius of pipe

$$r = \frac{D_{pipe_i}}{2} \tag{94}$$

Cross-sectional area of test section perpendicular to flow direction

$$A_{cs} = \pi \times r^2 \tag{95}$$

Liquid mass flux

$$G = \frac{\dot{m}_f}{A_{cs}} \tag{96}$$

Particle Reynolds number

$$Re_p = G \times \frac{D}{\mu_f} \tag{97}$$

Hagen number

$$Hg = Re_p\left(150(1-\epsilon) + 1.75Re_p\right)\left(\frac{1-\epsilon}{\epsilon^3}\right) \tag{98}$$

Friction factor

$$f = \left(\frac{2}{3}\right)\left(\frac{\epsilon}{(1-\epsilon)^{\frac{2}{3}}}\right) \tag{99}$$

Nusselt's number

$$\left(\frac{Nusselt}{Pr^{\frac{1}{3}}}\right) = 0.4038\left(2x_f Hgf\right)^{\frac{1}{3}} \tag{100}$$

$$Nusselt = h \times \frac{D}{k_f} \tag{101}$$

Volumetric heat transfer coefficient

$$h_v = h_a \tag{102}$$

$$a = 6\left(\frac{1-\epsilon}{D}\right) \tag{103}$$

Calculating NTU

Below is the simplification of the equations that will be used in the loops at the end of the programme.

$$NTU = \frac{h_v L}{G c_{pf}} \tag{104}$$

$$\tau = \left(\frac{m_s c_s}{\dot{m}_f c_{pf}}\right) \tag{105}$$

$$\Delta x = \frac{L}{x_{tot}} \tag{106}$$

$$\eta = 1 - \exp\left(-NTU\left(\frac{\Delta x}{L}\right)\right) \tag{107}$$

$$Constant1 = \left(\frac{\Delta t}{2}\right)\left(\frac{L}{\Delta x}\right)\left(\frac{1}{\tau}\right)\eta \tag{108}$$

The total time steps as well as the number of segments are selected based upon the length of the simulation that will be run. The longer the simulation needed the fewer segments and vice versa.

$$Duplicate\ t = 0, t_{tot} \tag{109}$$

$$T_f[0, t] = 61 \tag{110}$$

$$End$$

$$Duplicate\ x = 0, x_{tot} \tag{111}$$

$$T_s[x, 0] = 25 \tag{112}$$

$$End$$

$$Duplicate\ x = 1, x_{tot} \tag{113}$$

$$T_s[x, 0] = 25 \tag{114}$$

$$End$$

The outer loop and inner loop can be seen below. As the programme loops through, the segments and time steps the temperature of the HTF as well as that of the STM are calculated.

$$Duplicate\ t = 1, t_{tot} \tag{115}$$

$$Duplicate\ x = 0, x_{tot} - 1 \tag{116}$$

$$T_s[x,t] = T_s[x,t-1] \times (1 - Constant1) + T_f[x,t] \times \frac{2Constant1}{1 + Constant1} \tag{117}$$

$$T_f[x+1,t] = T_f[x,t-1] - \eta(T_f[x,t-1] - T_s[x,t-1]) \tag{118}$$

$$End$$

$$T_s[x_{tot},t] = (T_s[x_{tot},t-1] \times (1 - Constant1) + T_f[x_{tot},t]\left(\frac{2Constant1}{1 + Constant1}\right) \tag{119}$$

$$End$$

Table 17: Parameters for system charging time equations for detailed design

Symbol	Unit	Description
G	[kg/m^2.s]	Air mass flux $G=\dot{m}_f/A_{cs.}$
D	[m]	Particle hydraulic/equivalent diameter or size.
ϵ	[-]	Void fraction (porosity) of a material.
x_f	[-]	Frictional fraction of total pressure drop.
P_r	[-]	Fluid Prandtl number.
k_f	[W/mK]	Fluid thermal conductivity.
c_{pf}	[J/kgK]	Specific heat capacity of fluid at constant pressure.
L	[m]	Flow-wise length of the bed.
k_s	[W/mK]	Rock/solid thermal conductivity.
c_s	[J/kgK]	Specific heat capacity of rock/solid.
$\dot{m}_f$	[kg/s]	Mass flow rate of fluid flowing through bed cross section.
ρ_s	[kg/m^3]	Rock/solid density.
A_{cs}	[m^2]	Cross-sectional area of test section perpendicular to flow direction.
P_a	[N/m^2]	Ambient pressure.
Re_p	[-]	Particle Reynolds number $Re_p=\rho_f.v_s.D/\phi_f$''
v_s	[m/s]	Superficial speed through porous medium.
Φ_f	[kg/m.s]	Fluid (dynamic) viscosity
Hg	[-]	Hagen number.
f	[-]	Friction factor as defined for present method in this study.
Nusselt	[-]	Nusselt Number.
h_v	[W/m^3]	Volumetric heat transfer coefficient.

Table 18: Inputs for system charging time equations for detailed design

Symbol	Magnitude and unit	Description
D_{pipei}	0.327 [m]	Inside diameter of STM housing (measured value).
$D_{particle}$	0.05 [m]	STM particle diameter (Burg Refractories).
ϵ	0.275 [-]	Void fraction. (section 3.2.2)
x_f	0.197 [-]	Frictional fraction of total pressure drop.
Pr	2.99 [-]	Fluid Prandtl number.
k_f	0.609 [W/mK]	Fluid thermal conductivity.
L	5.25 [m]	Flow-wise length of the bed.
k_s	0.8 [W/mK]	Rock/solid (STM) thermal conductivity.
c_s	820 [J/kgK]	Specific heat capacity of rock/solid (section 3.2.1).
$\dot{m}_f$	0.017 [kg/s]	HTF flow rate.
ρ_s	9600 [kg/m^3]	Rock/solid (STM) density (section 3.2.1).
m_s	2786 [kg]	Mass of STM in system (section 4.1.1).
P_a	101 [kPa]	Ambient pressure.
T_f	100 [C]	Inflow temperature of HTF (received from the CSP designers).

Table 19: Results for system charging time equations for detailed design

Symbol	Unit	Magnitude
Time for all STM to heat up	[hours]	68.67

As mentioned above this will be the time that the system needs to heat up before it can be used. This heating up time is to avoid the heat pump cycle initially being run of design parameters (non-optimum).

This section calculates the number of sunshine hours that will be needed to fully charge the thermal storage system (68.67 h). Although this seems to be a very long time it is important to remember that this charging will only happen on the first start up.

4.2 Heat store containment

The storage system is designed as a simple cylinder as can be seen in Figure 14. A standard size steel pipe is used, in this case a pipe with inside diameter of 323 *mm* and a wall thickness of 2 *mm*. The eventual available length on the mobile rig is approximately 3.5 *m*. With the area available for the storage system having measurements of 3.5 *m* by 1.25 *m* by 1.25 *m*. Due to cost a dimensional scaled down model was not used, it was decided to rather use an approximate 15 *%* of the length of the full-scale heat store with the same diameter for testing. This amounted to 650 *mm*. This is also to keep the weight of the experimental storage setup low enough to be handled without any heavy machinery (the mobile rig chasse and suspension will be chosen to suite the total resulting weight of the whole rig).

At the ends of the pipe, flanges of 4 *mm* mild steel sheets are welded flush to the ends of the pipe. The flanges have an eight-hole bolt configuration for connecting to the endplates. The bolts will be M16 so as to make sure the endplates can be tightened to such a degree as to keep the system from leaking.

The endplates will have a 15 *mm* hole in the middle that will be used as the inflow and outflow of the storage system. The one endplate will have a hole at the bottom to be used for drainage of the system. The size of the connecting pipes was obtained from the solar collector's test rigs piping. The flow range for testing was also obtained from the solar panel test rig (see Section 6.4). In the solar panels and thermal heat storage system there will be varying flow throughout the day due solar irradiation changes during the day.

Inside the pipe expanded metal circles are to be welded 100 *mm* from the ends of the pipe as to create a plenum in the system. The plenums are there to help the flow stabilise when it enters the system, thus helping to heat the STM more evenly.

The STM will be placed on the expanded metal and then capped by the second expanded metal circle so as to sandwich the STM between the circles to keep the STM from moving while the system is moved.

Although this is the design for the experimental setup the same design will be used for the full-scale setup. The only change that will be made is to the length of the pipe. It can also be made modular and bolted together so as to make handling easier and to make the packing of the storage material easier.

Figure 14: Side view of the Solid Works model of the storage system for test setup

The detailed design drawing can be found in Appendix A.

4.3 Experimental setup

To do an accurate detailed design it is of the utmost importance to verify two design inputs. These two inputs are the specific heat of the STM (spinel) and the efficiency of the storage system. Both these inputs have a considerable effect on the amount of storage material that is needed in the system, and thus the price, volume and mass of the system.

Although the above-mentioned criteria are the main criteria when it comes to pricing it is not the only important variables that need to be established. Two others that will also be tested are the density of the material and the void fraction in the thermal heat storage system.

Thus, all four of the above-mentioned variables will be established via experiments. The pressure drop over the storage system will also be measured to be used as verification of the EES pressure drop calculation.

The experimental procedures of all the experiments can be found in Appendix B and the calibration process in Appendix C their risk assessments in Appendix D.

4.3.1 Specific heat of storage material

To determine the specific heat of a material a simple experiment can be done. A small piece of the material (with a known weight) is heated in an oven. It is left in the oven for an adequate time until the material is heated uniformly all the way to the centre of the core. The oven is set to 150 *°C.*

Then as quickly as possible transfer the material into a beaker which holds a known quantity of some much cooler water/liquid (which temperature must be measured beforehand). As the material cools, it will heat the liquid, until both reach the same temperature. This temperature is recorded using a thermometer.

It is assumed that all the heat lost by the material is absorbed by the water/liquid, although in the actual experiment heat transfer will not be 100 *%*. At 150 *°C* it is expected that there will be some heat loss due to the boiling of the water as the material is immersed. But if this immersion is done quickly this will be held to a minimum. The test will be done a second time using a liquid with a higher boiling point. These results will be used to as comparison to see if the results obtained using water is realistic.

Most of the heat loss can be mitigated by using proper insulation with the beaker and quick immersion of the material.

The process can be described by the following thermochemistry equations:

$$q_{material} = q_{water} \tag{120}$$

By substitution we have:

$$m_{material} \times \Delta t \times cp_{material} = m_{water} \times \Delta t \times cp_{water} \tag{121}$$

The difference in internal energies can be neglected in this experiment since the difference between initial and end value were used.

Where we solve for:

$$cp_{material} = (m_{water} \times \Delta t \times cp_{water})/(m_{material} \times \Delta t) \quad (122)$$

(Anon, 2014b)

4.3.2 Storage system void fraction

Although certain packing methods have known void fraction it can been seen from Singh *et al.* (2006) and Singh *et al.* (2013) in practice there might be some deviation from this number.

The void fraction can be defined as the ratio ε of the void volume V_f to the total volume V_o of a sample including both void and solid (Kenneth, 2010:16).

$$\varepsilon = \frac{V_f}{V_o} \quad (123)$$

An experiment can be done to establish the exact void fraction of the storage system. The bed can be packed in the manner it will be used in the completed system. Afterwards the system is filled with water. The amount of water is then what filled the voids. As the exact dimensions of the system are known the void fraction can then be calculated as follows:

$$\varepsilon = \frac{V_w}{V_s} \quad (124)$$

Where ε is the void fraction, V_w is the volume of water that it took to fill up the system and V_s is the system volume.

4.3.3 Storage material density

To calculate the density of the storage material a very elementary experiment is needed. The exact volume of an element needs to be established where after it needs to be weighed and then, using the following equations the density can be calculated:

$$V = L \times H \times W \quad (125)$$

$$\rho = M/V \tag{126}$$

4.3.4 Pressure difference over storage system

To do validation on the EES pressure drop over the storage system program a U-tube manometer will be used as illustrated in Figure 15 where one leg of the manometer will be connected to the inlet pipe just in front of the storage system on the test model and one on the outlet pipe after the storage system.

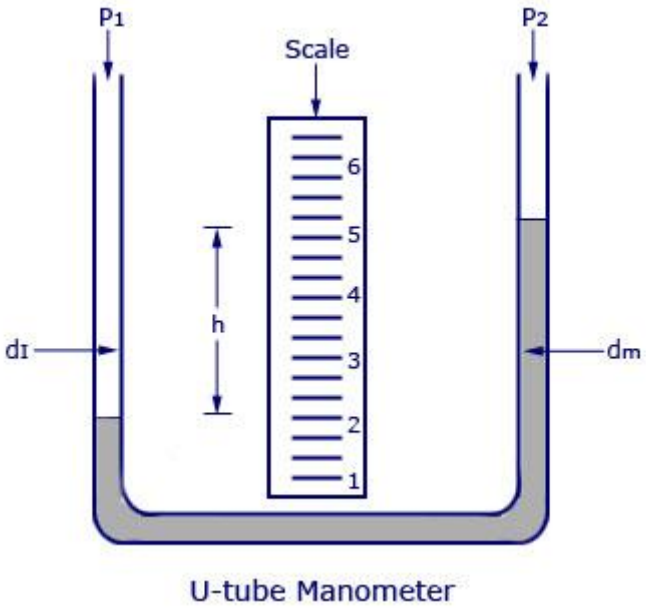

Figure 15: Example of a u-tube manometer (Smith, 2011)

Then by letting the HTF run through the system at a known flow rate a pressure difference should be observable. The pressure difference will be measured in millimetres. The millimetre value will then be converted into N/mm^2.

4.3.5 Energy store efficiency

To determine the thermal energy store's efficiency an experimental setup was developed. There are three main parts to the experiment are a circulation pump, heat store and heating element.

The CSP as used in the final system is replaced by a heating element. The 2 *kW* heating element in the experiment shall be a 100 *l* household geyser with an adjustable thermostat.

After the geyser, has reached the desired predetermined temperature, the circulation pump is used to circulate the HTF (in this case water) throughout the system.

The flow rate through the system will be managed using a combination of control valves and a flow meter. The flow will be set to replicate the expected operating flow. Circulation of the HTF will continue until all the thermocouples read the same temperature as that of the heating element, and this will indicate that the system is fully charged.

The discharging of the system will be done by changing the system to an open loop. Room temperature water will be pumped through the storage system discharging it. When all the thermocouples read the same temperature as the room temperature water, it can be assumed that the system is completely discharged.

The equations that will be used to determine the efficiency are as follows:

The amount of energy inserted into the system by the heating element:

$$Q_{in} = (\dot{m} \times t) \times cp_{HTF} \times \Delta T \quad (127)$$

The total amount of energy stored:

$$Q_{STM} = m_{STM} \times cp_{STM} \times \Delta T \quad (128)$$

The energy that was extracted:

$$Q_{out} = (\dot{m}_{HTF} \times t) \times cp_{HTF} \times \Delta T \quad (129)$$

There are two different efficiencies that can be calculated to determine how efficient the system is in storing the energy of the HTF that is pumped through as well as how much of that energy can then be extracted again.

This can be expressed as:

$$Eff_{store} = \frac{Q_{STM}}{Q_{in}} \quad (130)$$

And

$$Eff_{extract} = \frac{Q_{out}}{Q_{STM}} \quad (131)$$

4.3.6 Efficiency test setup

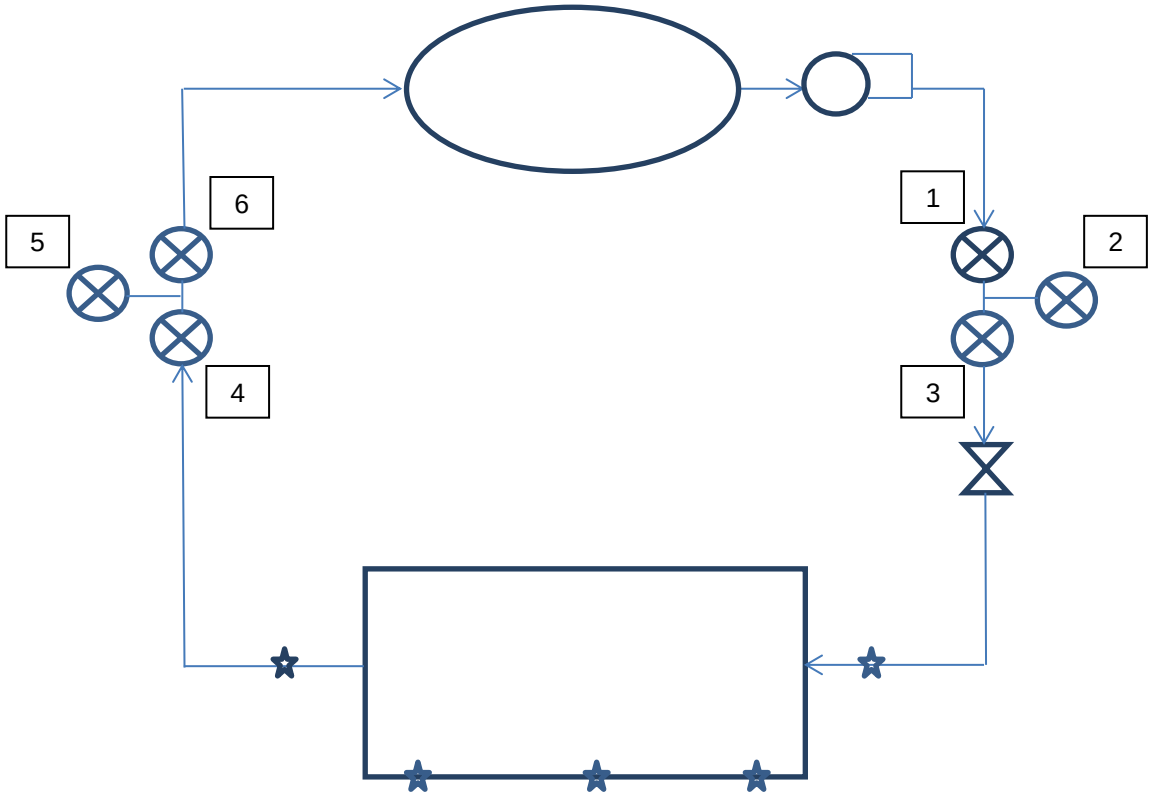

Figure 16: Schematic drawing of experimental setup

Table 20: Legend for the schematic drawing of the experimental setup

Legend	
100 Lt Geyser	
Tap	
Flowmeter	
One-way valve	
Pump	
Heat store	

4.4 Manufactured test bench

In this section, the manufactured test bench will be shown, with the main focus being on the most critical parts of the setup.

Figure 17 shows the manufactured storage system as described and illustrated in Section 4.2 On the top of the pipe small holes can be seen - this is where the thermocouples will be threaded through into storage material cubes to measure the temperature in the centre of those cubes.

Figure 17: Manufactured thermal heat storage system

Figure 18 shows how the thermocouples were installed into the storage material. This was done in three individual cubes which were spaced equally along the storage system.

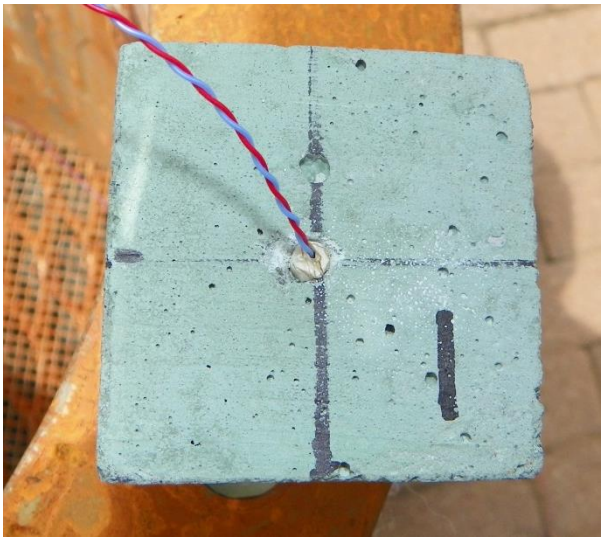

Figure 18: Thermocouple in storage material setup

The pump that was used in the experimental setup can be seen in Figure 19. The pump that was used is normally used as a circulation pump in solar power geysers. The pump specifications can be seen in the pump information sheet inserted in Appendix E.

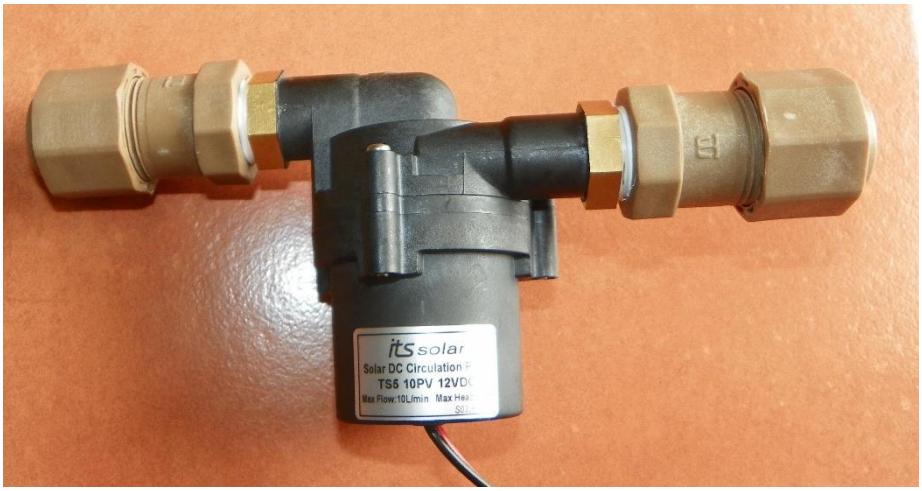

Figure 19: Circulation pump used

Figure 20 and Figure 21 show the manufactured inlet and outlet pipes of the storage system as depicted in the schematic presentation in Figure 16.

It can be seen that all the copper piping has been well insulated to keep heat loss to a minimum.

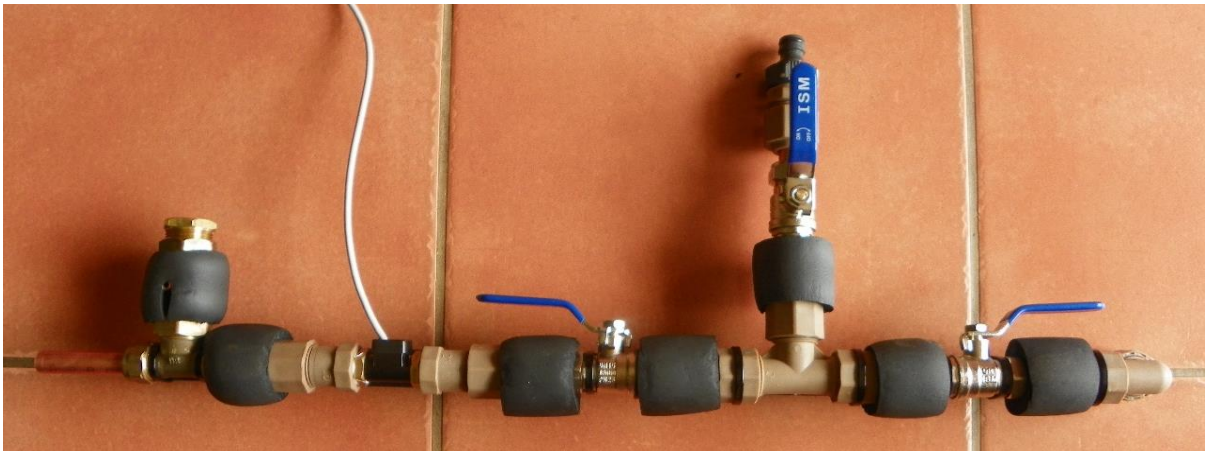

Figure 20: Storage system inlet pipe configuration

Figure 21: Storage system outlet pipe configuration

The fully assembled test bench can be seen in Figure 22. The green insulation around the storage system can also been seen in this figure. In Figure 20, 21 and 22 the excess insulation was removed for the purpose of these photographs to display the components used. All these services were covered with insulation during testing.

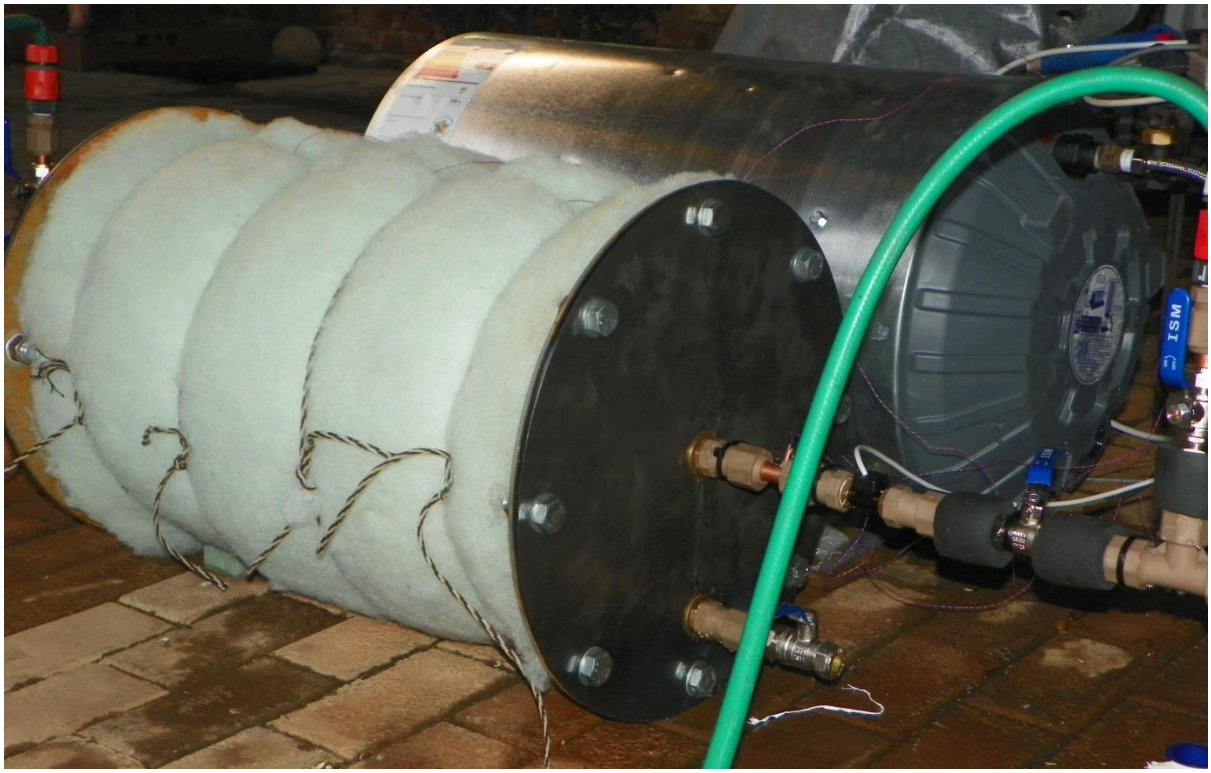

Figure 22: Picture of the full test bench

5 Test execution

This chapter only contains the readings for the specific heat of storage material test the storage material density test the pressure difference over storage system test and the energy store efficiency test. The calculated results can be found in Chapter 6.

5.1 Specific heat of storage material test

For this test, one of the casted spinel blocks was taken and a small piece was removed using a hammer and chisel. The piece was weighed using an electronic scale that is able to weigh to the nearest tenth of a gram. The weight of the spinel piece was measured to be 20.25 *g*

Using a marked beaker and scale 0.075 *kg* of liquid was measured out. The beaker was then insulated using normal glass fibre-based insulation.

The heating of the spinel was done using a drying oven at the NWU Mechanical Engineering laboratories with the oven being set to +-150 $°C$.

A Fluke 52 K/J thermometer was used to measure the temperature inside the oven as well as the water temperature where the water temperature was taken before and after the heated spinel piece was added.

5.1.1 Test data of specific heat of storage material test

The “Material temp” column is the temperature of the oven as it is assumed that the whole piece of spinel has uniformly heated up to the same temperature as the oven. The “Water/Glycerol temp” column refers to the temperature of the water before the experiment started whereas the “Combined stabilized temperature” is the temperature were the liquid settles after the heated spinel has been added.

Table 21: Test data of specific thermal heat storage capacity of material test using water

Specific heat of storage material calculation test data when using water			
Mass water	**Material temp**	**Water temp**	**Combined Stabilized Temperature**
[kg]	*[°C]*	*[°C]*	*[°C]*
0.0749	151.1	27.2	33.4
0.075	151.2	26.7	32.6
0.0748	149.8	26.9	33.1
0.075	150.2	27.3	33.5
0.0749	150.7	26.6	32.7

Table 22: Test data of specific thermal heat storage capacity of material test using glycerol

Specific heat of storage material calculation test data when using glycerol			
Mass Glycerol	**Material temp**	**Glycerol temp**	**Combined Stabilized Temperature**
[kg]	*[°C]*	*[°C]*	*[°C]*
0.0749	150.3	26.5	36.7
0.0747	151.4	26.8	37.1
0.0752	151.4	26.2	36.5
0.0751	150.6	25.9	36.2
0.0752	150.8	26.6	37.6

5.2 Storage system void fraction test

When conducting the test, the packing of the material was done as it would be in the actual setup. The cubes were packed in a Rhombohedral fashion. It is crucial to note that nearing the centre of the circular packing pattern, it became impossible to follow the packing method as the space became too limited as can be seen in Figure 23. The size of the blocks was dictated by the supplier due to economic reasons this was an existing cast and had a favourable volume to cost ratio. The size of the shell was a given as previous mentioned.

Figure 23: STM packing convention

When calculating the total volume of the storage system the size of the plenum was also calculated. See Section 4.2 and Table 23 below. This will need to be subtracted from the overall size of the storage system in order to get the space that is usable for holding of the STM.

5.2.1 Test data of the storage system void fraction test

Table 23: Test data of the storage system void fraction test

Storage system void fraction.	
Total storage system volume.	0.053261 [m3]
Plenum volume.	0.016388 [m3]
Amount of water to fill system.	22.7 [L]
Number of STM element packed into system.	176 [-]

The volume of the storage system and the plenum was calculated using the following equations:

$$A = \pi \left(\frac{C}{2\pi}\right)^2 \tag{132}$$

$$V = A \times L \tag{133}$$

5.3 Storage material density test

The volume of individual STM elements was calculated using measurements taken using a vernier calliper. The cubes mass was then measured using an electronic scale which is accurate to one-tenth of a gram.

As the cubes were cast the measurements seemed to be similar with these measurements being W, L and H is 0.05 *m.*

5.3.1 Test data of the storage material density test

Table 24: Test data of the storage material density experiment

Density of storage material	
Number	**Mass**
[-]	*[g]*
1	529.6
2	545.9
3	540.7
4	545.0
5	537.6
6	528.2
7	547.4
8	545.7
9	546.2
10	535.3
11	544.7
12	538.1
13	535.5
14	558.8
15	536.2
16	532.9
17	542.8
18	527.3
19	548.8
20	540.3

5.4 Pressure difference over storage system test

The pressure difference experiment was run with municipal water at room temperature. The flow rate was changed, after which the difference in *mm*, between the liquid, in the manometer's two legs was recorded.

In all the results the pressure was found to be higher on the incoming side of the storage thus the liquid in the leg connected to the incoming pipe was lower than that of the outgoing pipe.

5.4.1 Test data of the pressure difference over storage system

Table 25: Test data of pressure difference over storage system test

Pressure difference over storage system			
Number	**Flow**	**Real flow**	**Difference**
	[l/min]	*[l/min]*	*[mm]*
1	1	1.2	15
2	1	1.26	15
3	1	1.25	16
4	1	1.02	14
5	1	1.22	16
6	1	1.10	13
7	1	1.10	13
8	3	3.02	20
9	3	3.02	20
10	3	3.20	22
11	3	2.90	19
12	3	3.20	19
13	3	3.00	21
14	3	3.10	22
15	10	10.40	57
16	10	10.00	51
17	10	10.00	57
18	10	10.30	55
19	10	10.00	54
20	15	15.00	95

5.5 Energy store efficiency test

A total of four test runs were completed. The flow chosen for charging and discharging of the system was 3 *l/min* as this will be the most common flow rate experienced, once the system is incorporated into the larger solar driven aqua ammonia heat pump system. The temperature of the geyser was set to 80 *C* which is seen as a very good representation of the real working temperature. The instrument calibration process followed can be found in Appendix C.

5.5.1 Test data of the energy store efficiency test

Table 26: Test data of energy store efficiency test

Energy store efficiency									
Date	**Time**	**Status**	**T1**	**T2**	**T3**	**T4**	**T5**	**T6**	**Flow**
			Ave	Ave	Ave	Ave	Ave	Ave	Ave
			[°C]	*[°C]*	*[°C]*	*[°C]*	*[°C]*	*[°C]*	*[l/min]*
19.11.2016	23:23:20	OK	43.8	34.7	31.6	29.5	27.8	13.7	2.313
19.11.2016	23:23:40	OK	72.5	34.8	31.8	29.6	26.9	14	2.899

The table above is only a small sample of the data acquired during the test. An example of a full data sheets for 1 run will be attached in Appendix F. The table can be understood as follows:

1. Date: Date on which data are logged.
2. Time: The exact time data were logged. It can be seen that the times are 20 *s* apart these because data were logged every 20 *s*.
3. Status: Shows if all the input into the data logger is functional.
4. T1 to 5: They refer to the thermocouples where T1 is the thermocouple just before the storage system T2 is the first one in the storage system and T3 is the one in the middle of the system T4 is the one at the end and T5 is the thermocouple just after the storage system.
5. Flow: It is the flow meter reading.

All temperature and flow readings and the average over the 20 *s* time period data were logged. It is important to note that the test was done using the municipal water supply thus the flow rate is not perfectly constant.

6 Calculations and interpretation of results

In Sections 6.1-6.5 the experimental data stated in Chapter 5 will be calculated and evaluated. Then in Section 6.6 the calculations for the final design will be made using the experimental results.

6.1 Specific thermal heat storage of the storage material

When calculating the specific thermal heat storage of the material the following equation was used.

$$cp_{STM} = \frac{m_{liquid} \times cp_{liquid} \times \left(T_{together} - T_{liquid}\right)}{m_{STM} \times (T_{toghether} - T_{STM})} \quad (134)$$

Where the constant $cp_{water} = 4183\, J/kg.K$, $cp_{glycerol} = 2431\, J/kg.K$ and $m_{STM} = 20.25\, g$, with the results of the calculations being shown in Table 27 and Table 28. A constant specific heat capacity was chosen for the tests this is due to the fact that for water the specific heat capacity deviation of the water over the small temperature difference is in the region of 0.005489 %.

A second set of tests are also done using a 99 % pure food grade glycerol instead of water for the test. This is due to the fact that glycerol has a boiling temperature of 280 °*C* which will impede any steam from forming when material is added at 150 °*C*. It also has a lower specific heat capacity than water which leads to a higher ΔT in the equation used which in turn decreases the inaccuracy of the test.

Table 27: Specific thermal heat storage capacity calculations results when using water

Specific heat of storage material calculation results when using water				
Mass water	**Material temp**	**Water temp**	**Combined Stabilized Temperature**	cp_{STM}
[kg]	*[°C]*	*[°C]*	*[°C]*	*[J/kg.K]*
0.0749	151.1	27.2	33.4	809.5
0.075	151.2	26.7	32.6	772.0
0.0748	149.8	26.9	33.1	819.9
0.075	150.2	27.3	33.5	822.5
0.0749	150.7	26.6	32.7	797.2
			cp_{STM} **Average**	804.22

Table 28: Specific thermal heat storage capacity calculations results when using glycerol

Specific heat of storage material calculation results when using glycerol				
Mass glycerol	**Material temp**	**Glycerol temp**	**Combined Stabilized Temperature**	cp_{STM}
[kg]	*[°C]*	*[°C]*	*[°C]*	*[J/kg.K]*
0.0749	150.3	26.5	36.7	809.7
0.0747	151.4	26.8	37.1	807.0
0.0752	151.4	26.2	36.5	810.5
0.0751	150.6	25.9	36.2	807.9
0.0752	150.8	26.6	37.6	811.5
			cp_{STM} **Average**	809.32

The average $cp_{STM} = 804.22\, J/kg.K$ when using data gathered in the test using water. While using glycerol an average of $cp_{STM} = 809.32\, J/kg.K$. The percentage difference between these two sets of experiments is 1 % this small difference might be due to the fact that when the material is placed in the water at such a high temperature it can lead to a little steam forming before the material is fully submerged. The average between the two test sets is calculated to $cp_{STM} = 806.77\, J/kg.K$ and this will the specific heat value used for any further calculations.

When comparing this to the range of specific heat (800-820) as found in Section 3.2.1 it can be seen that the value achieved in the test is right in the expected range.

6.2 Storage system void fraction

The void fraction was calculated using two methods where one uses the water volume that could be added to the system after the STM was packed in the system. The second method used only the volume of STM elements added to system and sub-tracking that from the total volume of the system that is taken up by the STM elements.

The two methods can be expressed in the following equations:

$$\varepsilon = \frac{V_w}{(V_s - (Plenum\ volume \times 2)) * 1000} \tag{135}$$

and

$$\varepsilon = \frac{Number\ of\ STM\ elements \times V_{STM_{Element}}}{(V_s - (Plenum\ volume \times 2)} \tag{136}$$

Where the STM element volume is taken as $V_s = 0.000125\ m^3$.

Table 29: Storage system void fraction calculation results

Storage system void fraction.	
Total storage system volume.	0.053261 [m^3]
Plenum volume.	0.016388 [m^3]
Amount of water to fill system.	22.7 [L]
Number of STM element packed into system.	176 [-]
Void fraction water method.	0.62 [-]
Void fraction volume method.	0.60 [-]

When comparing the expected void fraction for a rhombohedral packing pattern, which is indicated to be 0.275 for spheres (Singh *et al.*, 2013:22), there is quite a large difference.

The difference between the measured values and the expected value is due to the fact that the packing pattern in the system is not a true rhombohedra packing pattern. This is because

only the two outermost rings could be packed in this pattern, as the space nearer to the middle was too small to fit the elements in in the chosen pattern. It also due to the fact that the test used cubes instead of the literatures spheres. The most realistic void fracture for the system was taken to be the average of the two measuring methods which is $\varepsilon = 0.61$.

6.3 Storage material density

The density was calculated using the simple equation:

$$\rho_{STM} = \frac{m_{STM}}{V_{STM}} \tag{137}$$

Where the volume of the STM element is taken as $V_{STM} = 0.000125\ m^3$.

The mass of the STM element is taken as the average of the 20 elements weighed. The average mass was $m_{STM} = 0.5403\ kg$ and thus the density is $\rho_{STM} = 9273.5\ kg/m^3$.

When comparing this to the expected density of $\rho_{STM} = 9200\ to\ 9600\ kg/m^3$ the density is at the lower end of the range but still in the range.

6.4 Pressure difference over storage system

To calculate the pressure difference over the system the following equation is used:

$$P = \rho_{MF} \times g \times h_{Diff} \tag{138}$$

(Engineers Edge, 2017)

Where *P* is the pressure difference ρ_{MF} is the manometer fluid density and h_{Diff} is the height difference between the fluid in the two legs of the manometer.
The results of these calculations can be seen in the pressure difference column of Table 30.

Table 30: Pressure difference over storage system calculation results

Pressure difference over storage system			
Number	**Flow measured**	**Difference**	**Pressure diff**
	[l/min]	*[mm]*	*[N/m^2]*
1	1.20	15	146.71
2	1.26	15	146.71
3	1.25	16	156.49
4	1.02	14	136.93
5	1.22	16	156.49
6	1.10	13	127.15
7	1.10	13	127.15
8	3.02	20	195.61
9	3.02	20	195.61
10	3.20	22	215.17
11	2.90	19	185.83
12	3.20	19	185.83
13	3.00	21	205.39
14	3.10	22	215.17
15	10.40	57	557.49
16	10.00	51	498.81
17	10.00	57	557.49
18	10.30	55	537.93
19	10	54	528.15
20	15	95	929.15

Using an EES program it is possible to develop a formula to predict the pressure drop over the system at different flow rates. The graph and equation can be seen in Figure 24.

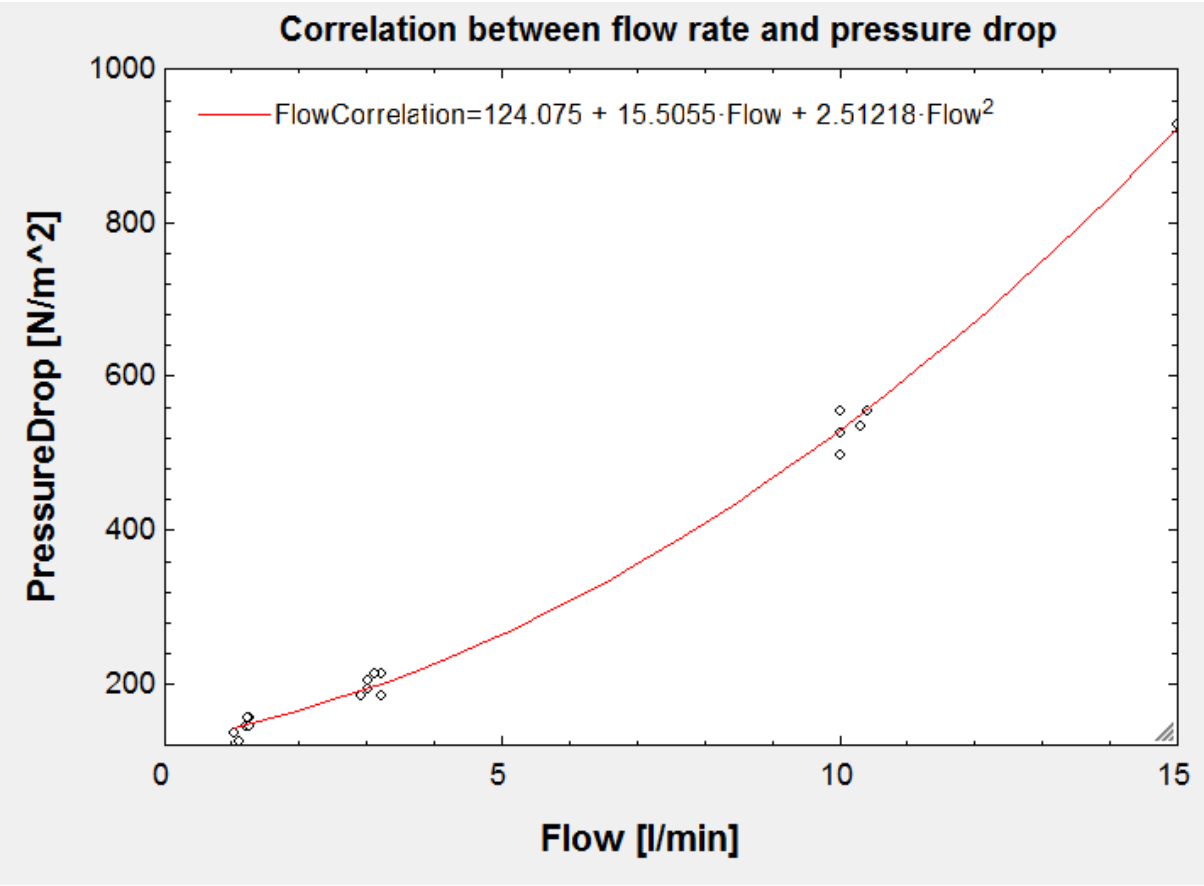

Figure 24: Graph of comparison between measured pressure drops and correlation curve

After calculating the pressure drop over the system as described in section 4.1.4 the results are tabulated in Table 31.

Table 31: Pressure difference over storage system EES calculation comparison

Pressure difference over storage system EES calculation comparison								
Run	**Flow Rate**	**Mass Flow**	**Measured pressure drop**	**Chandra and Willet**	**Ergun**	**RUC**	**Singh06**	**Singh13**
	[l/min]	*[kg/s]*	*[N/m^2]*	*[N/m^2]*	*[N/m^2]*	*[N/m^2]*	*[N/m^2]*	*[N/m^2]*
1	1.2	0.024	146.70855	6.961	15.58	0.002938	0	0
2	1.26	0.0252	146.70855	7.673	16.36	0.003171	0	0
3	1.25	0.025	156.48912	7.552	16.23	0.003132	0	0
4	1.02	0.0204	136.92798	5.032	13.24	0.002288	0	0
5	1.22	0.0244	156.48912	7.194	15.84	0.003015	0	0
6	1.1	0.022	127.14741	5.851	14.28	0.002568	0	0
7	1.1	0.022	127.14741	5.851	14.28	0.002568	0	0
8	3.02	0.0604	195.6114	44	39.21	0.01365	0	0
9	3.02	0.0604	195.6114	44	39.21	0.01365	0	0
10	3.2	0.064	215.17254	49.4	41.55	0.01512	0	0
11	2.9	0.058	185.83083	40.58	37.65	0.01271	0	0
12	3.2	0.064	185.83083	49.4	41.55	0.01512	0	0
13	3	0.06	205.39197	43.42	38.95	0.01349	0	0
14	3.1	0.062	215.17254	46.36	40.25	0.0143	0	0
15	10.4	0.208	557.49249	521.4	135	0.1344	0	0
16	10	0.2	498.80907	482	129.8	0.1247	0	0
17	10	0.2	557.49249	482	129.8	0.1247	0	0
18	10.3	0.206	537.93135	511.4	133.7	0.1319	0	0
19	10	0.2	528.15078	482	129.8	0.1247	0	0
20	15	0.3	929.15415	1084	194.8	0.2724	0	0

Where the table indicates 0 it shows that the specific conditions of that equation were not satisfied and thus that the equation could not be used to calculate the pressure drop over the system. Please note that the Ergun and RUC equations do not show 0 as no specific conditions were specified in the literature but it can be easily seen in Table 31 that these two equations are also not defined in the tested flow ranges.

Using a graph as in Figure 25 is becomes easy to see which equation gives a more accurate representation of the measured pressure drop.

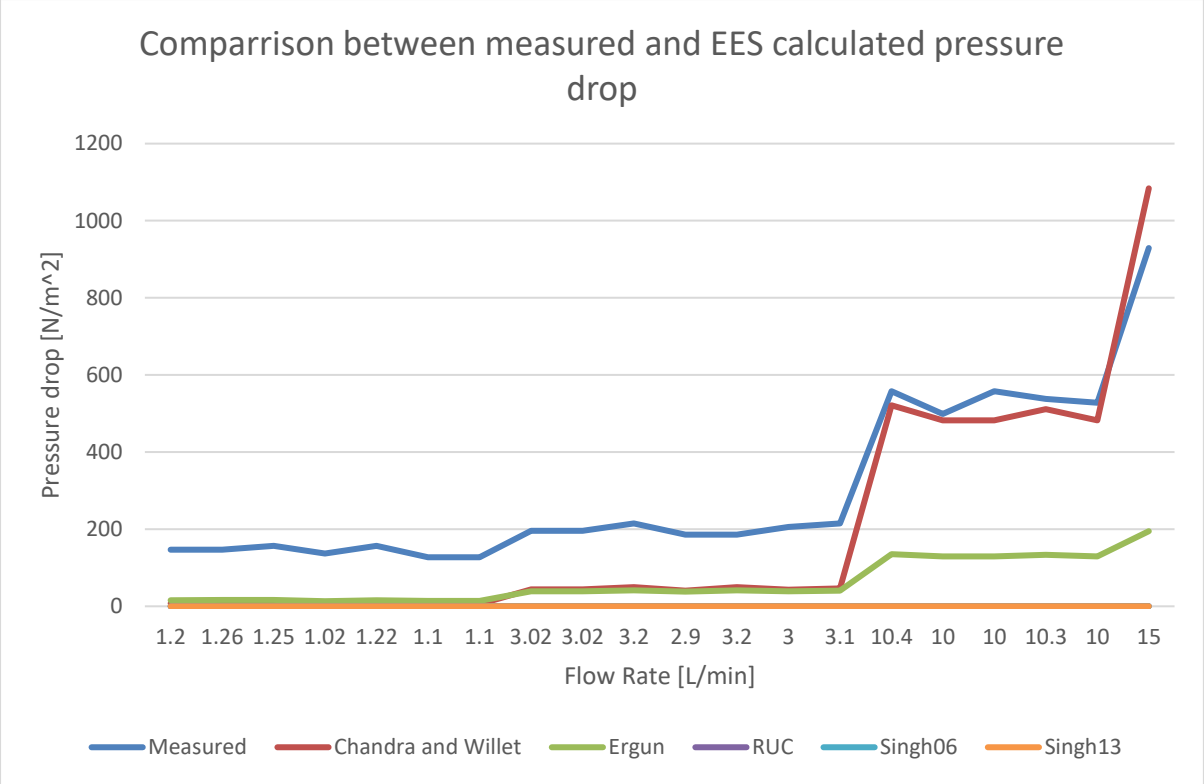

Figure 25: Comparison between measured and EES calculated pressure drop

After the examination of the graph it is clear to see that only Chandra and Willet's equation gives any short of accurate representation of the measured value, but only from a flow rate of about 10 *l/min*. The average deviation of Chandra and Willet's equation from the measured pressure drop for flow rates of 10 *l/min* have can be seen in Table 32. For flows below 10 *l/min* the Flow Correlation equation as per Figure 24 will be used.

Table 32: Average deviation between measured pressure drop and EES calculated pressure drop

Average deviation between measured pressure drop and EES calculated pressure drop				
Flow rate	**Measured**	**Chandra and Willet**	**Deviation**	**Percentage**
[L/min]	*[N/m^2]*	*[N/m^2]*	*[N/m^2]*	*[%]*
10.4	557.4	521.4	36.0	6%
10	498.8	482	16.8	3%
10	557.4	482	75.4	14%
10.3	537.9	511.4	26.5	5%
10	528.1	482	46.1	9%
15	929.1	1084	154.8	-17%

Using the available data, it will be more advantageous to use the equation derived from the measured data to make a prediction of the flow rate then using the equations as described in Section 4.1.4.

6.5 Energy store efficiency

In the calculation and interpretation phase the energy store efficiency table as seen in Table 26 is used. Three columns are added in Table 34: Energy store condition calculation table, being Time, Mass and Energy where the Time column is the time the experiment is running in minutes, the Mass column refers to the mass of water that has circulated into the system in the given time period. The equation used is as follows:

$$m_{HTF} = \frac{Flow}{3} \tag{139}$$

To calculate the mass of the water that has flown into the system the Flow is divided by 3 because the flow data are logged every 20 *s*.

The Energy column that is in Table 34 refers to the amount of energy that has flown into the system for that 20 *s* timespan. The equation used is as follows:

$$Q_{In} = (T1 - T5) \times c_{p_{HTF}} \times m_{HTF} \tag{140}$$

Where the T1 and T5 refers to the temperature at the 1st and 5th thermocouple. The $c_{p_{HTF}}$ =4.187 *kJ/kg.K* is the specific heat of water and m_{HTF} is the value in the Mass column.

By totalling all the answers in the Energy column for the whole charging period the total amount of energy that has entered the system can be calculated.

The same method is followed for calculating the amount of energy that was able to be extracted from the system - only difference is that is T5 minus T1. In an ideal experiment these two answers would be sufficient to calculate the efficiency of the storage system, but in practice there is energy that already in the system at the beginning of the experiment due to the STM having been heated up in previous experimental runs.

So, it is also necessary to calculate the amount of energy already in the system and add that to the amount of energy added to the system in this experimental run and then compare it to the amount of energy that could be extracted to get the efficiency of the system.

The amount of energy already in the heat storage material was calculated as follows:

$$Q_{In_{STM}} = (T2 - 23.7) \times m_{STM_{Elemnt}} \times \frac{NumberOfElements}{3} \times c_{s_{STM}} \quad (141)$$

Where the 23.7 *C* is the water temperature in the system as the experimental run starts. The number of elements is divided by 3 because this equation was done for T2, T3 and T4. This is to account for the temperature difference of the STM from the beginning to end of the storage system.

The amount of energy already in the heat transfer fluid was calculated as follows:

$$Q_{In_{HTF}} = (T5 - 23.7) \times c_{s_{HTF}} \times m_{HTF} \quad (142)$$

Where 23.7 °*C* is again there is the water temperature in the system as the runs starts and m_{HTF} is the mass of water inside the system as the runs starts.

Thus, by adding all three these answers to one another we are left with the total amount of energy in the system at the end of the charging cycle.

The next step is to compare the energy in and out to calculate the efficiency of the system. The results can be seen in Table 33 below.

Table 33: Final storage system efficiency results

Final storage system efficiency results			
Test	**In**	**Out**	**Efficiency**
	[kJ]	*[kJ]*	*[%]*
1	4829.9	3748.2	77.6
2	4390.4	3256.8	74.1
3	4633.0	3728.2	80.5
4	5917.6	4386.1	74.1
Average			76.5

Thus, the system has an efficiency of 76.5 %. This in layman's terms means that only 76.5 % of the energy that you put into the system can be extracted. It should be bore in mind that this efficiency is slightly lower than what it would have been with very low flow rates, approaching steady state condition. This experimental setup and procedure is more practically realistic since exaggerated transient conditions were mimicked. The rest of the energy has either been lost to the atmosphere furthermore, this the wort case scenario for practical overall efficiency.

Table 34: Energy store condition calculation table

Energy store transient condition data												
Date	**Time**	**Time**	**Status**	**T1**	**T2**	**T3**	**T4**	**T5**	**T6**	**Flow**	**Mass**	**Energy**
		Min		*Average*	*Average*	*Average*	*Average*	*Average*	*Average*	*Average*	*Average*	*Average*
				°C	*°C*	*°C*	*°C*	*°C*	*°C*	*L/min*	*kg*	*kJ*
20.11.2016	1:55:00	0	OK	51	40.4	34	36.2	51.4	13.9	2.719	0.906	1.518
20.11.2016	1:55:20	0.2	OK	50.3	40.5	34.1	36.3	51.2	13.9	2.716	0.905	3.412

6.6 Revised final design

Only now with the validation performed can the final design be done. This section will thus be focused on the calculations of the final dimensions of the thermal storage system.

As the same set of equations are being used as in Section 4.1 the table with the most important parameters have not been inserted again at each set of equations.

6.6.1 Storage material cost calculation

The equations used in this section is the same as per Section 4.1.1.

Table 35: Inputs for storage material cost calculation equations for final design

Symbol	Magnitude and unit	Description
Q_{in}	4804 [W.h]	Energy delivered by CSP on a clear day in March (received from the CSP designers).
$Q_{PumpDesigned}$	900 [W.h]	Energy consumed by bubble pump (received from the CSP designers).
T_{max}	140 [°C]	Maximum temperature in system (received from the CSP designers).
T_{min}	100 [°C]	Minimum temperature in system received from the CSP designers).
cp_{STM}	806.8 [J/kg.K]	Specific heat of the storage material (Section 6.1)
ρ_{STM}	9273.5 [kg/m^3]	Density of storage material (Section 6.2).
d_c	0.05 [m]	Side length of storage material cube (Burg Refractories).
CubePrice	14.26 [R]	Price of an individual cube (Burg Refractories).
MouldPrice	1800 [R]	Price of cube mould (Burg Refractories).
Housing	3000 [R]	Estimated price for manufacturing of storage system housing (estimated value).
Eff	76.5 [%]	Estimated effectivity of storage system (Section 6.5).

Table 36: Results for storage material cost calculation equations for final design

Symbol	Unit	Magnitude
$Q_{in6hours}$	[W]	28824
$Q_{pump1hourwatt}$	[W]	1126
$Q_{ToBeStored}$	[W]	166185
V_{STM}	[m^3]	0.3263
m_{STM}	[kg]	3026
V_{cube}	[m^3]	0.000125
m_{cube}	[kg]	1.159
PriceOfCubes	[R]	37219
HoursPumpCanRun	[h]	25.59
NumberOfCubes	[-]	2610

The most important design elements calculated in this section is the mass of storage material that will be needed (3026 *kg*). the number individual elements this equates to (2610) and the total volume of all these elements (0.03263 m^3). It can also be seen how long the pump can run solely for the thermal heat store (25.59 h)

6.6.2 Storage material housing size

The equations used in this section is the same as per Section 4.1.2.

Table 37: Inputs for storage housing size equations for final design

Symbol	Magnitude and unit	Description
D	0.327 [m]	Outside diameter of pipe.
N	2610 [-]	Number of cubes needed in storage system (Section 4.1.1).
d_c	0.05 [m]	STM cube side length (Burg Refractories).
Epsilon	0.61 [-]	Void fraction (Section 6.23.2.2).
t_{wall}	0.002 [m]	Pipe wall thickness (measured value).
H	0.1 [m]	Plenum size (measured value).

Table 38: Results for storage housing size equations for final design

Symbol	Unit	Magnitude
A_p	[m^2]	0.08197
L_p	[m]	6.428

The system will be housed in a standard size steel pipe. The inside diameter of this pipe is 323 *mm* and it has a wall thickness of 2 *mm*. This section calculates the total length needed of this pipe for the storage system (6.428 *m*).

6.6.3 Calculation of the maximum span between supports

The equations used in this section is the same as per Section 4.1.3.

Table 39: Inputs for calculation of the maximum span between supports equations for final design

Symbol	Magnitude and unit	Description
ρ_{STM}	9273.5 [kg/m^3]	Density of storage material (Section 6.3).
ρ_{HTF}	1000 [kg/m^3]	Density of heat transfer fluid.
ρ_{pipe}	7850 [kg/m^3]	Density of pipe material.
ε	0.61 [-]	Void fraction of packing configuration (Section 6.2).
S_a	115.1e3 [kPa]	Allowable stress in pipe.
$E_{Constant}$	0.7 [-]	Quality factor from ASME B31.3 Table A-1A or A-1B.
$Y_{constant}$	0.4 [-]	Coefficient of material from ASME B31.3.
w_{con}	0 [N]	Concentrated weight on pipeline.
C_a	0 [m]	Corrosion allowance.
E	195122e3 [kPa]	Modulus of elasticity of pipe.
t_c	0.002 [m]	Pipe wall thickness (measured value).
D_{pipeO}	0.327 [m]	Outside diameter of pipe (measured value).
P_{pipeI}	101 [kPa]	Pressure inside storage system.

Table 40: Results for calculation of the maximum span between supports equations for final design

Symbol	Unit	Magnitude
t	[m]	0.0000002050
L	[m]	3.584
y_a	[m]	0.005974
y	[m]	0.001451

This section calculates the maximum space between the support struts (3.584 *m*).

6.6.4 System charging time

The equations used in this section is the same as per Section 4.1.5.

Table 41: Inputs for system pressure drop equations for final design

Symbol	Magnitude and unit	Description
D_{pipei}	0.347 [m]	Inside diameter of STM housing (measured value).
$D_{particle}$	0.05 [m]	STM particle diameter (Burg Refractories).
ϵ	0.61 [-]	Void fraction. (Section 6.2)
x_f	0.197 [-]	Frictional fraction of total pressure drop.
Pr	2.99 [-]	Fluid Prandtl number.
k_f	0.609 [W/mK]	Fluid thermal conductivity.
L	6.42 [m]	Flow-wise length of the bed (Section 6.6.3).
k_s	0.8 [W/mK]	Rock/solid (STM) thermal conductivity.
c_s	806.77 [J/kgK]	Specific heat capacity of rock/solid (Section 6.1).
$\dot{m}_f$	0.017 [kg/s]	HTF flow rate.
ρ_s	9273.5 [kg/m^3]	Rock/solid (STM) density (Section 6.3).
m_s	3026 [kg]	Mass of STM in system (Section 6.6.1).
P_a	101 [kPa]	Ambient pressure.
T_f	100 [C]	Inflow temperature of HTF (received from the CSP designers).

Table 42: Results for system pressure drop equations for final design

Symbol	Unit	Magnitude
Time for all STM to heat up	[hours]	74.67

This section calculates the number of sunshine hours that will be needed to fully charge the thermal storage system (74.67 *h*).

6.7 Revised heat store containment design

The thermal heat stores design is based on the design in Section 4.2 that was used to build the test setup. Again, the pipe that will be used will be a mild steel pipe with an inside diameter of 323 *mm* and a wall thickness of 2 *mm.* The same flange and endplate configuration will be used.

From Section 6.6.2 it can be seen that the total length of pipe needed to house the appropriate amount of storage material is 6.428 *m.* Due to the fact that there is only an area of 3.5 *m* by 1.25 *m* by 1.25 *m* available to mount the system on the mobile rig the final design will be a stacked system. This entails that two units of exact same length are to be made and stacked on top of each other. They are then connected to each other with pipes in order to function as one long inline system. The plenum size is also made smaller to 0.05 *m* at each end of each unit in order to save some space.

A representation of the system can be seen in Figure 26.

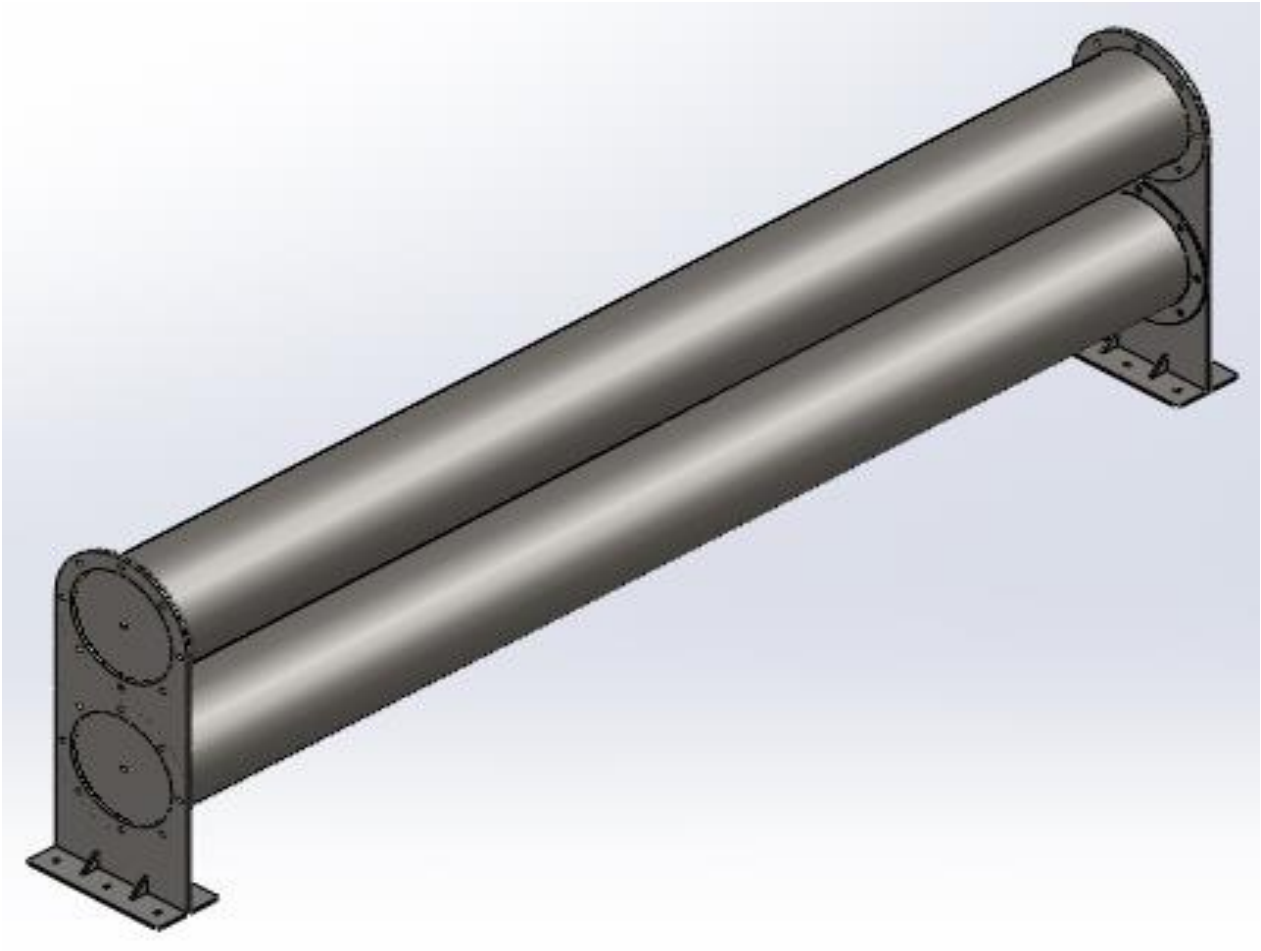

Figure 26: Solid Works model of final design of thermal storage system

When looking at results obtained in Section 6.6.3 it was estimated that only two struts will be needed one on each this is due to the fact that each unit is 3.314 m long and the maximum span between supports can be 3.584 m.

The units can be broken down into as smaller sections if need be to facilitate with setup ext. All these smaller sections can then be bolted together to eventually provide the same configuration in the figure above.

The detailed design drawing can be found in Appendix G.

---

7 Conclusion and recommendations

For solar power aqua ammonia heat pumps to become a viable alternative the system needs to be optimized. The team under Prof. C.P. Storm has made good headway in achieving this goal. The system has been optimized by determining an optimum generator temperature for each varying system pressure which in turn leads to relatively low energy requirement to function. The system is made up of several sub systems. This dissertation focuses specifically on the thermal storage system that allows the heat pump to run continuously 24 *h* a day.

As the thermal heat storage system is one of the sub systems associated with the solar power aqua ammonia heat pump there were several fixed parameters that needed to be used in the design.

These include:

- The amount of energy available for storage (30 *kW.h* for 6 hours a day).
- The temperature range in which the energy is to be stored (60-140 °*C*).
- The energy needed by the aqua ammonia heat pump (0.9 *kW.h*).
- The flow rate of the HTF from the solar collectors (1-3 *l/min*).
- The area available on the mobile test rig to mount the heat store in.
- The heat transfer fluid to be used (a water glycol mixture in the full-scale setup and water in the experiments). A water glycol mixture was chosen as the water gives the heat transfer fluid a very high specific heat capacity and the glycol increases the boiling temperature of the water to above 140 °*C*.

Given the limitations as mentioned above a thermal heat store was designed that is able to power the aqua ammonia heat pump for 25.59 *h* on one charge. This was done using cubic spinel elements packed in a rhombohedral pattern in cylindrical housings with a combined length of 6.428 *m* as seen in Section 6.6.6.

7.1 Conclusions

7.1.1 Design

The design of the full-scale storage system has been done (Section 6.6) based on extrapolated data from the scaled test model. The test model was not a dimensionally scaled down model, but just 15 *%* of the size of the full-scale system regarding length/mass of system. This was done due to the limited budget available for the project.

7.1.2 Storage material shape

The cubical shape and the 0.05 *m* side length of the material is adequate as per the test results.

7.1.3 Detailed design equations

All EES programs namely the storage material cost calculation, storage material cost calculation, storage material housing size, calculation of the maximum span between supports and pressure drop calculations used were verified with Excel. The validation for the pressure drop calculations, however, only correlated with the Chandra and Willet's equation for flows over 10 *l/min*. For lower flow rates the derived equation can be used.

7.1.4 Experimental setup

The specific thermal heat storage of the storage material, storage system void fraction, storage material density, pressure difference over storage system and energy store efficiency experimental setups all worked as planned. The experimental data gathered during pressure difference over storage system test correlated with the Chandra and Willet's equation for the calculation of the pressure drop over the system as mentioned in Section 7.1.3.

7.1.5 Test results

A summary of the final tests results can be found in Table 43.

Table 43: Summery of all test results

Specific heat capacity of material	806.8 *J/kg.K*
Storage system void fraction	0.61
Storage material density	9273.5 kg/m^3
Pressure difference of system	$\Delta P\ [Pa]\ = 124.075 + 15.5055 Flow + 2.51218 Flow^2$
Energy store efficiency	76.5 %

The specific heat capacity of the chosen material was tested to be 806.8 *J/kg.K* which is in line with the predicted 800-820 *J/kg.K* for spinel (Markgraaff, 2010:10).

The storage system void fraction is measured to be 0.61 which is higher than the normal 0.27 (Singh *et al.*, 2013:23) for rhombohedral packing. This is due the fact that near the middle of the system it was not possible to keep the same packing pattern.

The storage material density was calculated to be 9273.5 kg/m^3 which is again in line with the expected 9200-9600 kg/m^3 for spinel (Markgraaff, 2010:10).

The Chandra and Willet equation as per *Tesfay & Venkatesan* is the only pressure drop equation that correlates with the test data. This correlation also only happens when the heat transfer fluid has a flow of 10 *l/min* and more. Where the equation has a 7.4 % deviation from the measured value at a flow of 10 *l/min*. Thus, rather than using one of the equations as listed in Section 3.3an equation was rather formulated using the data gathered during the experiment to be used for further pressure drop predictions.

The overall efficiency of the thermal storage system was found to be 76.5 % which is relatively close to the efficiency of 82.5 % (Kantole, 2012:75) found in the literature consulted.

7.2 Recommendations

7.2.1 Storage material shape

Although the test indicated that a cubic shape will work for the storage material, further study into the storage material shape can be advised. This is advised in order to help lower the manufacturing costs even further as well as to limit the void fraction in the storage material. Through consultation with Mr P. Burger of Burg Refractories and Prof C.P. Storm it was concluded that one of the shapes that might need further investigation is a cuboid.

7.2.2 Experimental setup

Once the full-scale rig is built it will have to be commissioned in any case. This will serve as a full-scale test based on the partial massed test in this document (Chapter 5). It is expected that the full-scale model will have an improved performance as compared to the test setup. This will be due to the greater mass of storage material (with the same diameter) that would cause a more gradual ΔT over the individual blocks for the same energy and overall ΔT. Also, the actual setup can be configured to have a counter flow heat transfer mode between storage and recovery.

8 References and Bibliography

8.1 References

Anon. 2014a. *Australian sun energy*. http://www.australiansunenergy.com.au/stratification-water-tanks/ Date of access: May 5. 2015.

Anon. 2014b. How to determine the spesific heat of a substance. http://www.chemteam.info/Thermochem/Determine-Specific-Heat.html Date of access: September 27. 2016.

Camacho, E.F., Berenguel, M., Rubio, F.R. & Martínez, D. 2012. Control of solar energy systems. Berlin: Springer Science & Business Media.

David, I. 2015. How does a RV refrigerator work? . http://www.ehow.com/how-does_4572467_rv-refrigerator-work.html Date of access: May 5. 2015.

Department Of Electrical Engineering Indian Institute of Technology. 2008. 40 lessons on refrigeration and air conditioning from iit kharagpur. useful training material for mechanical engineering students college, or as reference for engineer. 1st ed. India: Department Of Electrical Engineering Indian Institute of Technology.

Duffie, J.A. & Beckman, W.A. 2013. Solar engineering of thermal processes. 4th Ed ed. Hoboken, New Jersey: John Wiley.

Engineers Edge. 2017. Manometer application equation for pressure. http://www.engineersedge.com/fluid_flow/manometer_application_equation_13257.htm Date of access: Januaries 21. 2017.

Henry, A. & Prasher, R. 2015. The prospect of high temperature solid state energy conversion to reduce the cost of concentrated solar power. *Energy & environmental science,* (6):1819.

Kantole, J.B. 2012. Modelling and design of a latent heat thermal storage system with reference to solar absorption refrigeration. Johannesburg: University of Johannesburg. (Masters: Mechanical Engineering).

Kenneth, G.A. 2010. Performance characteristics of packed bed thermal energy storage for solar thermal power plants. University of Stellenbosch: University of Stellenbosch. (Master of Science in Engineering).

Kumar V, P. & Sharma, M. 2014. Analysis of heat transfer fluids in concentrated solar power (CSP). *International journal of engineering research and technology,* 3(12):239-240.

Markgraaff, J. 2010. High-temperature heat transfer characterisation of castable shaped ceramics for thermal energy storage. 2-33. (Unpublished).

Sharma, A., Tyagi, V.V., Chen, C.R. & Buddhi, D. 2009. Review on thermal energy storage with phase change materials and applications. *Renewable and sustainable energy reviews,* 13(2):318-345.

Singh, H., Saini, R.P. & Saini, J.S. 2013. Performance of a packed bed solar energy storage system having large sized elements with low void fraction. *Solar energy,* (87):22-24.

Smith, J. 2011. Manometer. http://www.instrumentationtoday.com/manometer/2011/09/ Date of access: March 8. 2017.

Srikhirin, P., Aphornratana, S. & Chungpaibulpatana, S. 2001. A review of absorption refrigeration technologies. *Renewable and sustainable energy reviews,* 5(4):343-372.

Stine, W.B. & Geyer, M. 2001. Power from the sun. http://www.powerfromthesun.net/book.html Date of access: September 20. 2016.

Tamme, D.R., Laing, D., Steinmann, W. & Bauer, T. 2012. Thermal energy storage. (In Anon. Encyclopedia of sustainability science and technology. Meyers, Robert A. ed. Springer New York. p. 10551-10577).

Tesfay, M. & Venkatesan, M. 2013. Simulation of thermocline thermal energy storage system in C. *International journal of innovation and applied studies,* 3(2):354-360.

Ullah, K.R., Saidur, R., Ping, H.W., Akikur, R.K. & Shuvo, N.H. 2013. A review of solar thermal refrigeration and cooling methods. *Renewable and sustainable energy reviews,* 24(0):499-513.

Vakharia, D.R. & Farooq A, M. 2009. Determination of maximum span between pipe supports using maximum bending stress theory. *International journal of recent trends in engineering,* 1(6):46-48.

van der Walt, S. 2012. The design and optimisation of a bubble pump for an aqua-ammonia diffusion absorption heat pump. Potchefstroom: North-West University. (Masters: Mechanical Engineering).

.

8.2 Bibliography

Auwerda, G., Kloosterman, J., Winkelman, A., Groen, J. & Van Dijk, V. 2010. Comparison of experiments and calculations of void fraction distributions in randomly stacked pebble beds. *Advances in reactor physics to power the nuclear renaissance, 9-14.*

BAE Resources. 2011. Standards – pipe schedules chart. http://baeresources.com/downloads/pipe-charts/ Date of access: July 1. 2015.

Dincer, I. & Rosen, M.A. 2011. Thermal energy storage. 7th ed. United Kingdom: John Wiley & Sons.

Heller, L. & Gauche, P. 2012. Rock bed storage-based simulation of a 5mwe combined cycle solar power plant. South African solar energy conference, Stellenbosch, May 21-23. http://scholar.sun.ac.za/handle/10019.1/83969 Date of access: June 11, 2015.

Kalaiselvam, S. & Parameshwaran, R. 2014. Thermal energy storage technologies for sustainability. 3rd ed. USA: Elsevier.

Kalogirou, S.A. 2014. Solar energy engineering processes and systems. 2nd ed. United States of America: Elsevier.

Kuppan, T. 2000. Heat exchanger design handbook. 1st ed. New York: Marcel Dekker.

Modi, A. & Perez-Segarra, C.D. 2014. Thermocline thermal heat storage systems for concentrated solar power plants: One-dimensional numerical model and comparative analysis. Solar energy, 100(1):84-93.

Subramanian, R.S. 2015. Heat transfer to or from a fluid flowing through a tube. https://www.studystandard.com/document/heat-transfer-to-or-from-a-fluid-flowing-through-a-tube-in-flow-through-conduits-r-shankar-subramanian-126932.html Date of access: October 10. 2015.

van Antwerp, W. 2009. Modelling the effective thermal conductivity in the near-wall region of a packed pebble bed. Potchefstroom: North-West University. (Doctor of Philosophy).

9 Appendices

9.1 Appendix A

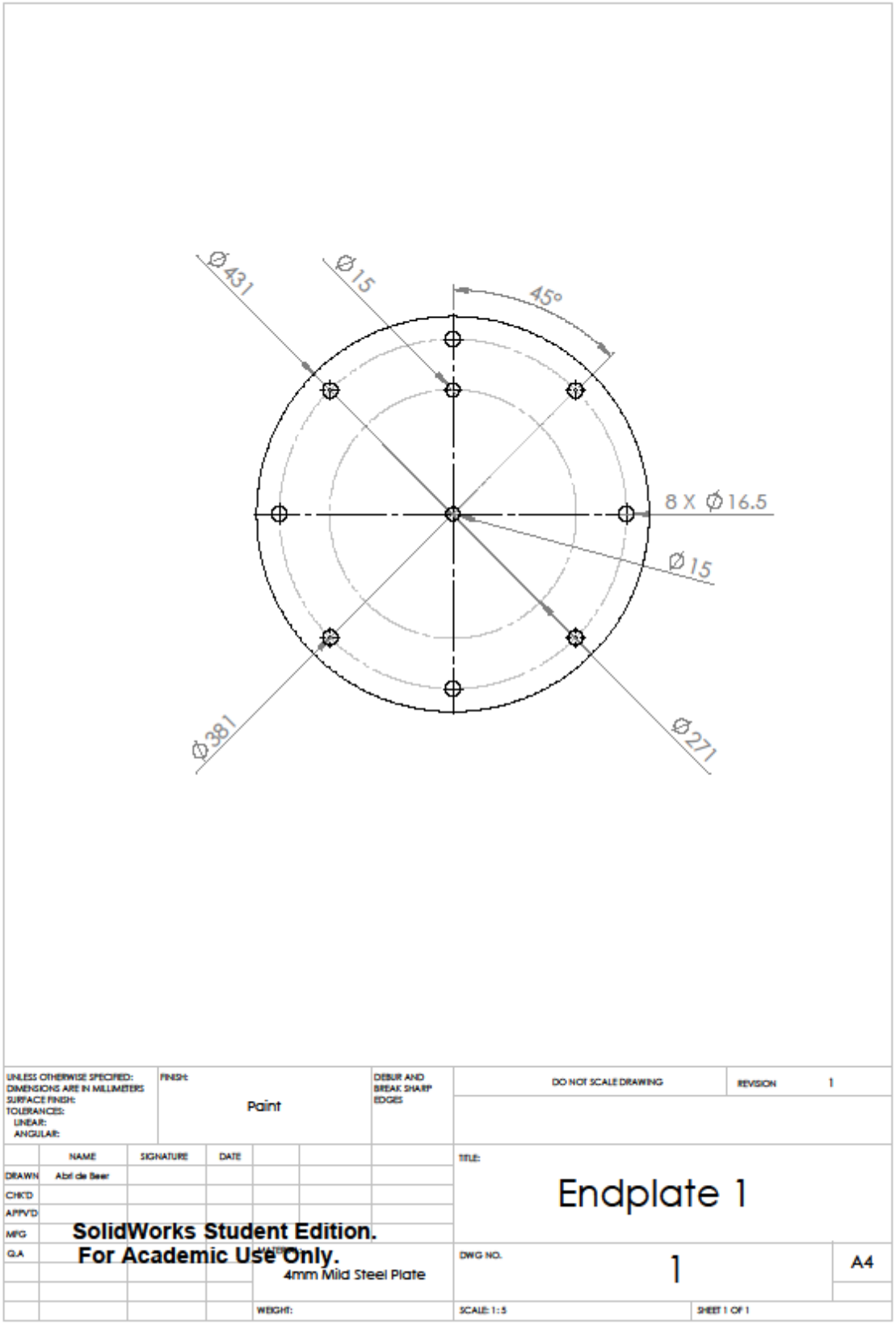

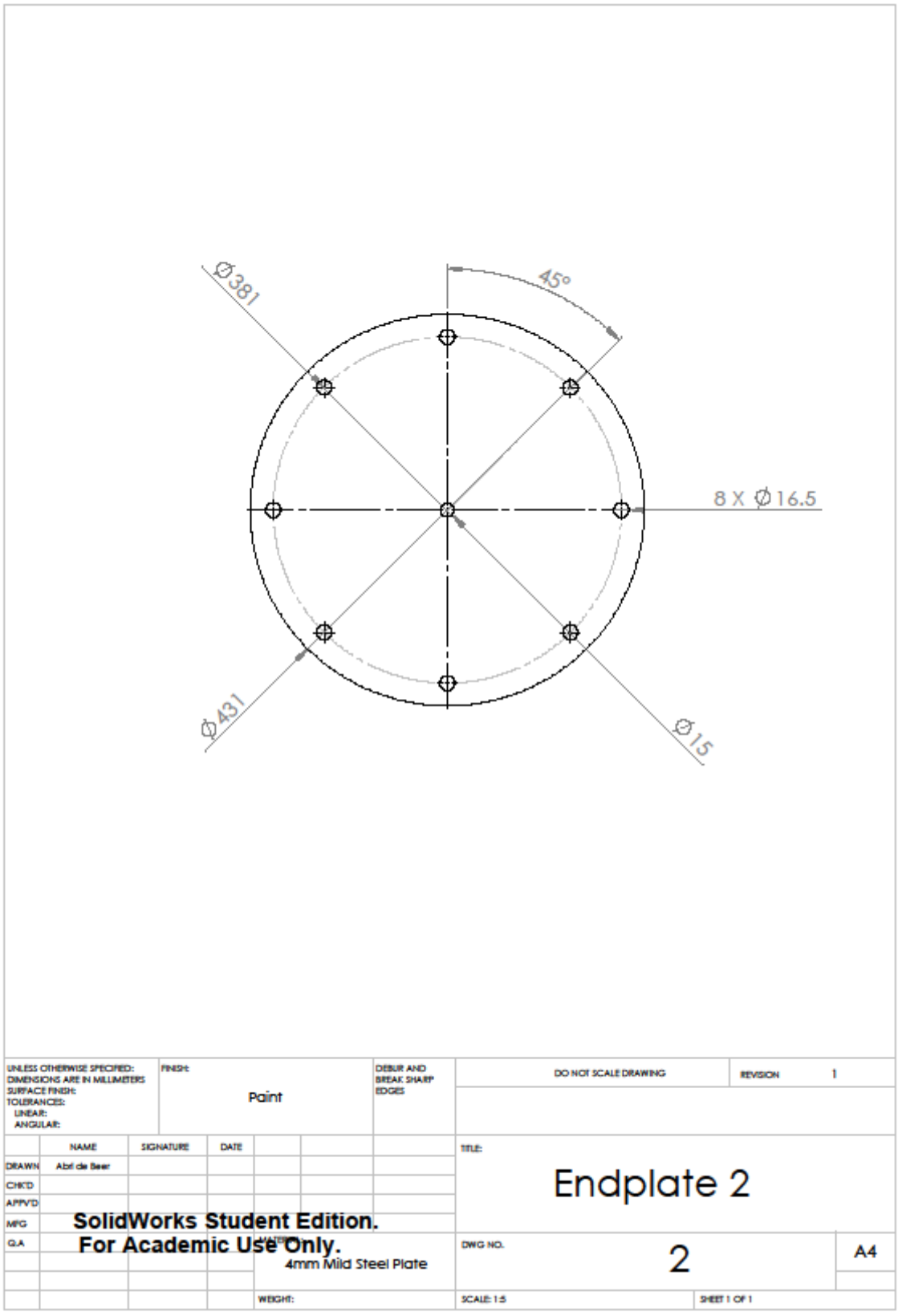
Ø381
45°
8 X Ø16.5
Ø431
Ø15
UNLESS OTHERWISE SPECIFIED:
DIMENSIONS ARE IN MILLIMETERS
SURFACE FINISH:
TOLERANCES:
LINEAR:
ANGULAR:
FINISH:
Paint
DEBUR AND BREAK SHARP EDGES
DO NOT SCALE DRAWING
REVISION 1
NAME
SIGNATURE
DATE
DRAWN Abri de Beer
CHK'D
APPV'D
MFG
Q.A
MATERIAL:
4mm Mild Steel Plate
WEIGHT:
TITLE:
Endplate 2
DWG NO.
2
A4
SCALE: 1:5
SHEET 1 OF 1
SolidWorks Student Edition.
For Academic Use Only.

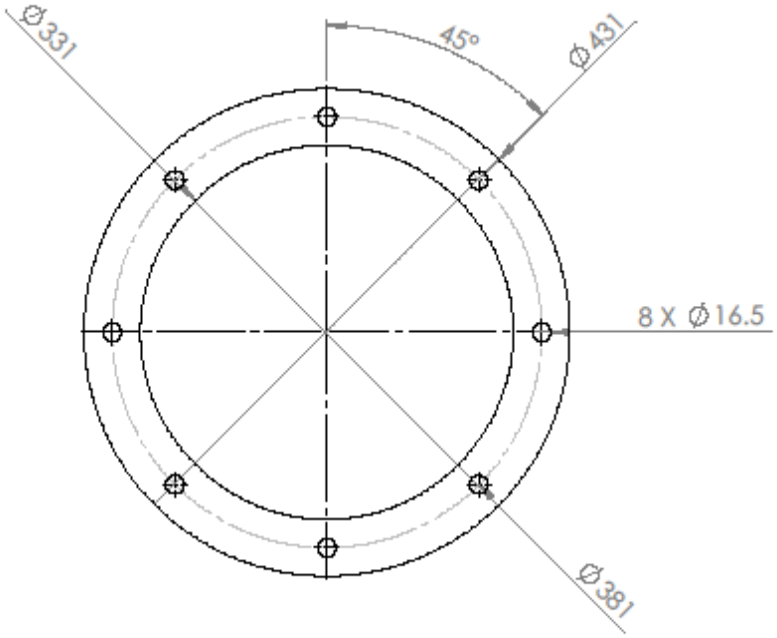

UNLESS OTHERWISE SPECIFIED: DIMENSIONS ARE IN MILLIMETERS SURFACE FINISH: TOLERANCES: LINEAR: ANGULAR:		FINISH: Paint		DEBUR AND BREAK SHARP EDGES	DO NOT SCALE DRAWING	REVISION 1	
	NAME	SIGNATURE	DATE		TITLE: Flange		
DRAWN	Abri de Beer						
CHK'D							
APPV'D							
MFG							
Q.A					DWG NO. 3		A4
				MATERIAL: 4mm Mild Steel Plate			
				WEIGHT:	SCALE: 1:5	SHEET 1 OF 1	

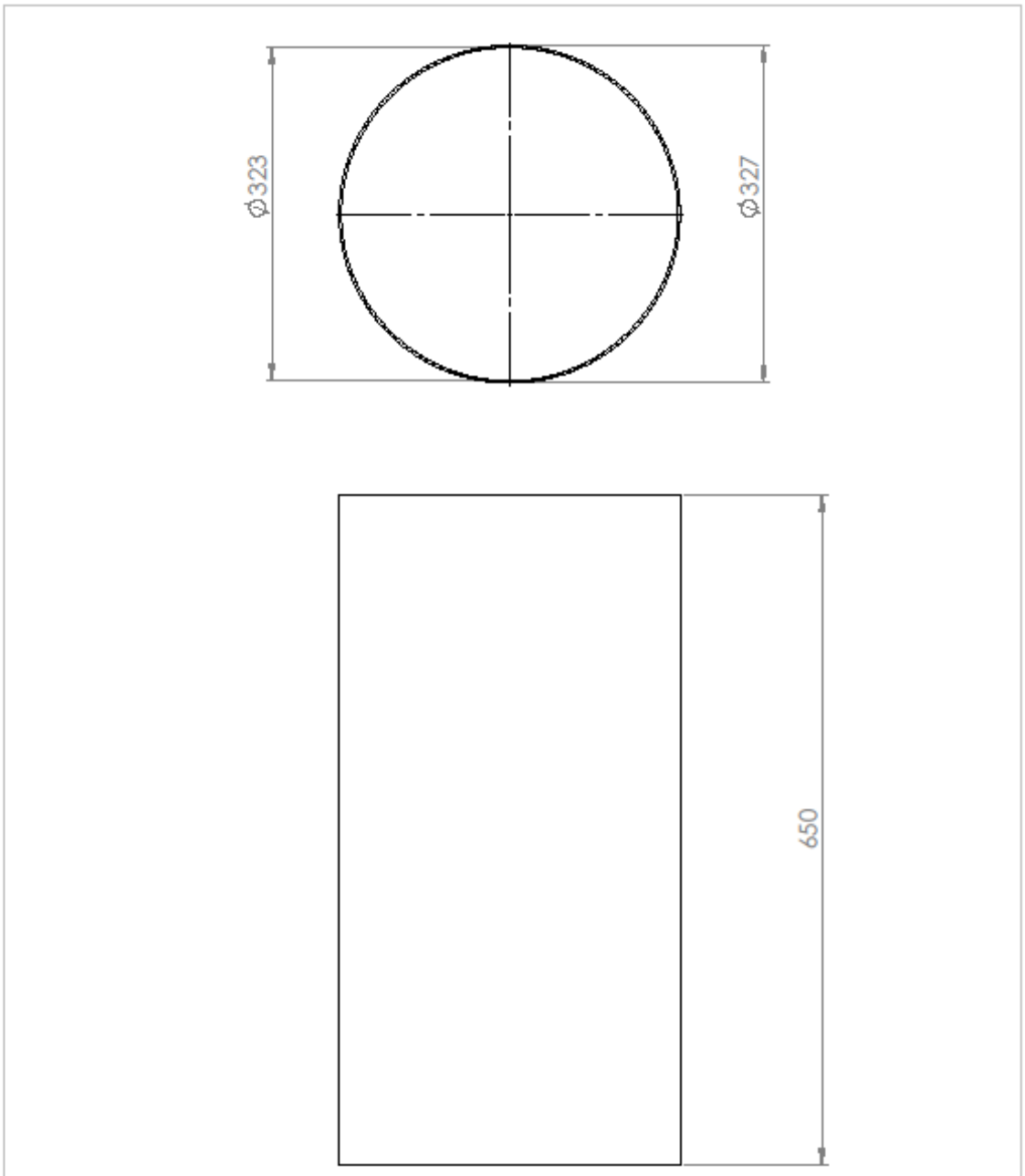
Φ323
Φ327
650
UNLESS OTHERWISE SPECIFIED:
DIMENSIONS ARE IN MILLIMETERS
SURFACE FINISH:
TOLERANCES:
LINEAR:
ANGULAR:
FINISH:
Paint
DEBUR AND BREAK SHARP EDGES
DO NOT SCALE DRAWING
REVISION 1
NAME
SIGNATURE
DATE
DRAWN
Abri de Beer
CHK'D
APPV'D
MFG
Q.A
MATERIAL:
Mild Steel
WEIGHT:
TITLE:
Pipe
DWG NO.
4
A4
SCALE: 1:5
SHEET 1 OF 1
SolidWorks Student Edition.
For Academic Use Only.

9.2 Appendix B

Experimental procedure

Specific heat of storage material

1. Pour 0.075 *kg* in a beaker.
2. Weigh a small piece of storage material approximately 20 *g* (it can be any shape).
3. Use oven to heat the material to 150 °*C*.
4. While material is heating, measure temperature of water in another beaker and note it.
5. After 15 *min* quickly remove material from oven and insert into the beaker.
6. Continually monitor water temperature until it stabilizes and note the temperature.

Storage system void fraction

1. Measure exact volume of housing to be filled by storage material.
2. Make sure all the taps that might lead the housing to leak are firmly closed.
3. Pack the storage material in desired configuration till the whole housing volume is filled.
4. Use a 2 *l* measuring cylinder to begin and fill the housing with water.
5. Fill the housing to the top and work out what volume of water it took to fill the housing.

Storage material density

1. Use a vernier calliper to measure the exact length, width and height of the STM element.
2. Make use of a suitable accurate scale to measure the mass of the STM element that was measured using the vernier calliper.

Pressure difference over storage system

1. Use the efficiency test rig.
2. Close valves 1 to 6.
3. Connect municipal water supply to valve 2.
4. Open valves 2, 4 and 5.
5. Open the municipal water.
6. Use valve 3 to throttle the flow to desired magnitude.
7. Read the pressure difference in mm of the manometer.

Energy store efficiency

Charging system

1. Close all valves in the system.
2. Switch on geyser.
3. Let geyser warm up till desired temperature.
4. When geyser is on temperature open valves 1, 3, 4 and 6 all the way.
5. Switch on circulation pump.
6. Throttle flow using valve 1 until flowmeter 1 measured desired flow.
7. Leave experiment until all thermos couples in system give the same reading.

Discharging system

1. Close all valves in the system.
2. Connect water from house plumbing line to connection point 1.
3. Open valves 2, 3, 4 and 5 completely.
4. Throttle flow using valve 3 until flowmeter 1 measured desired flow.
5. Leave experiment until all thermos couples in system give the same reading.

9.3 Appendix C

Calibration of measuring instruments

The thermocouples used in the experiment were type T. These were used in combination with the Memograph M RSG 40 Endress+Hauser data logger.

Before testing commenced all thermocouples where calibrated using a 2-step process with the help of Mr. Willem van Tonder at the Mechanical Engineering Laboratories at the NWU.

The first step is to make an ice slush - as we know that this slush will be at a constant 0 °*C*. All the points of the thermocouples were then bound together thus eliminating any temperature differences that might occur in the slush. All the thermocouples were then manually set to 0 °*C*.

After the thermocouples, had been manually set, a heating element with a calibrated adjustable thermostat was used in the second part of the calibration process. The thermostat was first set to 10 *C* when the water reached the desired temperature the temperature of the thermocouples was noted. This was again done at 20 °*C*. The following pictures show an example of what step 2 of the calibration looked like.

The flow meter was bought new and factory calibrated.

Programmable thermostat with heating element used in calibration

Example of step 2 of the calibration process

9.4 Appendix D

Risk assessments

Specific heat of storage material

Storage material for specific heat experiments risk assessment

Potential hazard	Preventative measures
Beaker breaking while heating.	1. Make sure only SABS approved beakers are used. 2. Make sure beaker doesn't boil dry. 3. Use applicable protective clothing.
Burns from oven.	1. Use suitable tongs to handle material sample. 2. Use applicable protective clothing.

Storage system void fraction

Storage system void fraction experiment risk assessment

Potential hazard	Preventative measures
System falling over when water and storage material are added.	1. Never work underneath system when it has been fully loaded. 2. Make sure the supports are firmly in place before loading in the storage material and water.

Storage material density

Density of storage material experiment risk assessment

Potential hazard	Preventative measures
Storage elements following on one's feet.	1. Make sure to wear safety boots.

Pressure difference over storage system

Pressure difference over storage system experiment risk assessment

Potential hazard	Preventative measures
Storage elements falling on one's feet.	1. Make sure to wear safety boots.

Energy store efficiency

Energy store efficiency experiments risk assessment

Potential hazard	Preventative measures
Burns from hot water pipes.	1. Make sure pipes are suitably insulated. 2. Use applicable protective clothing.
Bursting hot water geyser.	1. Make sure geyser is fitted with appropriate safety features. This includes pressure valves and overflow.
The risk of storage system falling over.	1. Do not ever work underneath the storage system while it is fully loaded.

9.5 Appendix E

TSS SOLAR DC CIRCULATION PUMP

Specifications

Voltage: 8V-24V DC (Standard:12V DC)
Max Flow Rate: 12 L/Min
Max Water Head: 3M
Brass 1/2" BSP / NPT male Inlet/Outlet
Max system pressure: 10Bar
Max working temperature: 110℃ (230° F)

Application

The TS5 solar DC pump can be used for most circulation pump applications without connection to the power grid. Highly efficient, the TS5 can be connected directly to a photovoltaic panel and is characterized by its small size, high efficiency, and extreme low power consumption.

The long life brushless motor technology provides maintenance free and quiet service life.

This pump is perfect for single family home thermal solar systems or any circulation pump application where conventional power is not available.

Features

- DC brushless motor with energy efficient technology by micro processor
- Soft start at very low in-rush current, good convenient working directly with PV panel
- Durable permanent magnetic rotor/impeller and fine ceramic shaft
- Advanced magnetic drive technology for static-impeller, without any leakage for ever
- Long life brushless pump, ideal life for 30000 hours
- Heavy duty work, can sustain continual 24 hours' work
- Automatic overload protection
- Automatic over-temperature protection
- Automatic dry-running protection
- Low or no maintenance
- Low power consumption

Areas of use

Hot Water Circulation
Radiant Floor Heating
Solar Applications
Liquid Transfer
General Purpose Pumping

9.6 Appendix F

Run 2 charging cycle test data

Date	Time	Time	Status	T1	T2	T3	T4	T5	T6	Flow
		Min		Average	Average	Average	Average	Average	Average	Average
				°C	°C	°C	°C	°C	°C	L/min
20.11.2016	10:43:20	0	OK	42.4	20.4	19.8	19.8	20.9	21.4	1.211
20.11.2016	10:43:40	0.2	OK	65.8	20.4	19.9	19.8	20.5	21.3	0.953
20.11.2016	10:44:00	0.4	OK	69.4	20.4	19.9	19.9	20.4	21.4	1.264
20.11.2016	10:44:20	1	OK	70.5	20.4	19.9	19.9	20.4	21.6	0.974
20.11.2016	10:44:40	1.2	OK	70.9	20.5	20	20	20.4	21.7	1.087
20.11.2016	10:45:00	1.4	OK	71.1	20.5	20	20	20.4	21.6	1.421
20.11.2016	10:45:20	2	OK	71.4	20.6	20	20	21	22.1	1.513
20.11.2016	10:45:40	2.2	OK	71.2	20.7	20.1	20.1	21.4	22.7	1.358
20.11.2016	10:46:00	2.4	OK	71	20.8	20.1	20.1	22.6	22.3	1.003
20.11.2016	10:46:20	3	OK	70.7	20.9	20.2	20.2	29.7	22.1	0.72
20.11.2016	10:46:40	3.2	OK	70.6	21.2	20.2	20.2	29.7	21.9	1.068
20.11.2016	10:47:00	3.4	OK	71.3	21.4	20.2	20.3	30.6	21.9	1.337
20.11.2016	10:47:20	4	OK	71.5	21.7	20.3	20.4	30.6	22.1	1.779
20.11.2016	10:47:40	4.2	OK	71.5	22	20.3	20.5	31.6	22.4	2.141
20.11.2016	10:48:00	4.4	OK	71.4	22.4	20.4	20.6	34.9	22.8	6.44
20.11.2016	10:48:20	5	OK	71.1	22.8	20.4	20.7	37.1	22.7	3.802
20.11.2016	10:48:40	5.2	OK	70.8	23.2	20.4	20.9	43.5	22.2	3.692
20.11.2016	10:49:00	5.4	OK	70.8	23.6	20.4	21	45	22.1	3.187
20.11.2016	10:49:20	6	OK	70.9	24	20.5	21.1	45.7	22.3	3.025
20.11.2016	10:49:40	6.2	OK	70.9	24.5	20.5	21.3	47.8	22.2	3.018
20.11.2016	10:50:00	6.4	OK	71	24.9	20.5	21.5	49.7	22.7	3.011

20.11.2016	10:50:20	7	OK	70.9	25.4	20.5	21.7	51.4	22.8	3.005
20.11.2016	10:50:40	7.2	OK	70.9	25.8	20.5	21.8	52.3	23.1	3.001
20.11.2016	10:51:00	7.4	OK	70.9	26.3	20.5	22.1	53	22.9	2.999
20.11.2016	10:51:20	8	OK	70.8	26.8	20.6	22.4	54.4	22.7	2.991
20.11.2016	10:51:40	8.2	OK	70.8	27.2	20.6	22.6	55.4	22.8	2.99
20.11.2016	10:52:00	8.4	OK	71	27.7	20.7	22.9	56.1	22.7	2.985
20.11.2016	10:52:20	9	OK	71	28.2	20.7	23.1	57	23	2.98
20.11.2016	10:52:40	9.2	OK	70.8	28.6	20.8	23.5	57.4	22.9	2.981
20.11.2016	10:53:00	9.4	OK	70.8	29.1	20.9	23.9	58	23.5	2.981
20.11.2016	10:53:20	10	OK	70.8	29.5	20.9	24.2	58.5	23.6	2.98
20.11.2016	10:53:40	10.2	OK	70.8	30.1	21	24.5	58.8	22.8	2.966
20.11.2016	10:54:00	10.4	OK	70.8	30.6	21.1	24.9	59.2	23.1	2.966
20.11.2016	10:54:20	11	OK	70.7	31	21.1	25.1	59.3	23.1	2.957
20.11.2016	10:54:40	11.2	OK	70.7	31.4	21.1	25.4	59.5	23.3	2.954
20.11.2016	10:55:00	11.4	OK	70.7	31.8	21.2	25.7	59.6	23.7	2.962
20.11.2016	10:55:20	12	OK	70.7	32.2	21.3	26.2	59.7	23.7	2.955
20.11.2016	10:55:40	12.2	OK	70.7	32.7	21.4	26.6	59.9	24	2.895
20.11.2016	10:56:00	12.4	OK	70.7	33.1	21.6	27	59.9	23.9	2.819
20.11.2016	10:56:20	13	OK	70.7	33.5	21.7	27.3	60.1	23.5	2.959
20.11.2016	10:56:40	13.2	OK	70.7	33.9	21.6	27.6	60.2	23.6	2.955
20.11.2016	10:57:00	13.4	OK	70.6	34.3	21.7	27.9	60.4	23.7	2.945
20.11.2016	10:57:20	14	OK	70.6	34.7	21.9	28.3	60.4	23.6	2.948
20.11.2016	10:57:40	14.2	OK	70.6	35.1	22	28.6	60.6	23.2	2.949
20.11.2016	10:58:00	14.4	OK	70.7	35.5	22.1	28.9	60.9	23.3	2.94
20.11.2016	10:58:20	15	OK	70.6	35.9	22.1	29.3	60.9	23.2	2.945
20.11.2016	10:58:40	15.2	OK	70.6	36.2	22.3	29.6	61	23.3	2.938
20.11.2016	10:59:00	15.4	OK	70.5	36.6	22.4	30	61.1	23.7	2.941
20.11.2016	10:59:20	16	OK	70.5	37.1	22.6	30.4	61.2	23.5	2.94

20.11.2016	10:59:40	16.2	OK	70.5	37.5	22.8	30.7	61.3	23.4	2.938
20.11.2016	11:00:00	16.4	OK	70.5	37.8	22.8	30.9	61.4	23.7	2.936
20.11.2016	11:00:20	17	OK	70.4	38.1	22.9	31.2	61.5	23.6	2.936
20.11.2016	11:00:40	17.2	OK	70.5	38.5	23	31.5	61.7	23.9	2.934
20.11.2016	11:01:00	17.4	OK	70.5	38.8	23	31.7	61.7	23.7	2.937
20.11.2016	11:01:20	18	OK	70.5	39.2	23.3	32.1	61.9	23.2	2.936
20.11.2016	11:01:40	18.2	OK	70.5	39.7	23.5	32.5	61.9	23.4	2.934
20.11.2016	11:02:00	18.4	OK	70.4	40	23.6	32.7	62	23.7	2.932
20.11.2016	11:02:20	19	OK	70.3	40.4	23.8	33.1	62.1	23.9	2.934
20.11.2016	11:02:40	19.2	OK	70.3	40.6	23.8	33.2	62.2	24.2	2.94
20.11.2016	11:03:00	19.4	OK	70.3	40.9	23.9	33.5	62.2	24.1	2.93
20.11.2016	11:03:20	20	OK	70.2	41.2	24	33.8	62.3	23.9	2.936
20.11.2016	11:03:40	20.2	OK	70	41.5	24.3	34.2	62.3	23.9	2.938
20.11.2016	11:04:00	20.4	OK	69.9	41.8	24.5	34.5	62.4	24.2	2.93
20.11.2016	11:04:20	21	OK	69.8	42.1	24.6	34.7	62.5	24.2	2.93
20.11.2016	11:04:40	21.2	OK	69.7	42.4	24.9	35.1	62.3	23.9	2.931
20.11.2016	11:05:00	21.4	OK	69.7	42.7	25	35.4	62.4	24	2.93
20.11.2016	11:05:20	22	OK	69.6	43	25.3	35.7	62.4	23.8	2.928
20.11.2016	11:05:40	22.2	OK	69.4	43.3	25.5	36	62.4	23.8	2.922
20.11.2016	11:06:00	22.4	OK	69.3	43.5	25.7	36.2	62.4	24.3	2.923
20.11.2016	11:06:20	23	OK	69.1	43.8	25.9	36.5	62.4	24.4	2.914
20.11.2016	11:06:40	23.2	OK	69	44	26	36.7	62.6	24.6	2.922
20.11.2016	11:07:00	23.4	OK	68.8	44.2	26.1	36.8	62.5	24.7	2.92
20.11.2016	11:07:20	24	OK	68.6	44.4	26.3	37.2	62.3	24.6	2.924
20.11.2016	11:07:40	24.2	OK	68.4	44.7	26.5	37.4	62.4	24.5	2.92
20.11.2016	11:08:00	24.4	OK	68.2	44.9	26.7	37.6	62.3	24.6	2.76
20.11.2016	11:08:20	25	OK	68.1	45.1	27	37.9	62.3	24.6	2.604
20.11.2016	11:08:40	25.2	OK	67.8	45.4	27.3	38.3	62.3	24.2	2.598

20.11.2016	11:09:00	25.4	OK	67.7	45.7	27.5	38.5	62.1	24.4	2.594
20.11.2016	11:09:20	26	OK	67.4	45.8	27.7	38.7	61.8	24.5	2.59
20.11.2016	11:09:40	26.2	OK	67.2	46.1	27.9	38.9	61.9	24.4	2.76
20.11.2016	11:10:00	26.4	OK	66.8	46.2	28.1	39.1	61.4	24.7	3.293
20.11.2016	11:10:20	27	OK	66.6	46.5	28.4	39.3	61.6	24.8	3.285
20.11.2016	11:10:40	27.2	OK	66.4	46.7	28.5	39.4	61.6	24.9	3.279
20.11.2016	11:11:00	27.4	OK	66	46.7	28.5	39.5	61.5	25	3.265
20.11.2016	11:11:20	28	OK	65.6	46.8	28.7	39.6	61.4	24.9	3.262
20.11.2016	11:11:40	28.2	OK	65.3	47	29	40	61.2	24.8	3.251
20.11.2016	11:12:00	28.4	OK	65.1	47.2	29.2	40.2	61.1	25	1.763
20.11.2016	11:12:20	29	OK	65.3	47.3	29.4	40.3	61	24.9	0.836

Run 2 discharging cycle test data

Date	Time	Time	Status	T1	T2	T3	T4	T5	T6	Flow
		Min		Average	Average	Average	Average	Average	Average	Energy
				°C	°C	°C	°C	°C	°C	L/min
20.11.2016	11:14:40	0	OK	33.2	48.5	31	41.6	58.9	24.3	2.496
20.11.2016	11:15:00	0.2	OK	28.9	48.6	31.2	41.8	59.2	24.3	2.31
20.11.2016	11:15:20	0.4	OK	29.2	48.7	31.5	42	59.3	24.6	3.729
20.11.2016	11:15:40	1	OK	28	48.9	31.7	42.3	59.2	24.9	3
20.11.2016	11:16:00	1.2	OK	27.1	49	31.7	42.2	58.6	25.2	2.968
20.11.2016	11:16:20	1.4	OK	26.5	49.1	32	42.5	57.6	25	2.962
20.11.2016	11:16:40	2	OK	26.1	49.1	32.2	42.7	56.3	25.2	3.006
20.11.2016	11:17:00	2.2	OK	25.9	49.2	32.4	42.8	54.8	25.5	3.027
20.11.2016	11:17:20	2.4	OK	25.9	49.3	32.6	42.9	54.1	25.3	3.039
20.11.2016	11:17:40	3	OK	25.9	49.3	32.7	42.9	51.4	25	3.04
20.11.2016	11:18:00	3.2	OK	25.9	49.3	32.9	43	49.6	25.1	3.03
20.11.2016	11:18:20	3.4	OK	25.9	49.3	33.1	43.2	48.6	25.2	3.019
20.11.2016	11:18:40	4	OK	25.8	49.2	33.3	43.2	47.6	25.1	3.031
20.11.2016	11:19:00	4.2	OK	25.8	49.2	33.5	43.4	46.4	24.9	3.015
20.11.2016	11:19:20	4.4	OK	25.9	49.3	33.8	43.5	45.6	24.9	2.992
20.11.2016	11:19:40	5	OK	26	49.5	34.1	43.5	44.9	25.3	2.994
20.11.2016	11:20:00	5.2	OK	26.1	49.4	34.1	43.5	43.8	25.1	2.98
20.11.2016	11:20:20	5.4	OK	26.1	49.4	34.2	43.4	42.7	25	2.997
20.11.2016	11:20:40	6	OK	26.1	49.3	34.2	43.3	42.2	25.2	3.006
20.11.2016	11:21:00	6.2	OK	26.2	49.4	34.7	43.5	41.4	25.6	2.999
20.11.2016	11:21:20	6.4	OK	26.1	49.4	35	43.6	40.8	24.9	2.924
20.11.2016	11:21:40	7	OK	26	49.3	35.1	43.7	40.6	24.5	2.899

20.11.2016	11:22:00	7.2	OK	26	49.1	35.2	43.7	40	24.3	2.915
20.11.2016	11:22:20	7.4	OK	26	49.1	35.3	43.7	39.4	24.8	2.894
20.11.2016	11:22:40	8	OK	26.2	49.2	35.6	43.8	39.5	25.2	2.907
20.11.2016	11:23:00	8.2	OK	26.1	49	35.7	43.7	39.4	25.5	2.918
20.11.2016	11:23:20	8.4	OK	26.1	49	35.9	43.8	38.6	25.5	2.914
20.11.2016	11:23:40	9	OK	26	48.9	36.1	43.8	38	25.5	2.896
20.11.2016	11:24:00	9.2	OK	26.1	48.9	36.1	43.7	37.3	26	2.911
20.11.2016	11:24:20	9.4	OK	26.1	48.8	36.1	43.5	36.9	25.7	2.886
20.11.2016	11:24:40	10	OK	26.1	48.7	36.3	43.6	37	25.3	2.889
20.11.2016	11:25:00	10.2	OK	26.1	48.6	36.5	43.7	37.2	25.3	2.877
20.11.2016	11:25:20	10.4	OK	26.1	48.6	36.7	43.7	38.1	24.9	2.865
20.11.2016	11:25:40	11	OK	26.1	48.6	36.9	43.7	37.3	25	2.888
20.11.2016	11:26:00	11.2	OK	26.1	48.5	37	43.7	37.5	25.1	2.888
20.11.2016	11:26:20	11.4	OK	26.2	48.5	37.2	43.7	36.9	25.1	2.88
20.11.2016	11:26:40	12	OK	26.2	48.4	37.1	43.6	35.8	25.4	2.869
20.11.2016	11:27:00	12.2	OK	26.2	48.3	37.3	43.6	35.6	25.2	2.885
20.11.2016	11:27:20	12.4	OK	26.2	48.2	37.5	43.7	34.7	25.4	2.884
20.11.2016	11:27:40	13	OK	26.2	48.2	37.7	43.8	34.5	25.8	2.886
20.11.2016	11:28:00	13.2	OK	26.2	48.1	37.9	43.8	34.4	25.8	2.895
20.11.2016	11:28:20	13.4	OK	26.2	48.2	38.1	43.8	34.1	25.7	2.895
20.11.2016	11:28:40	14	OK	26.2	48	38	43.6	33.3	25.9	2.896
20.11.2016	11:29:00	14.2	OK	26.1	47.8	38	43.6	33.2	25.3	2.884
20.11.2016	11:29:20	14.4	OK	26.1	47.7	38.2	43.6	32.7	25.3	2.886
20.11.2016	11:29:40	15	OK	26.1	47.6	38.3	43.6	32.4	25.5	2.885
20.11.2016	11:30:00	15.2	OK	26.2	47.5	38.4	43.6	32.2	25.5	2.881
20.11.2016	11:30:20	15.4	OK	26.2	47.4	38.5	43.6	31.8	25.3	2.876
20.11.2016	11:30:40	16	OK	26	47.2	38.4	43.4	31.5	25.7	2.89

20.11.2016	11:31:00	16.2	OK	25.9	47	38.4	43.4	31.2	25.5	2.877
20.11.2016	11:31:20	16.4	OK	26	47.1	38.7	43.4	31	25.4	2.873
20.11.2016	11:31:40	17	OK	26	47	38.7	43.4	31.2	25.5	2.897
20.11.2016	11:32:00	17.2	OK	26.1	46.8	38.8	43.3	31.3	25.5	2.894
20.11.2016	11:32:20	17.4	OK	26.1	46.8	38.9	43.4	31.1	25.7	2.893
20.11.2016	11:32:40	18	OK	26.3	46.8	39	43.3	31.2	25.8	2.902
20.11.2016	11:33:00	18.2	OK	26.3	46.7	39	43.2	31.2	25.6	2.915
20.11.2016	11:33:20	18.4	OK	26.3	46.7	39.1	43.3	30.8	25.6	2.906
20.11.2016	11:33:40	19	OK	26.3	46.5	39.1	43.1	31.2	26	2.925
20.11.2016	11:34:00	19.2	OK	26.2	46.4	39.2	43.2	30.9	25.9	2.945
20.11.2016	11:34:20	19.4	OK	26.2	46.3	39.3	43.1	30.5	25.9	2.946
20.11.2016	11:34:40	20	OK	26.2	46.2	39.3	43.1	31	26.1	2.939
20.11.2016	11:35:00	20.2	OK	26.2	46.1	39.4	43.1	31	25.7	2.936
20.11.2016	11:35:20	20.4	OK	26.2	46	39.4	43	30.5	25.5	2.914
20.11.2016	11:35:40	21	OK	26.2	45.9	39.5	43	30.2	25.3	2.909
20.11.2016	11:36:00	21.2	OK	26.2	45.7	39.5	42.9	29.8	25.6	2.916
20.11.2016	11:36:20	21.4	OK	26.2	45.6	39.6	43	29.5	25.3	2.911
20.11.2016	11:36:40	22	OK	26.2	45.5	39.6	43	29.7	25.6	2.91
20.11.2016	11:37:00	22.2	OK	26.2	45.4	39.7	43	29.5	26	2.921
20.11.2016	11:37:20	22.4	OK	26.3	45.3	39.7	42.9	29.3	25.8	2.919
20.11.2016	11:37:40	23	OK	26.3	45.2	39.6	42.7	29.1	25.9	2.942
20.11.2016	11:38:00	23.2	OK	26.3	45	39.6	42.7	28.7	25.5	2.94
20.11.2016	11:38:20	23.4	OK	26.3	44.9	39.6	42.6	28.8	25.6	2.961
20.11.2016	11:38:40	24	OK	26.2	44.7	39.6	42.6	28.5	25.6	2.974
20.11.2016	11:39:00	24.2	OK	26.3	44.7	39.8	42.7	28.5	26.2	2.97
20.11.2016	11:39:20	24.4	OK	26.3	44.6	39.9	42.7	28.3	26.3	2.937
20.11.2016	11:39:40	25	OK	26.2	44.4	39.8	42.6	28.4	26	3

20.11.2016	11:40:00	25.2	OK	26.2	44.3	39.8	42.6	28.1	25.6	3.013
20.11.2016	11:40:20	25.4	OK	26.3	44.3	39.9	42.5	28.1	26	3.036
20.11.2016	11:40:40	26	OK	26.3	44.2	39.9	42.5	28.2	25.9	3.032
20.11.2016	11:41:00	26.2	OK	26.3	44.1	39.9	42.4	28.2	25.9	3.027
20.11.2016	11:41:20	26.4	OK	26.2	43.9	39.7	42.2	28.2	25.9	2.965
20.11.2016	11:41:40	27	OK	26.2	43.7	39.7	42.1	27.9	26.2	2.965
20.11.2016	11:42:00	27.2	OK	26.3	43.7	39.8	42.1	28.3	26.2	2.961
20.11.2016	11:42:20	27.4	OK	26.3	43.5	39.6	41.9	27.9	26.2	2.959
20.11.2016	11:42:40	28	OK	26.4	43.4	39.5	41.7	28	26.4	2.985
20.11.2016	11:43:00	28.2	OK	26.4	43.3	39.5	41.7	27.7	26.3	2.992
20.11.2016	11:43:20	28.4	OK	26.4	43.3	39.7	41.7	27.6	26.3	3.026
20.11.2016	11:43:40	29	OK	26.3	43.1	39.5	41.6	27.3	26.2	3.042
20.11.2016	11:44:00	29.2	OK	26.3	43	39.6	41.6	27.5	26.1	3.04
20.11.2016	11:44:20	29.4	OK	26.2	42.8	39.6	41.6	27.3	26.2	3.042
20.11.2016	11:44:40	30	OK	26.2	42.7	39.7	41.6	27.4	26	1.925
20.11.2016	11:45:00	30.2	OK	26.5	42.5	39.7	41.6	27.5	26.2	0
20.11.2016	11:45:20	30.4	OK	26.7	42.5	39.6	41.5	26.7	26	0

9.7 Appendix G

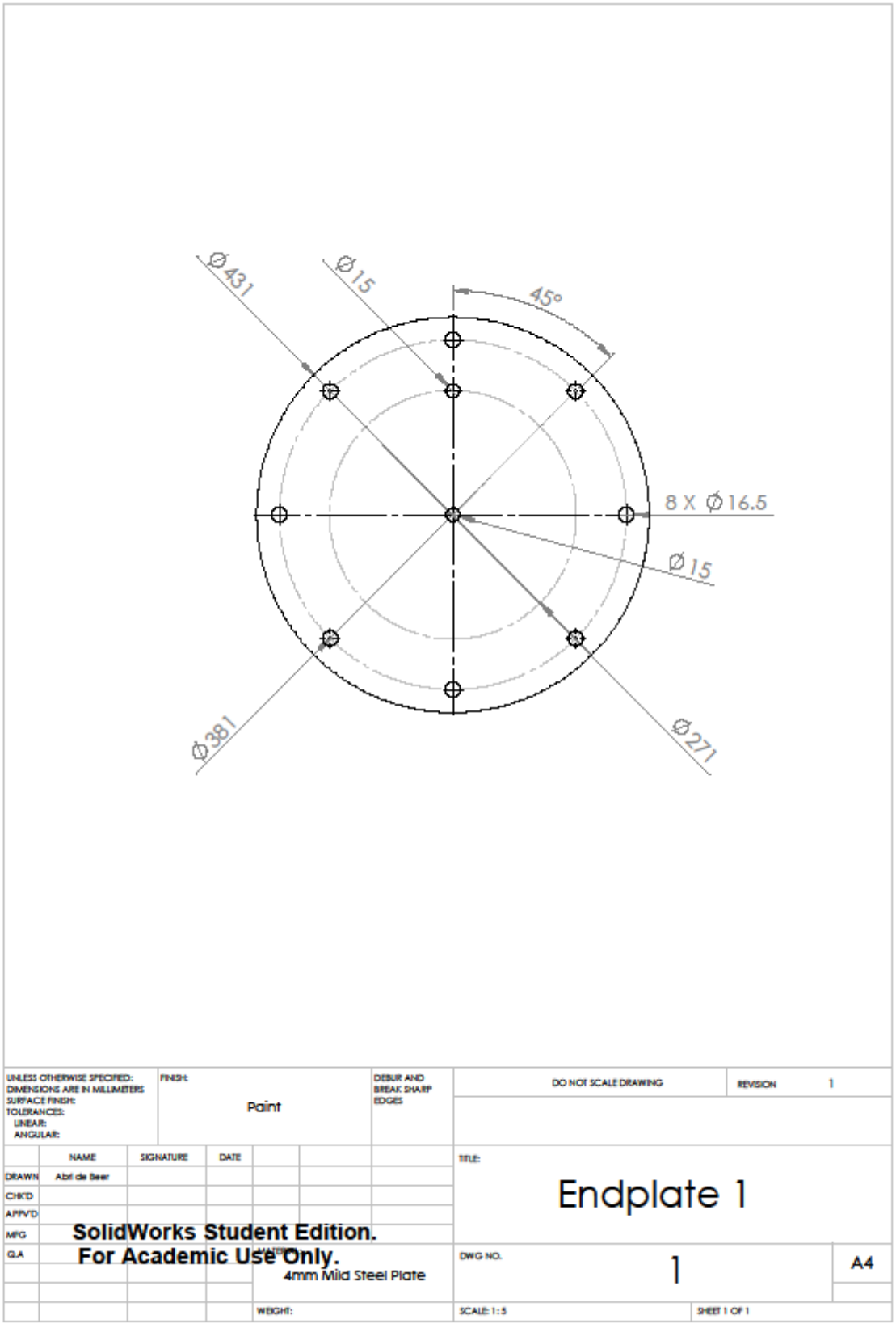

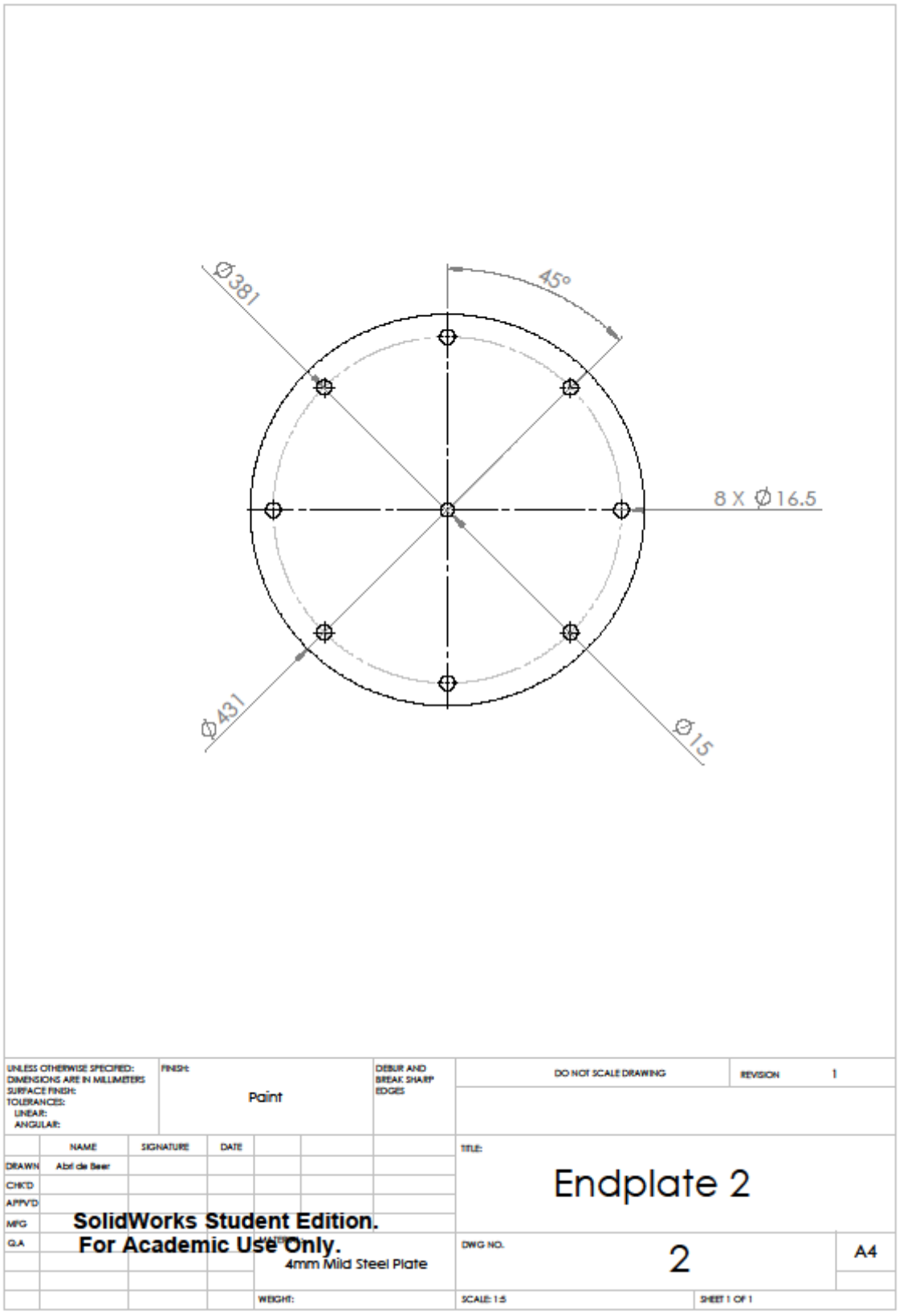
Ø381
45°
8 X Ø16.5
Ø431
Ø15
UNLESS OTHERWISE SPECIFIED:
DIMENSIONS ARE IN MILLIMETERS
SURFACE FINISH:
TOLERANCES:
LINEAR:
ANGULAR:
FINISH:
Paint
DEBUR AND BREAK SHARP EDGES
DO NOT SCALE DRAWING
REVISION 1
NAME
SIGNATURE
DATE
DRAWN Abri de Beer
CHK'D
APPV'D
MFG
Q.A
MATERIAL:
4mm Mild Steel Plate
WEIGHT:
TITLE:
Endplate 2
DWG NO.
2
A4
SCALE: 1:5
SHEET 1 OF 1
SolidWorks Student Edition.
For Academic Use Only.

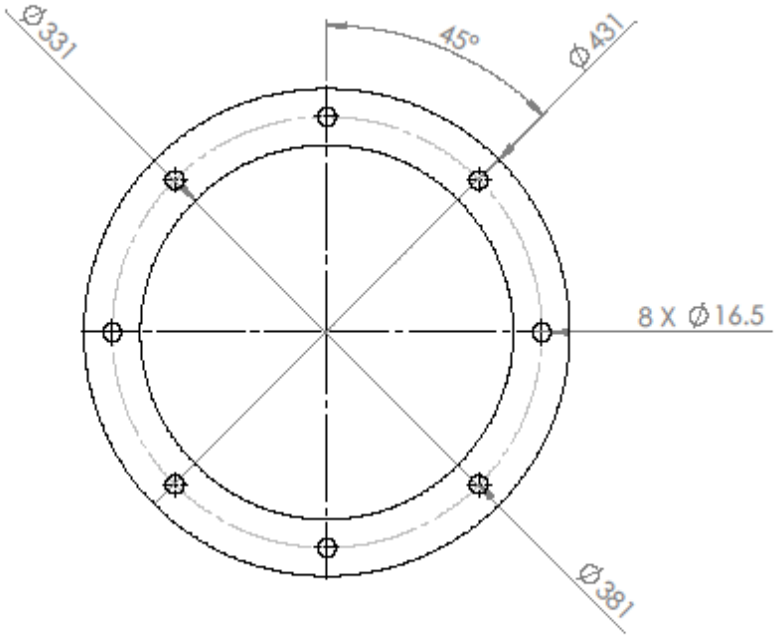

UNLESS OTHERWISE SPECIFIED: DIMENSIONS ARE IN MILLIMETERS SURFACE FINISH: TOLERANCES: LINEAR: ANGULAR:			FINISH: Paint			DEBUR AND BREAK SHARP EDGES	DO NOT SCALE DRAWING REVISION 1
	NAME	SIGNATURE	DATE				TITLE: Flange
DRAWN	Abri de Beer						
CHK'D							
APPV'D							
MFG							
Q.A							DWG NO. 3 A4
				MATERIAL: 4mm Mild Steel Plate			
				WEIGHT:			SCALE: 1:5 SHEET 1 OF 1

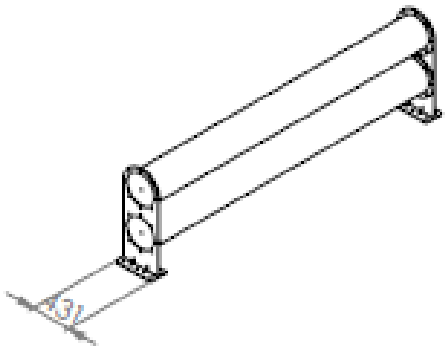

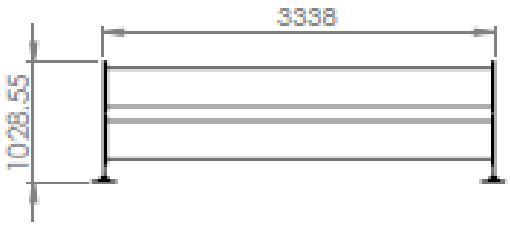

UNLESS OTHERWISE SPECIFIED: DIMENSIONS ARE IN MILLIMETRES SURFACE FINISH: TOLERANCES: LINEAR: ANGULAR:		FINISH:				DRILLER AND REMAC SHARP EDGES:	DO NOT SCALE DRAWING	REVISION
	NAME	SIGNATURE	DATE				TITLE: Final Design Ass	
DRAWN								
CHK'D								
APP'VD								
MFG								
Q.A							DWG NO.	A4
				MATERIAL:			SCALE: 1:20	SHEET 1 OF 1

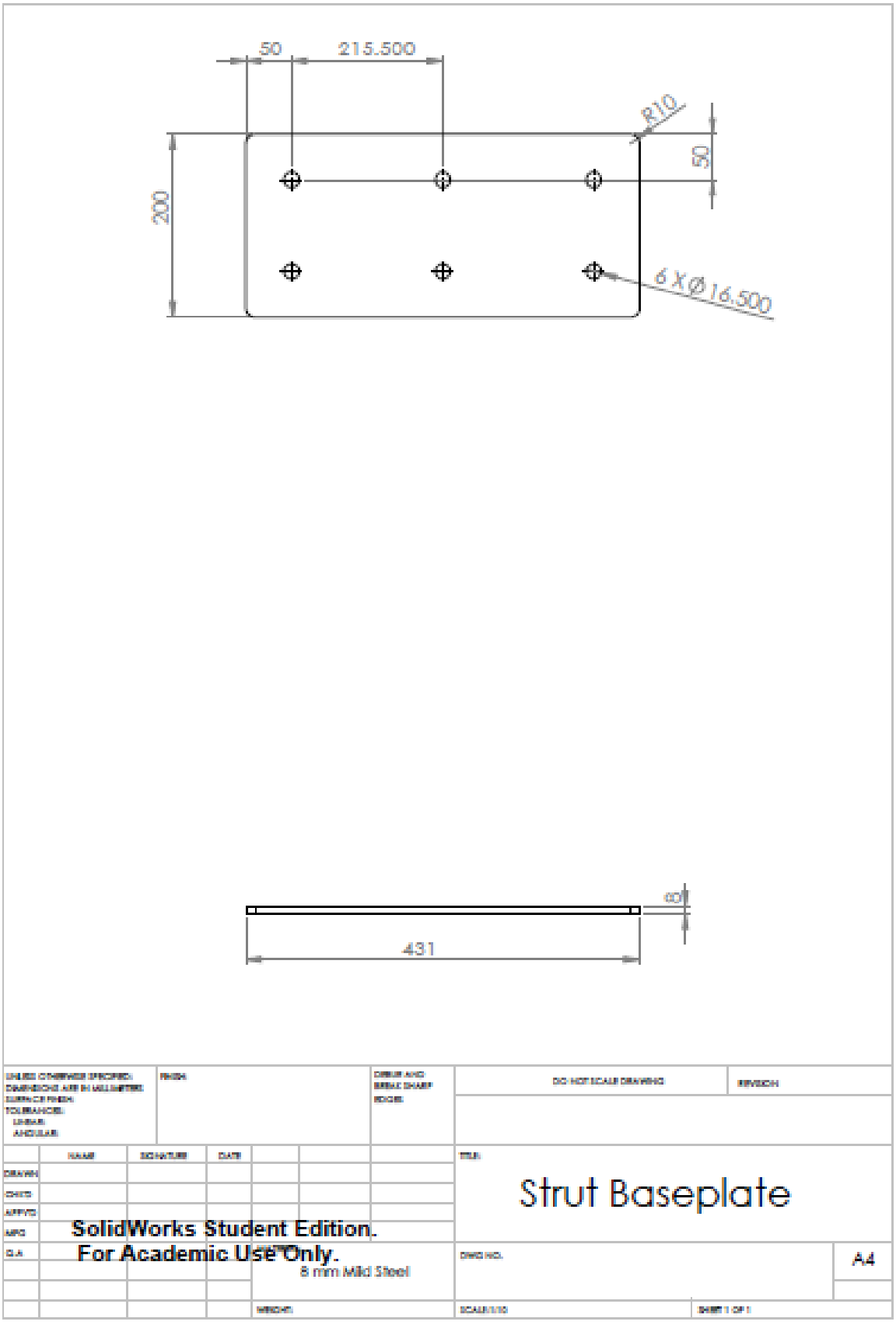
50
215.500
R10
50
200
6 X Ø 16.500
8
431
SolidWorks Student Edition.
For Academic Use Only.
8 mm Mild Steel
Strut Baseplate
A4

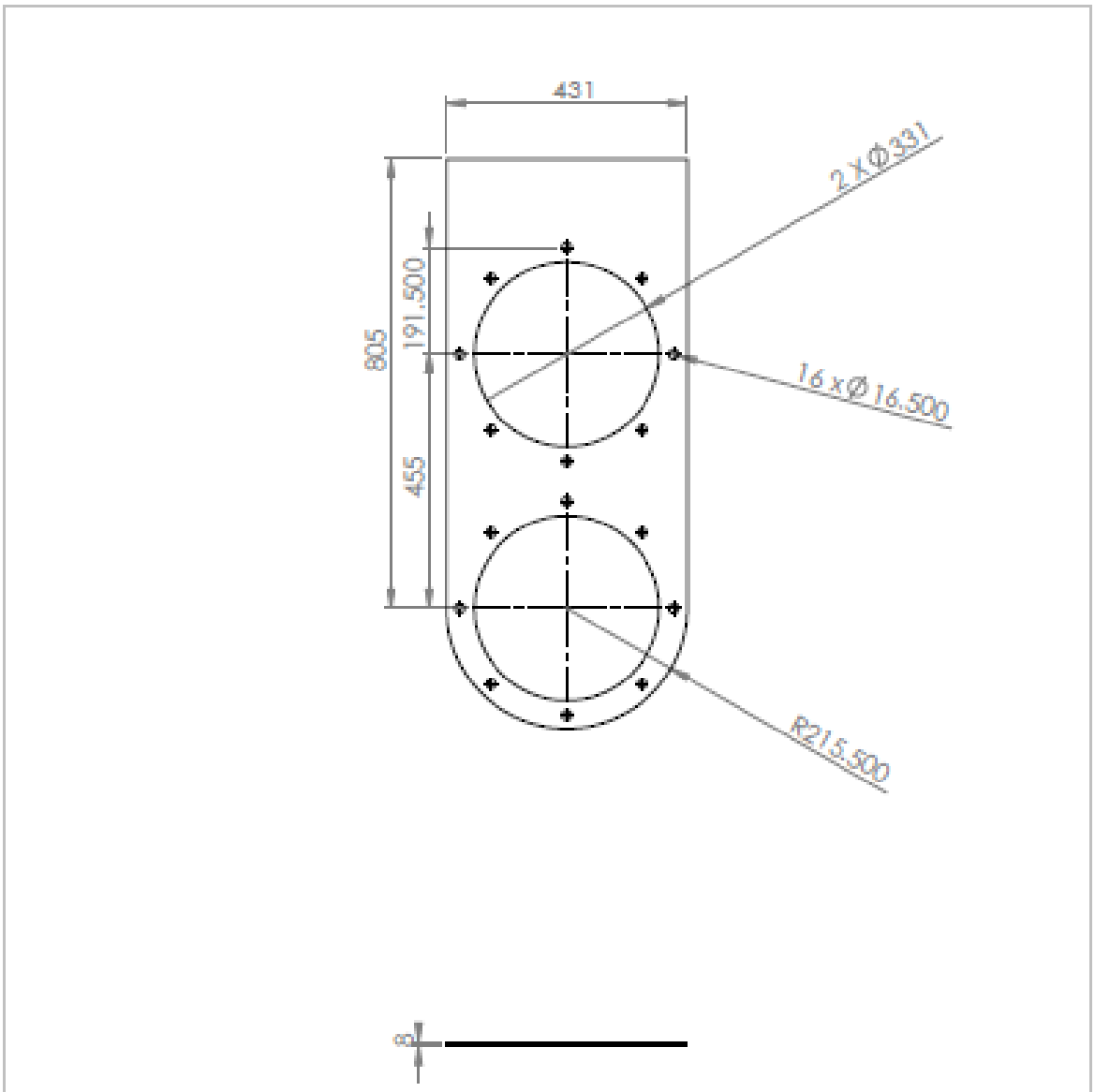

UNLESS OTHERWISE SPECIFIED: DIMENSIONS ARE IN MILLIMETRES SURFACE FINISH: TOLERANCES: LINEAR: ANGULAR:		FINISH:			DEBUR AND BREAK SHARP EDGES	DO NOT SCALE DRAWING	REVISION
	NAME	SIGNATURE	DATE			TITLE: Strut	
DRAWN							
CHK'D							
APP'D							
MFG							
Q.A						DWG NO.	A4
					8 mm Mild Steel		
				WEIGHT:		SCALE:1:10	SHEET 1 OF 1

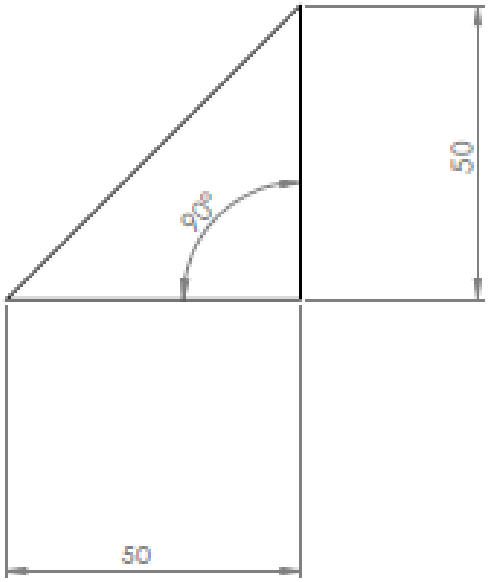

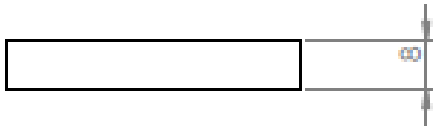

UNLESS OTHERWISE SPECIFIED: DIMENSIONS ARE IN MILLIMETERS SURFACE FINISH: TOLERANCES: LINEAR: ANGULAR:		FINISH:		DEBUR AND BREAK SHARP EDGES	DO NOT SCALE DRAWING		REVISION
	NAME	SIGNATURE	DATE		TITLE: Strut support		
DRAWN							
CHK'D							
APP'D							
MFG							
Q.A					DWG NO.		A4
				8 mm Mild Steel			
				WEIGHT:	SCALE:1:1	SHEET 1 OF 1	

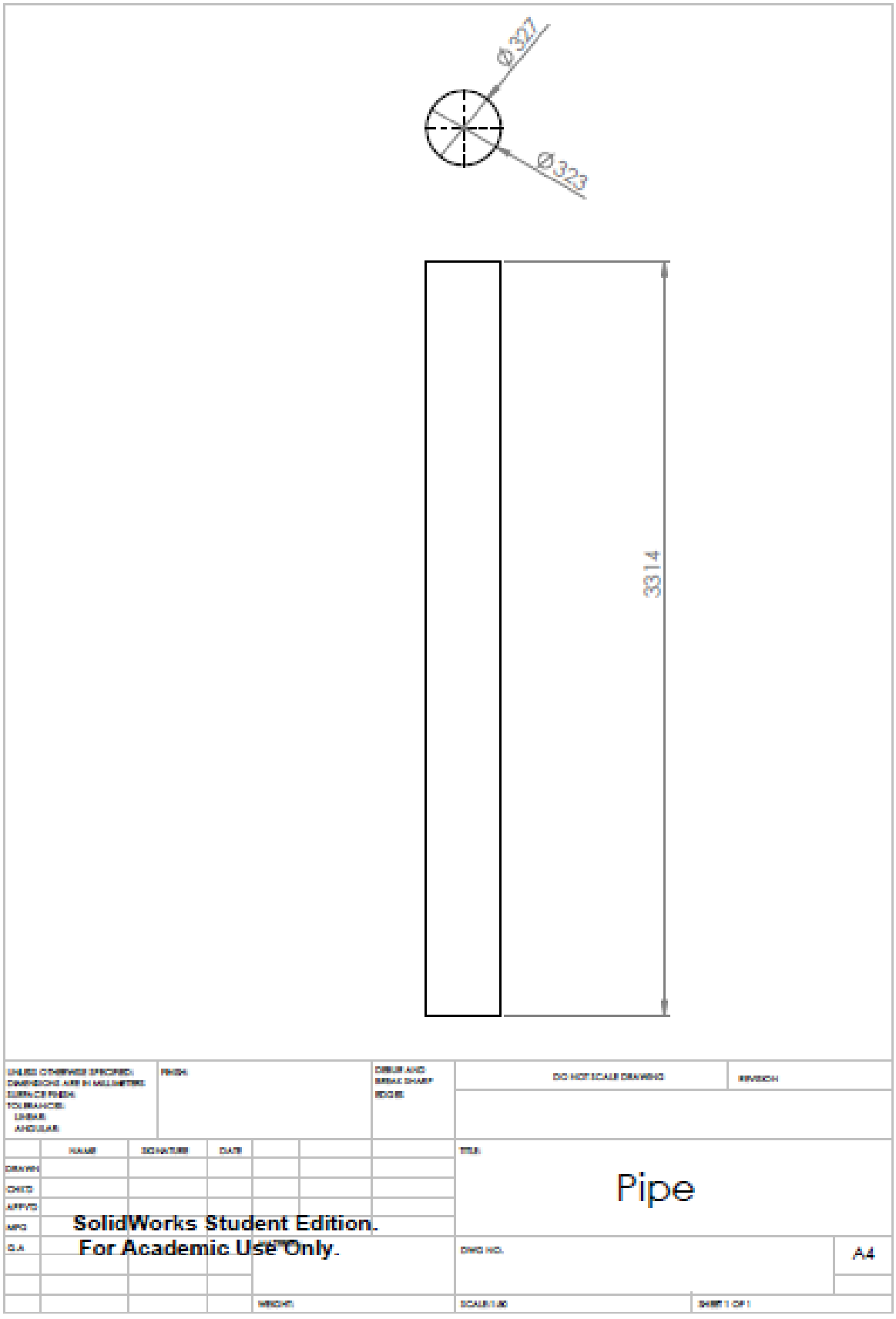
Ø327
Ø323
3314
DO NOT SCALE DRAWING
REVISION
Pipe
SolidWorks Student Edition.
For Academic Use Only.
A4